

## ABSTRACT

Title of Dissertation:                   PHYSICAL FACTORS IN B CELL  
  SIGNALING AND ACTIN DYNAMICS

Christina Merrill Ketchum  
Doctor of Philosophy, 2016

Dissertation directed by:           Professor Arpita Upadhyaya  
  Department of Physics

Cells adapt to their changing world by sensing environmental cues and responding appropriately. This is made possible by complex cascades of biochemical signals that originate at the cell membrane. In the last decade it has become apparent that the origin of these signals can also arise from physical cues in the environment.

Our motivation is to investigate the role of physical factors in the cellular response of the B lymphocyte. B cells patrol the body for signs of invading pathogens in the form of antigen on the surface of antigen presenting cells. Binding of antigen with surface proteins initiates biochemical signaling essential to the immune response. Once contact is made, the B cell spreads on the surface of the antigen presenting cell in order to gather as much antigen as possible. The physical mechanisms that govern this process are unexplored. In this research, we examine the role of the physical parameters of antigen mobility and cell surface topography on B cell spreading and

activation. Both physical parameters are biologically relevant as immunogens for vaccine design, which can provide laterally mobile and immobile antigens and topographical surfaces. Another physical parameter that influences B cell response and the formation of the cell-cell junction is surface topography. This is biologically relevant as antigen presenting cells have highly convoluted membranes, resulting in variable topography. We found that B cell activation required the formation of antigen-receptor clusters and their translocation within the attachment plane. We showed that cells which failed to achieve these mobile clusters due to prohibited ligand mobility were much less activation competent.

To investigate the effect of topography, we use nano- and micro-patterned substrates, on which B cells were allowed to spread and become activated. We found that B cell spreading, actin dynamics, B cell receptor distribution and calcium signaling are dependent on the topographical patterning of the substrate.

A quantitative understanding of cellular response to physical parameters is essential to uncover the fundamental mechanisms that drive B cell activation. The results of this research are highly applicable to the field of vaccine development and therapies for autoimmune diseases. Our studies of the physical aspects of lymphocyte activation will reveal the role these factors play in immunity, thus enabling their optimization for biological function and potentially enabling the production of more effective vaccines.



PHYSICAL FACTORS IN B CELL ACTIN DYNAMICS AND ACTIVATION

by

Christina M. Ketchum

Dissertation submitted to the Faculty of the Graduate School of the  
University of Maryland, College Park, in partial fulfillment  
of the requirements for the degree of  
Doctor of Philosophy  
2016

Advisory Committee:

Dr. Arpita Upadhyaya, Chair

Dr. Kimberly Stroka

Dr. Garegin A. Papoian

Dr. Wenxia Song

Dr. John Fourkas, Dean's Representative

© Copyright by  
Christina Merrill Ketchum  
2016

# Acknowledgements

There are many people who I would like to thank for aiding in the completion of this dissertation. Foremost, I would like to thank Arpita for her role as my advisor. Her guidance and insight into biophysical problems has been invaluable. For many professors striking the balance between motivation and understanding the needs of their students is a challenge but Dr. Upadhyaya does this with grace and understanding. For many reasons would also like to thank my fellow labmates. Dr. King Lam Hui and Dr. Brian Grooman I thank especially for providing the knowledge and support that only seasoned lab members can offer. Brian gets a special thanks for devising a release mechanism out of an empty coke can when I jammed a bike lock key in my car door in a sleep deprived state. Dr. Mike Azatov was my comrade in arms. We learned Matlab together and exchanged so many program fragments that it is hard to know who wrote what. Ivan and David, I hope that I helped you the way King and Brian helped me. If not, then I hope I didn't scare you too much. I would also like to acknowledge our collaborators Dr. Wenxia Song, her students, Heather Miller and Michelle Lazzaro, for their Immunology advice and for providing me with primary B cells. Dr. John Fourkas and his students, Xiaoyu Sun and Lexi Suberi for providing us with patterned substrates. There are also two undergraduates who helped me acquire some of my data, so I would also like to thank Ming Zhang and Ashley Matos.

I wouldn't have gotten very far without the love and support of my family. My parents Dr. Barb Vail and Robert Ketchum were always supportive of my choices, even though they took me far away from home. Special thanks to my father for being the most interesting thing to ever happen to Billings, Montana and my mother for teaching me how to laugh at my failures. I can only hope to emulate them in my career and as a parent. Thank you to my sister, Karey Ketchum, for her quick wit, her tough as nails attitude, and for putting family above all else. She was there for my parents when I couldn't be.

I want to thank my husband Valentin Solotych for just about everything. He is the most hardworking, patient, and loyal human being I've ever met. He helped me solve Matlab issues, among many, many other things. I probably don't deserve him, so I hope he doesn't read this and figure it out. Thank you to my daughter, Natalie Ketchum, for being so amazing and so patient with me while I finish my degree. And thank you to Yuri Solotych, who helped take care of Natalie, and who single handedly held our little family together while Vali and I wrote our dissertations.

# Table of Contents

Acknowledgements.....	ii
Table of Contents.....	iv
List of Figures.....	vii
List of Abbreviations.....	x
Chapter 1: Introduction.....	1
1.1 Overview of the Thesis.....	1
1.2 The B Lymphocyte and the Adaptive Immune System.....	2
1.2.1 Innate and adaptive immunity in mammals.....	2
1.2.2 The role of the B cell in immunity.....	4
1.3 B Cell Activation.....	8
1.3.1 BCR signaling pathway.....	8
1.3.2 Models of BCR triggering and oligomerization.....	12
1.3.3 Nanoscale barriers to BCR cluster formation.....	14
1.3.4 Store operated calcium entry.....	16
1.4 The Actin Cytoskeleton.....	18
1.4.1 Actin and actin binding proteins.....	18
1.4.2 BCR engagement leads to remodeling of the actin cytoskeleton.....	21
1.4.3 The role of actin associated proteins in B cell activation.....	24
1.5 The Importance of Ligand Mobility.....	25
1.5.1 Factors in plasma membrane mobility.....	25
1.5.2 Ligand mobility in hematopoietic cells.....	26
1.6 Topography and Cell Biology.....	31
1.6.1 Topography influences a variety of cell types.....	31
1.6.2 Techniques for studying the role of topography.....	32
1.6.3 Topography and immune cells.....	35
Chapter 2: Ligand Mobility Regulates B Cell Receptor Clustering and Signaling Activation.....	38
2.1 Introduction.....	38
2.2 Ligand lateral mobility modulates B cell spreading and BCR aggregation.....	40
2.2.1 Cell spread area is larger on immobile ligand presenting surfaces.....	40
2.2.2 BCR accumulation is greater on a bilayer substrate.....	43
2.2.3 Syk-mediated B cell signaling is greater with mobile ligand.....	45
2.3 Effect of ligand mobility on BCR microcluster formation, dynamics, and signaling.....	47
2.3.1 BCR cluster formation is less efficient when bound to immobile ligand.....	47
2.3.2 BCR cluster motion is dependent on ligand mobility.....	50
2.3.3 Primary B cells recapitulate mobile and immobile cluster behavior.....	53
2.4 Actin organization with respect to BCR and receptor cluster formation and signaling.....	55
2.4.1 Actin patches are colocalized with BCR clusters.....	55
2.4.2 Actin modulates BCR signaling by controlling cluster conformations.....	58

2.4.3 Actin cytoskeleton integrity is essential for BCR cluster formation and translocation.....	61
2.5 Discussion.....	64
Chapter 3: Substrate Topography Guides Actin dynamics and Calcium Oscillations in B Cells.....	68
3.1 Introduction.....	68
3.2 Recurring actin contractions are induced on patterned substrates.....	72
3.2.1 Nanotopographic substrates alter B cell morphology and spreading.....	73
3.2.2 Contact with multiple ridges cause repeated actin enrichments.....	75
3.2.3 Signaling downstream of BCR cross-linking is necessary for actin-based contractions.....	80
3.2.4 Myosin IIA regulates actin oscillations.....	85
3.2.5 Role of topography on BCR clustering.....	86
3.3 Small ridge spacings induce actin protrusions.....	90
3.3.1 Protrusion velocity and length are modulated by pattern width.....	90
3.3.2 N-WASP and ARP2/3 branching are necessary for actin based protrusions.....	93
3.3.3 Patterned substrates induce waves and oscillations in primary B cells....	94
3.4 B cell signaling is modulated by ridge spacing.....	97
3.4.1 Calcium oscillation frequency dependent on ridge spacing.....	97
3.5 Discussion.....	101
Chapter 4: Conclusions and Future Directions.....	104
4.1 Conclusions.....	104
4.2 Future Directions.....	106
4.2.1 Other topographically patterned geometries.....	106
4.2.2 Curvature sensing proteins.....	107
4.2.3 Substrate stiffness and B cell activation.....	108
Chapter 5: Materials and Methods.....	110
5.1 Cells and Reagents.....	110
5.1.1 Reagents.....	110
5.1.2 Cell culture.....	110
5.2 Substrate Preparation.....	111
5.2.1 Glass substrates.....	111
5.2.2 Bilayer substrates.....	111
5.2.3 Topographically patterned substrates.....	113
5.3 Microscopy.....	114
5.3.1 Microscopy of live cells.....	114
5.3.2 Immunofluorescence imaging.....	115
5.4 Image Analysis.....	115
5.4.1 Cluster identification and tracking.....	115
5.4.2 Autocorrelation analysis.....	115
Appendices.....	117
A: Additional Ligand Mobility Data.....	117
A.1 Streptavidin accumulation in the B cell contact zone.....	117
A.2 Photobleaching correction of fluorescence intensity.....	118
A.3 BCR peak cluster intensity is proportional to total cluster intensity.....	119

A.4 BCR cluster motion and intensity is actin dependent on mobile ligand substrates.....	120
B: Additional Patterned Substrate Data .....	122
B.1 Photobleaching correction of calcium fluorescence intensity.....	122
B.2 Protrusion widths vary by ridge spacing .....	122
Bibliography .....	124

# List of Figures

- 1.1 The innate and adaptive immune systems
- 1.2 B cell activation and antibody production
- 1.3 Structure of the B cell receptor (BCR)
- 1.4 Signaling cascade of BCR and TCR clusters
- 1.5 Formation of BCR clusters and the immune synapse
- 1.6 Models of cross-linking activation
- 1.7 The dissociation activation model
- 1.8 Store operated calcium entry
- 1.9 Actin filament treadmilling
- 1.10 Actin network as a corral
- 1.11 Stages of B cell spreading, BCR clustering and actin reorganization
- 1.12 The influence of ligand mobility on cSMAC formation
- 1.13 Physical effects of a ligand mobility limiting substrate
- 1.14 Epithelial cell alignment along topographically patterned substrate
- 1.15 Migratory T cells on topographically patterned substrates
- 2.1 Effect of ligand mobility on spreading and BCR accumulation of A20 B cells
- 2.2 Signaling levels are affected by ligand mobility
- 2.3 BCR cluster formation is distinct on bilayer and glass surfaces
- 2.4 BCR cluster dynamics depends on ligand mobility
- 2.5 Spreading and BCR clustering in mouse primary B cells
- 2.6 Actin dynamics are distinct on bilayer and glass substrates

- 2.7 Actin organization is distinct on bilayer and glass substrates
- 2.8 Role of actin polymerization in BCR movement
- 3.1 Example images of nanostructures encountered by B cells in vivo
- 3.2 A20 B cells spreading dynamics on patterned substrates
- 3.3 Effect of topographically patterned substrates of 3  $\mu\text{m}$  and 5  $\mu\text{m}$  spacings on B cells
- 3.4 Actin oscillation and ridge-adjacent accumulation analysis
- 3.5 Transferrin controls
- 3.6 Actin contractions are mediated by Syk
- 3.7 Actin contractions are mediated by non-muscle myosinIIA
- 3.8 BCR analysis on patterned substrates
- 3.9 Technique for measuring protrusion length
- 3.10 Patterned substrates induce actin-based protrusions on ridge separations less than 2 microns
- 3.11 Actin protrusions on small ridge spacings (0.8 $\mu\text{m}$  – 1.5 $\mu\text{m}$ ) are stalled by Arp2/3 and N-WASP inhibition
- 3.12 Primary B Cells exhibit actin and calcium oscillations on patterned substrates
- 3.13 Patterned substrates influence the distribution of BCR clusters and intracellular calcium signaling
- 4.1 Scanning electron micrographs showing nano-posts fabricated using MAP/RAPID lithography
- 4.2 Traction force microscopy
- 5.1 FRAP evaluation of planar lipid bilayer mobility

- 5.2 ELISA assay showing levels of streptavidin density on bilayer and glass substrates
  - A.1 Labeled bilayer shows that streptavidin does not accumulate within the contact zone
  - A.2 Fluorescence intensity curves to assess photobleaching rates
  - A.3 BCR cluster peak intensity and integrated cluster intensity are correlated
  - A.4 Disruption of actin polymerization inhibits BCR cluster movement and growth
- B.1 Protrusions width is influenced by ridge spacing

# List of Abbreviations

APC	Antigen presenting cell
BCR	B cell receptor
BLNK	B cell linker protein
Btk	Bruton's tyrosine kinase
cSMAC	Central supramolecular activation cluster
DAG	Diacylglycerol
DC	Dendritic cell
dSTORM	Direct stochastic optical reconstruction microscopy
ELISA	Enzyme-linked immunosorbent assay
ER	Endoplasmic reticulum
ERM	Ezrin, radixin and moesin
FRET	Forster resonance energy transfer
IP3	Inositol triphosphate
IRM	Interference reflection microscopy
ITAM	Immunoreceptor tyrosine-based activation motif
KLD	Kullback-Leibler distance
KS test	Kolmogorov–Smirnov test
Lat-A	Latrunculin-A
MFI	Mean fluorescence intensity

MLCK	Myosin light chain kinase
NFAT	Nuclear factor of activated T cells
N-WASP	Neuronal Wiskott–Aldrich Syndrome protein
PI3K	Phosphoinositide 3-kinase
pY	Phosphotyrosine
SLO	Secondary lymphoid organ
SOCE	Store-operated calcium entry
Syk	Spleen tyrosine kinase
TCR	T cell receptor
TIRF	Total internal reflection fluorescence
WASP	Wiskott–Aldrich Syndrome protein



# Chapter 1: Introduction

## 1.1 Overview of the Thesis

The function of a cell in a multicellular organism is to interpret extracellular stimuli and respond by making gene expression decisions. While the collective efforts of scientists over decades has given us a schematic for how cells interpret chemical and molecular stimuli, it has only recently become clear that the physical environment of a cell can also have profound effects on cell behavior. The discoveries that stem cell differentiation can be controlled by substrate stiffness alone [1] and that cancer cells during metastasis are often guided by topographical cues [2, 3], imply that elucidating cellular response to physical stimuli is critical to obtain a complete understanding of cell function.

B cells, as key mediators of the immune response, encounter a wide variety of tissues and form close contacts with other cell types. B cells often migrate through tissues and within the lymph nodes and spleen, which present different tissue stiffnesses and architectures. Additionally, as B cells often form immune junctions with a variety of antigen presenting cells, the topography of those cells as well as the fluidity of their membranes may be of importance. These physical signals can be communicated across the B cell membrane through the B cell receptor as it participates in many types of feedback with the underlying actin network or through the manipulation of the actin network itself. Given that misregulation of B cell signaling leads to immune

dysfunction and impacts human health, it is imperative that we understand the physical factors and mechanisms that contribute to optimal immune function.

This thesis will focus on the role of ligand mobility (Chapter 2) and surface topography (Chapter 3) in B cell function and how this information is communicated to the cell. The actin cytoskeleton, as the regulator of cell shape change and force generation, will be the key target of our investigations. This information is then examined along with B cell signaling outputs in order to piece together a picture of the role of physical cues in directing B cell behavior.

## 1.2 The B Lymphocyte and the Adaptive Immune System

### 1.2.1 Innate and adaptive immunity in mammals

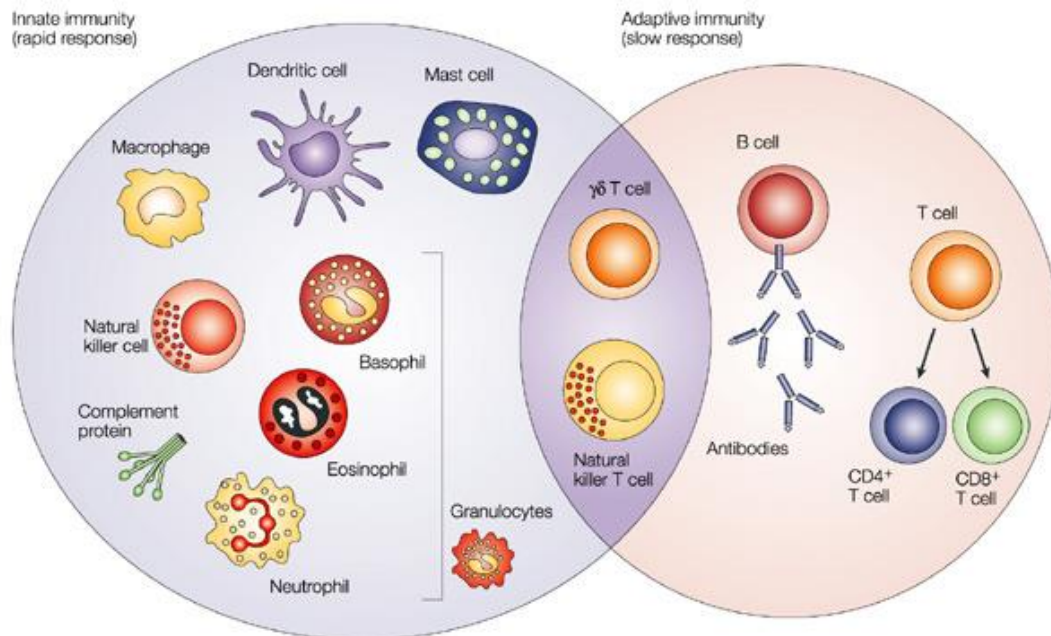
The defense of an organism against invading pathogens is mediated by a collection of cells and molecules known as the immune system. Pathogen invasion in an organism initiates the two stages of immune response in vertebrates, the relatively rapid innate immune response and the adaptive immune response [4].

The innate immune system is evolutionarily older than the adaptive immune system, and found in more primitive organisms, such as small, multicellular organisms and fungi as well as animals. Consisting of many different pathogen fighting strategies,

the innate immune system responds to invading pathogens in a non-specific manner. These strategies include barrier tissues, such as skin and epithelia, inflammation coordinated by chemical signals released from injured cells, and the complement system, which tags pathogens for destruction by cellular agents. The innate immune system recognizes molecular patterns that are common to many pathogens through mediators such as phagocytic cells, natural killer cells, blood proteins and cytokines. However, this response is non-specific and does not confer long lasting immunity to the organism [5].

The adaptive immune system provides a second layer of defense against invading pathogens. It consists of two branches, the cell-mediated immune response, which is mediated by T lymphocytes, and the humoral immune response, which is mediated by B lymphocytes (Fig.1.1). While the innate immune response occurs almost immediately upon the invasion of a foreign body, the adaptive immune system requires between four to seven days to reach full efficacy. The adaptive immune response involves the translocation of B and T cells from circulation to the site of infection and then identification of the invading pathogen by cell surface receptors. T cells then multiply quickly and differentiate into helper T cells, killer T cells, memory T cells, and regulatory T cells, which fight the infection directly, killing either the bacteria or infected host cells. Upon recognizing the infectious pathogen, B cells differentiate into plasma B cells, and memory B cells, which produce antibodies and then store information about the infection, respectively. While T cells are quite

effective at eliminating infection directly, the memory B cell is the key effector of immune system adaptivity, and preservation of immunity [5].



Nature Reviews | Cancer

**Figure 1.1: The innate and adaptive immune systems.** The cells and proteins that comprise the immune system. Images are from [6]. All images used with permission.

### 1.2.2 The role of the B cell in immunity

Also known as B lymphocytes, B cells are responsible for the production of high-affinity antibodies (immunoglobulin, Ig), which bind with cognate antigen rendering it incapable of infection and targeting it for destruction by T cells or macrophages. B cells recognize extracellular (either soluble or cell surface) antigen and then differentiate into plasma B cells, which secrete antibodies [5]. Antibodies are Y-shaped protein complexes consisting of two identical heavy chains joined to two identical light chains (Reth M1 1991, Reth M 1991). The two branches of the

antibody are regions of high sequence variation, which allow for the large range of binding diversity available over the lifetime of the organism [7]. The five major isotypes of antibody are determined by the conserved region of the antibody in the C-terminus. While naïve B cells normally express IgM and IgD isotypes, exposure to antibody leads to isotype switching allowing for the expression of IgG, IgA, and IgE isotypes. Once the B cell matures into a plasma B cell, it begins producing antibodies with the same antigen-binding region as the B cell receptor (BCR) that first recognized the antigen (Fig. 1.2). These secreted antibodies serve to bind to the pathogen and prevent it from infecting a cell, and also to target the pathogen for destruction by neutrophils and macrophages. While these antibodies only have half-lives of a few days, some plasma B cells can actively secrete antibodies at low levels for years.

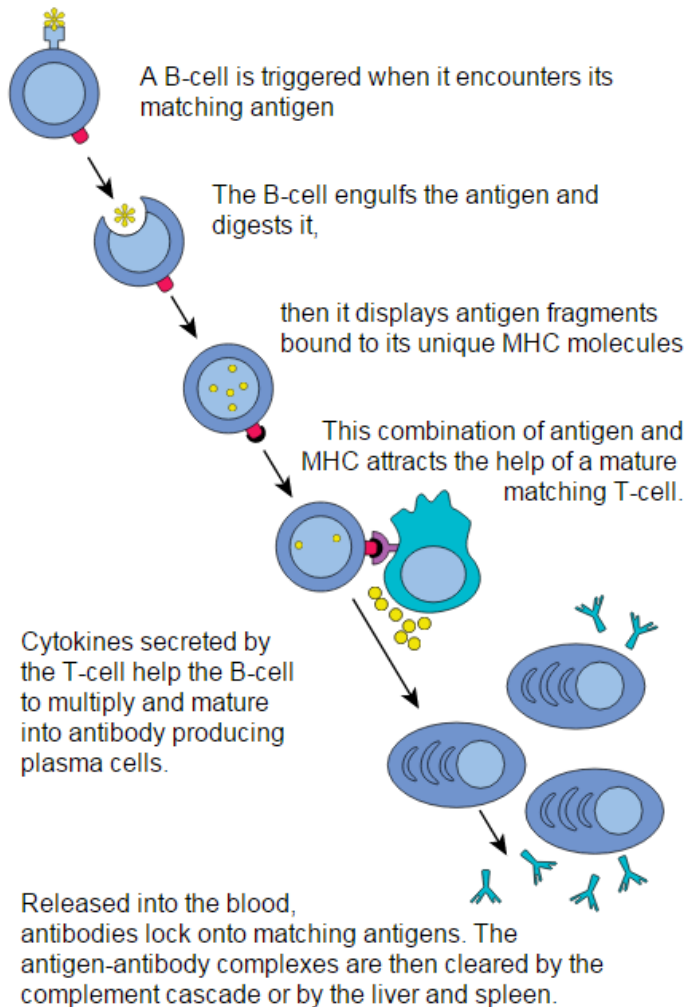


**Figure 1.2: B cell activation and antibody production.** B cell is triggered when antigen is encountered. Once antigen is processed it is presented on the cell surface for binding with a T cell. Finally the plasma B cells release antibodies into the blood. Image is from [8].

Membrane bound Ig, which is non-covalently associated with an  $I\alpha/I\beta$  heterodimer, is known as the B-cell receptor (Michael 1995) (Fig. 1.3). Signaling through the BCR leads to cell proliferation and survival, as well as exacting gene expression changes allowing for the production of antibodies, which is known as “activation”.

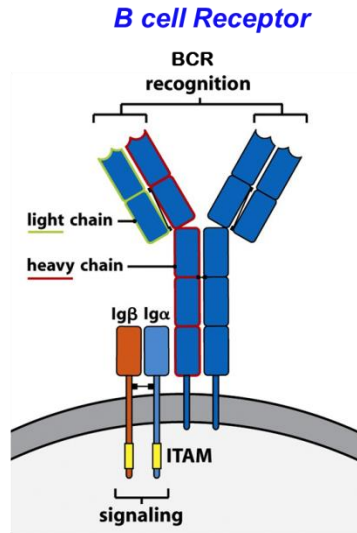


**Figure 1.3: Structure of the B cell receptor (BCR).** Two identical light chains are connected to a heavy chain, which non-covalently associates with an Ig $\alpha$  and Ig $\beta$  possessing transmembrane activation regions. Image is from [9].

Cell-cell interactions require that antigen be captured and displayed on the surface of antigen presenting cells (APCs), the most specialized of which are dendritic cells. APCs and lymphocytes group together in lymphoid organs in order to interact and initiate the immune response, but lymphocytes are also able to circulate in the blood. Lipids and polysaccharides that bind to the BCR induce the production of a class of antibody called immunoglobulin M (IgM). Protein antigens induce the production of a number of different antibody classes, such as IgG, IgA, IgE. Furthermore, a small number of B cells will differentiate into memory B cells, which remain in the body for years to provide a rapid antibody response if the same pathogen is reintroduced to the body, which is a key feature of long term immunity [5].

## 1.3 B Cell Activation

### 1.3.1 BCR signaling pathway

B cells detect antigen through the BCR. Two identical heavy and light chains comprise the mIg, each of which is capable of binding two identical antigenic epitopes simultaneously [10]. Ig $\alpha$  and Ig $\beta$  are transmembrane proteins linked by disulfide bonds in the extracellular domains. Each of their cytoplasmic domains contains one immunoreceptor tyrosine-based activation motif (ITAM). ITAM regions are signaling conduction motifs that are conserved throughout different types of immune system cells, most notably the T cell receptor [11].

Although activation and development of B cells is a complex and lengthy process, many key events of B cell activation take place in the first few minutes of B cell – antigen contact. The initial event is the binding of foreign antigen by the BCR. Evidence suggests that antigen binding may induce a conformational change in the cytoplasmic domain of the Ig $\alpha$ /Ig $\beta$  heterodimer from a closed to an open conformational state, which can then allow for the phosphorylation of ITAMs [12]. The BCR then preferentially associate with cholesterol enriched lipid rafts where the BCR are able to contact Src kinases, such as Lyn, which cause the phosphorylation of those ITAMs at their tyrosine residues and leads to the downstream recruitment of kinases and adaptor proteins [13-15]. The key mediator of this response is the spleen tyrosine kinase (Syk), which binds to fully phosphorylated ITAMs and allows it to act as a tyrosine kinase. Disruption of Syk function precludes downstream signaling

propagation [16]. In its active form Syk then phosphorylates and recruits the adaptor proteins Grb2 and BLNK, as well as PI3K, and Bruton's tyrosine kinase (Btk). Activation is also aided by the recruitment of costimulatory coreceptor Cd19 [17, 18]. Together these proteins form the signalosome, a structure involving the spatiotemporal rearrangement of BCR and signaling molecules into clusters, which propagates a signaling cascade within the cytoplasm. Furthermore, Btk and Syk work in concert to activate PLC $\gamma$ 2, which by cleaving PIP2 creates inositol triphosphate (IP3) and diacylglycerol (DAG) [19-21]. IP3 can then move to the endoplasmic reticulum and, by binding to a receptor, triggers the release of intracellular calcium stores (Fig.1.4).

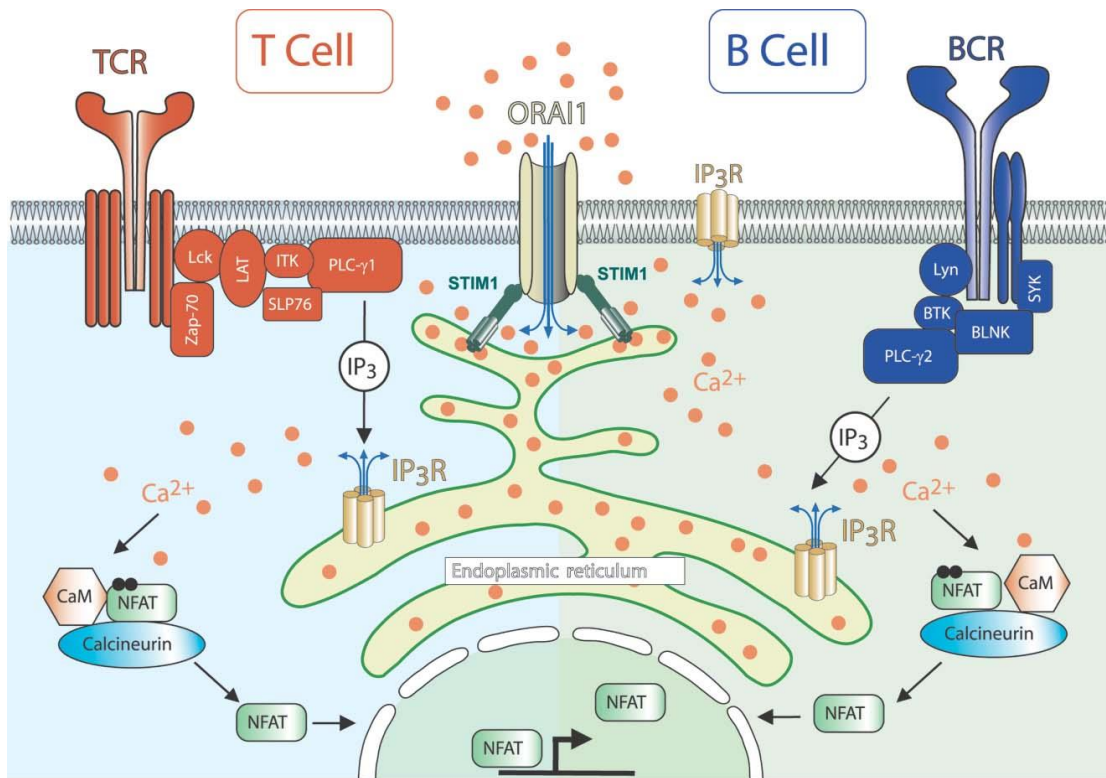


**Figure 1.4: Signaling cascade of BCR and TCR clusters.** Following actin binding of the BCR, Syk is recruited to the membrane, then activates BLNK and BTK, which

then activates PLC $\gamma$ 2 and creates IP3, which then allows for the release of calcium from the endoplasmic reticulum. An increase in calcium allows for the translocation of NFAT into the nucleus, which then changes gene expression. Image is from [22].

These proteins act in concert to eventually propagate gene expression changes resulting in the production of infection fighting antibodies. Cytoplasmic signaling is, however, not the complete process involved in early B cell activation events. It has been shown that the predominant form of antigen contact *in vivo* is membrane bound antigen on the surface of specialized antigen presenting cells, such as the dendritic cell [23]. This contact then brings the membrane of both cells into close contact, allowing them to form a junction. The B cell undergoes drastic physical changes in order to maximize the amount of contact between B cell receptors and surface-bound antigen. The initiation of BCR binding, leading to the activation response, requires the cross-linking of BCR through multivalent antigens into oligomers, which reorganizes the BCR into microclusters on the membrane surface [24, 25]. These events are concurrent with a transient increase in BCR mobility lasting tens of seconds [26, 27]. These microclusters steadily grow in size as more BCR oligomerize and microclusters merge. Simultaneously, receptor clusters translocate along the cell-cell junction in a roughly centripetal trajectory toward the center of the contact zone (Fig. 1.5).

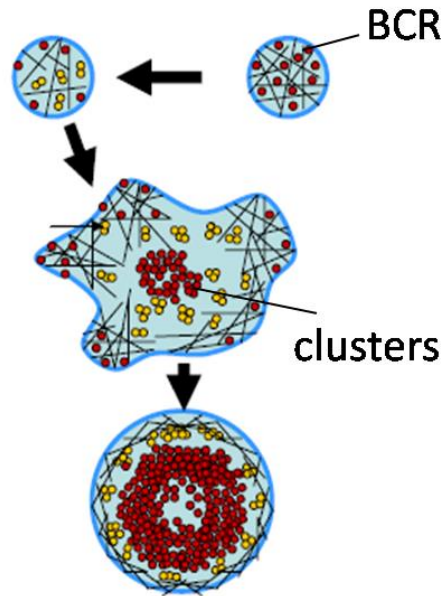


**Figure 1.5: Formation of BCR clusters and the immune synapse.** BCR clusters, upon binding antigen encounter each other and oligomerize. These clusters then move centripetally toward the center of the contact zone while simultaneously growing. Image is from [28].

Antigen mediated BCR clustering has been shown to be necessary for the initiation of B cell signaling [23, 29]. However, some studies show that small BCR oligomers exist on the surface of the B cell prior to antigen contact. The existence of preclusters was demonstrated using the single molecule imaging technique, direct stochastic optical reconstruction microscopy (dSTORM) [30], as well as observing the direct molecular interactions using Forster resonance energy transfer (FRET) [31]. These pre-clusters are too small to be visible using standard fluorescence microscopy, but their existence and translocation within the plane of the membrane has a probable role in the tonic signaling of the B cell [30], in which it is postulated that their

conformational arrangement serves an inhibitory function for signaling. Cells lacking the ability to form these pre-clusters were found to be hyperactive [32].

### 1.3.2 Models of BCR triggering and oligomerization

Although the signaling pathway of the BCR has been well characterized, the mechanism driving the transition from inactive BCR to a signaling state is still a matter of debate. Several different models have been proposed to explain this transition, each with some supportive evidence. The cross-linking model is both the oldest and most supported hypothesis of BCR activation. Under this scheme the BCR is assumed to exist as a monomer in its inactive state. Upon binding with a multivalent antigen, the BCR would then be able to crosslink with another BCR and thereby form a stable group (Fig. 1.6). Cross-linking is the basis for the formation of microclusters, which are recognized as the fundamental signaling platform in B cells. Notably, B cells were only found to become activated when stimulated with F(ab)<sub>2</sub> bivalent antibody fragments, but not with monovalent F(ab) fragments [33]. Furthermore, crystal structure analysis of the BCR revealed a hinge between the Fab and Fc portions of the receptor, which may preclude the transmission of a conformational change from the antigen binding site to the cytoplasmic portion of the BCR. The cross-linking model does not require the presence of a conformational change (2010 Jianying Yang, Michael Reth).

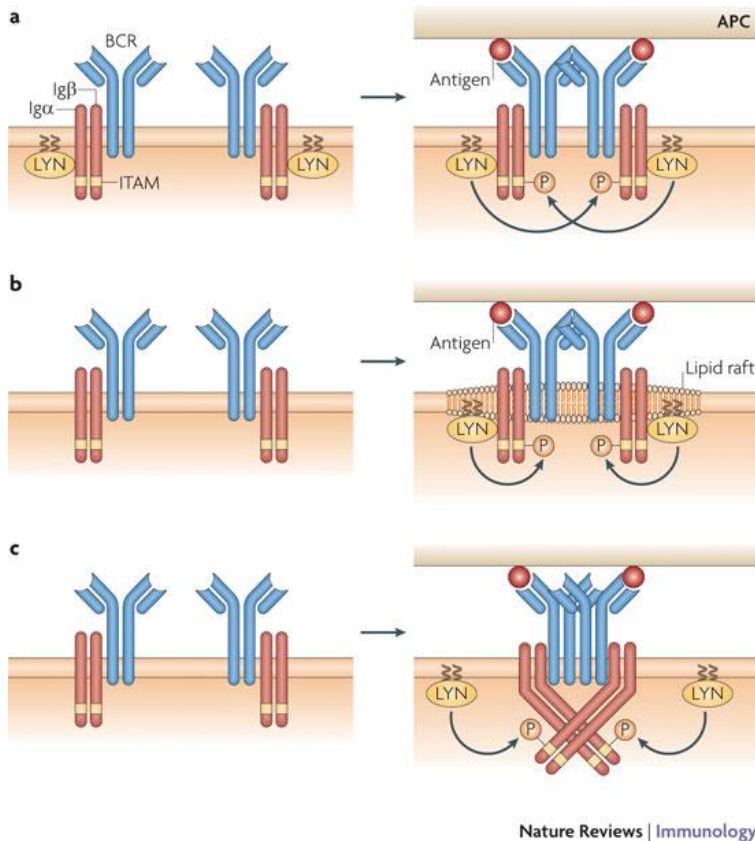


**Figure 1.6: Models of cross-linking activation.** (a) Proposed model in which cross-linking allows BCR associated Lyn to trans-phosphorylate each other. (b) Model in which cross-linking perturbs the local lipid environment, allowing for a formation of lipid rafts and associated Lyn accumulation. (c) Model where oligomerization causes conformational changes in the Ig $\alpha$ /Ig $\beta$  regions allowing for phosphorylation of ITAMs. Images from [34].

However, this model fails to explain some experimental results. The cross-linking model assumes that BCR naturally exist in solely a monomeric state, which has been shown to be not entirely accurate, as small BCR clusters are observed in unstimulated

cells. For a good review of these results see [35]. Furthermore, other receptors that are known to be activated by cross-linking have a highly regulated cross-linked distance. BCRs do not share this feature as they can be activated by antigens of a wide range of sizes.

A model that may resolve these contradictions is known as the dissociation activation model [32]. This model posits that unstimulated BCRs exist predominantly in auto-inhibitory oligomers along with a small percentage of non-signaling monomers. Upon the binding of antigen, BCRs undergo a conformational change which allows them to crosslink (Fig. 1.7).

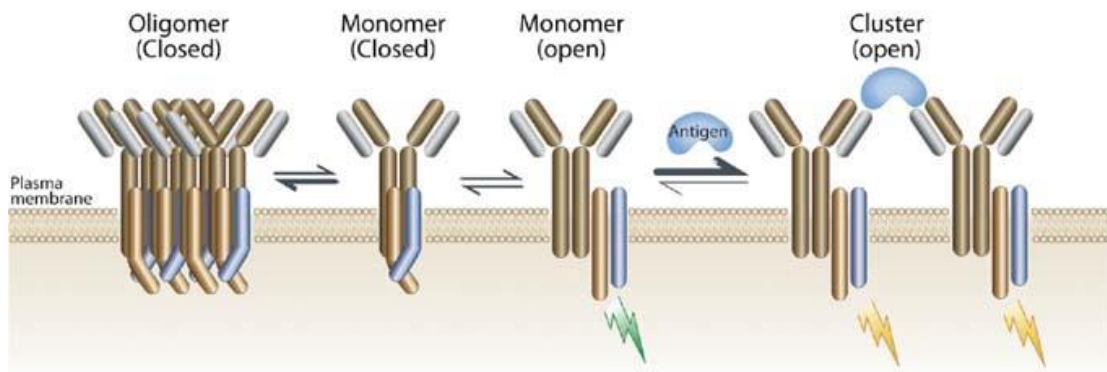


**Figure 1.7: The dissociation activation model** posits two oligomeric states, one in which the ITAM regions are inhibited by a conformational change and one in which the cross-linking through antigen allows for the accessibility of the ITAM regions, thus allowing signaling. Image is from [32].

### 1.3.3 Nanoscale barriers to BCR cluster formation

Given the importance of nanoscale BCR cross-linking and organization in the propagation of signaling and B cell activation, it is therefore essential that the

physical factors that control this organization are well understood. The model of the cellular membrane posited by Singer and Nicolson as a featureless, fluid 2D lipid environment [36] has since been amended to include a host of features that can influence the local membrane fluidity. One such limit is the presence of phase separated regions possessing high concentrations of cholesterol and glycosphingolipids, known as lipid rafts. These regions, while estimated to be small (100 - 200 nm in diameter) [37] have been shown to cover a sizeable percentage of the membrane surface area – measured between 13% [38] and 50% [38, 39]. Due to their high cholesterol content, lipid rafts provide less fluidity of the membrane and can thereby inhibit receptor diffusion. Furthermore, a subset of tyrosine kinases such as Lyn and Syk and transmembrane receptors including BCR have been found to colocalize with lipid rafts under certain conditions [40-42]. Thus, lipid rafts may be viewed as a “signaling platform” wherein both receptors and tyrosine kinases are held in close contact to promote efficient signaling by limiting local diffusion.

Further modulation of the membrane diffusion landscape is performed by the actin network. Actin and spectrin form a dense network underlying the plasma membrane. This network connects to the membrane through lipid-binding proteins, transmembrane proteins, or membrane-attached proteins. These connections lead to the formation of “corrals” on the cytoplasmic side of the membrane that further impede free diffusion of transmembrane proteins [43]. These corrals, as measured by single molecule tracking experiments, have been found to be on the order of 230 nm [44].

Both lipid rafts and actin corrals provide real, mobility-altering obstacles to transmembrane proteins. As these obstacles change the time-frame and scale on which BCRs may encounter each other and oligomerize to produce a signaling BCR cluster, it is important that we understand the role of ligand mobility in influencing BCR cluster motion and the effects on B cell signaling.

### 1.3.4 Store operated calcium entry

It has long been known that changes in intracellular calcium concentration regulate a wide variety of cell behaviors, from cell division, to migration, to apoptosis. A rise in intracellular calcium can occur through two routes, either the release of calcium stored within the endoplasmic reticulum or the influx of calcium through plasma membrane calcium channels. Often, these two mechanisms work in concert to regulate intracellular calcium concentrations.

An increase in intracellular calcium is one of the major signaling transmitters of lymphocyte activation. Calcium influx occurs after the engagement of the cell membrane receptor, which then triggers the production of secondary messenger inositol 1,4,5 triphosphate (IP<sub>3</sub>). IP<sub>3</sub> then binds to the IP<sub>3</sub> receptors on the ER, causing the release of calcium stores. A drop in concentration of Ca<sup>2+</sup> within the ER causes a conformational change in the STIM1 protein, which can then bind to the ORAI1 plasma membrane calcium channel [45]. Binding causes the opening of the ORAI

calcium channels, thus resulting in a secondary calcium influx. The second part of this process is known as store-operated calcium entry (SOCE) (Fig. 1.8).

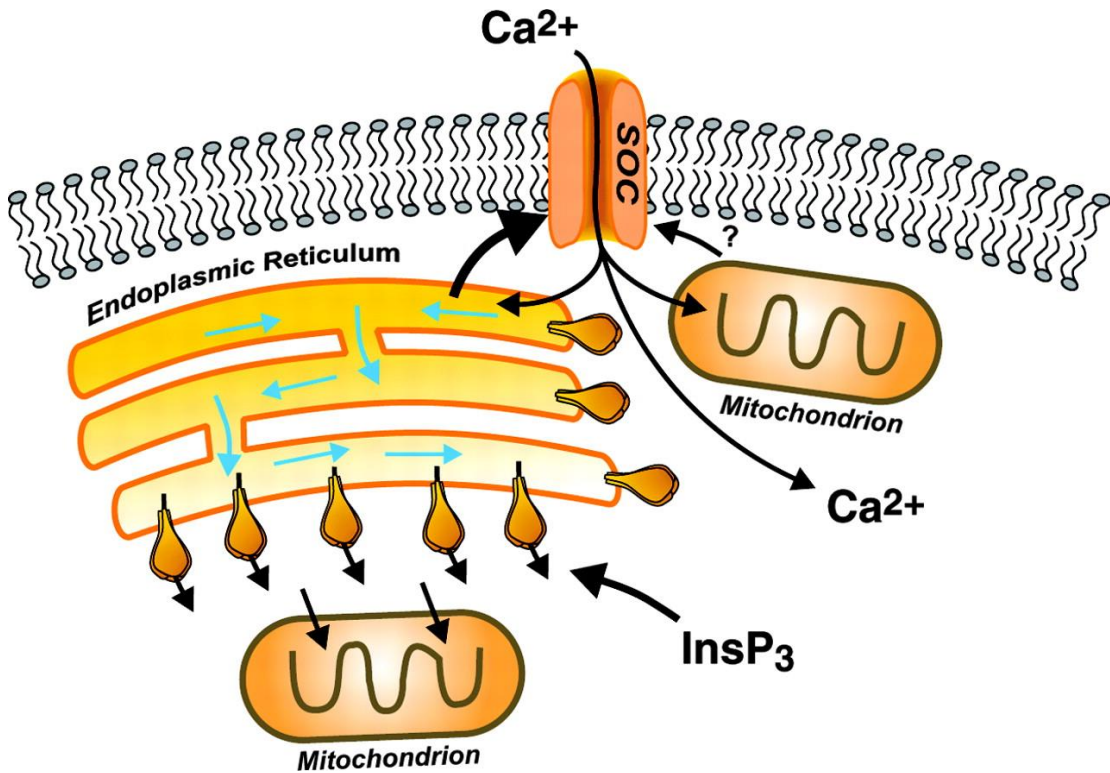


**Figure 1.8: Store operated calcium entry.** InsP<sub>3</sub> allows the calcium stored within the ER to be released. Subsequently, calcium channels in the plasma membranes are opened to allow for a secondary influx of calcium. Image is from [46].

Calcium influx, regardless of the pathway, is an important signaling mechanism in cells. The magnitude and duration of calcium influx in cells relates directly to the modification of cellular processes. In lymphocytes, for example, a higher magnitude of calcium influx has been correlated with higher levels of activation and eventual antibody production. A single influx of calcium in lymphocytes often lasts only minutes until the immune synapse is fully formed.

Furthermore, calcium enrichment is known to have direct effects on the organization of the actin cytoskeleton [47]. Heightened calcium levels allow more  $\text{Ca}^{2+}$  to bind to calmodulin, which in turn activates myosin light chain kinase (MLCK). The myosin light chain is then phosphorylated by MLCK, enabling myosin to move. On a larger scale the increase in myosin activity results in a local contraction of the actin network.

On smaller time and length scales, calcium flickers have also been found to direct the dynamics of actin polymerization [48]. Calcium flickers have been found to steer the migration of some cell types. Interestingly, calcium concentrations were found to be much higher in the front lamellipodial extension of migrating cells in a 4:1 ratio front to back [48].

## 1.4 The Actin Cytoskeleton

### 1.4.1 Actin and actin binding proteins

The cytoskeleton exists to provide cells with structure and allow them to transmit forces, resulting in either external physical changes (such as morphology changes or cell movement) or internal reorganization (such as relocation of the nucleus). Three components of the cytoskeleton: actin, microtubules, and intermediate filaments, share these abilities. Each has specific contributions for the function to which it is

most suited. The role of each cytoskeletal component is in part dictated by the biophysical properties of the filaments and their protein components.

Actin, with a diameter of 7 nm and a persistence length of 17.7  $\mu\text{m}$  [49], is preferentially associated with the plasma membrane, but due to high turnover rates and an abundance of property-altering, actin associated proteins provides for a dynamic and heterogeneous network. Due to the intrinsic polarity of actin filaments, actin monomers preferentially associate with the barbed end of the filament and dissociate from the pointed end, in a process known as actin treadmilling (Fig. 1.9). Filament polarity is further supported by the hydrolysis of ATP, as hydrolyzed ATP has a higher concentration toward the pointed end of the filament. Treadmilling allows actin filaments to grow and shrink dynamically as well as to exert force on the plasma membrane by polymerizing against it. These qualities lend themselves to making actin the main driving force behind cellular motility and cell shape changes.

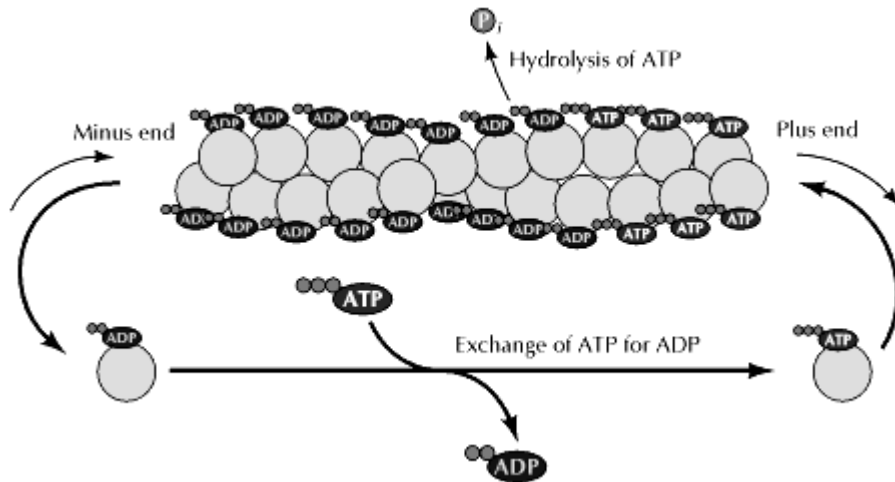


**Figure 1.9: Actin filament treadmilling.** Actin monomers form a double helical strand. ATP-bound monomers preferentially associate at the plus end of the filament. Hydrolysis of the ATP to ADP results in monomers which more readily disassociate from the minus end of the filament. Non-uniform actin monomer association allows the continual growing of the filament on one side and shrinking on the other, which is known as treadmilling [50].

In the B lymphocyte, actin is generally isotropically distributed in an actin-rich cortex beneath the plasma membrane, while the B cell circulates in the blood and lymph systems. Upon contact with antigen, the actin cytoskeleton undergoes dramatic remodeling to allow for maximal antigen contact and activation. Although there are countless actin binding and modifying proteins, some specific proteins that are tightly intertwined with the B cell signaling network help provide more detailed insight into the redistribution and functionality of actin during B cell activation.

## 1.4.2 BCR engagement leads to remodeling of the actin cytoskeleton

The mechanism by which B cells engage APCs and cluster and translocate BCRs has been investigated in recent years. This process is both rapid and complex, taking part in four distinct phases. Upon initial contact with activating ligand, the B cell actin cortex undergoes a rapid depolymerization for ~10 seconds, which is concurrent with an increase in BCR mobility [51]. The actin network is therefore thought to act as a corral, reducing the perceived BCR mobility (Fig. 1.10).

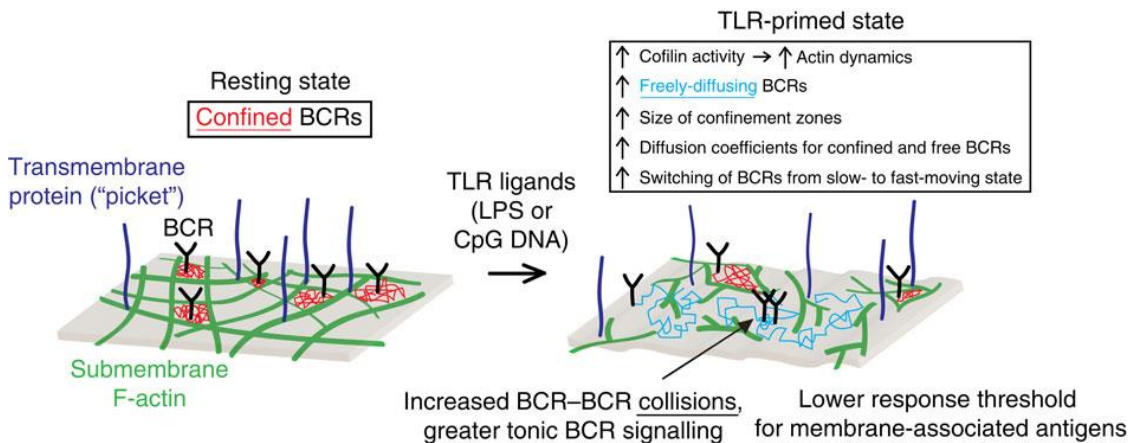


**Figure 1.10: Actin network as a corral.** Cross-linking of actin and spectrin on the cytoplasmic side of the membrane, which are held in place by transmembrane “picket” proteins are known as actin corrals. These corrals limit BCR diffusion and their dissolution allows for BCR oligomerization. Image is from [52].

Subsequently, actin re-polymerization at the cell-cell interface drives a dramatic spreading of the B cell membrane on the surface of the APC. This rapid spreading, which lasts between four and six minutes, maximizes the amount of contact between

the B cell and the antigen presenting cell, and occurs concurrently with BCR cluster formation. Cell spreading allows for maximal BCR binding and promotes B cell activation. The extent of spreading has been shown to be dependent on the ligand affinity [53]. After the completion of spreading, the B cell membrane at the contact site begins to contract: a process driven by actin retrograde flow. As a well-characterized mode of actin dynamics, retrograde flow is associated with lamellipodial protrusions. Rapid polymerization of actin against the leading membrane leads to centripetally oriented actin treadmilling. When combined with myosin-mediated actin network contraction at the rear of the lamellipodium, this results in a steady state flow of actin from the periphery to the center of the cell. In B cells, actin retrograde flow drives contraction of the cell spread area, while BCR clusters are simultaneously transported centripetally towards the center of the contact zone. Eventually, a central target-like pattern is formed, called the immune synapse. The formation of the immune synapse is concurrent with a downregulation of BCR signaling. A summary diagram in Figure 1.11 illustrates the phases of actin dynamics during B cell spreading and contraction.

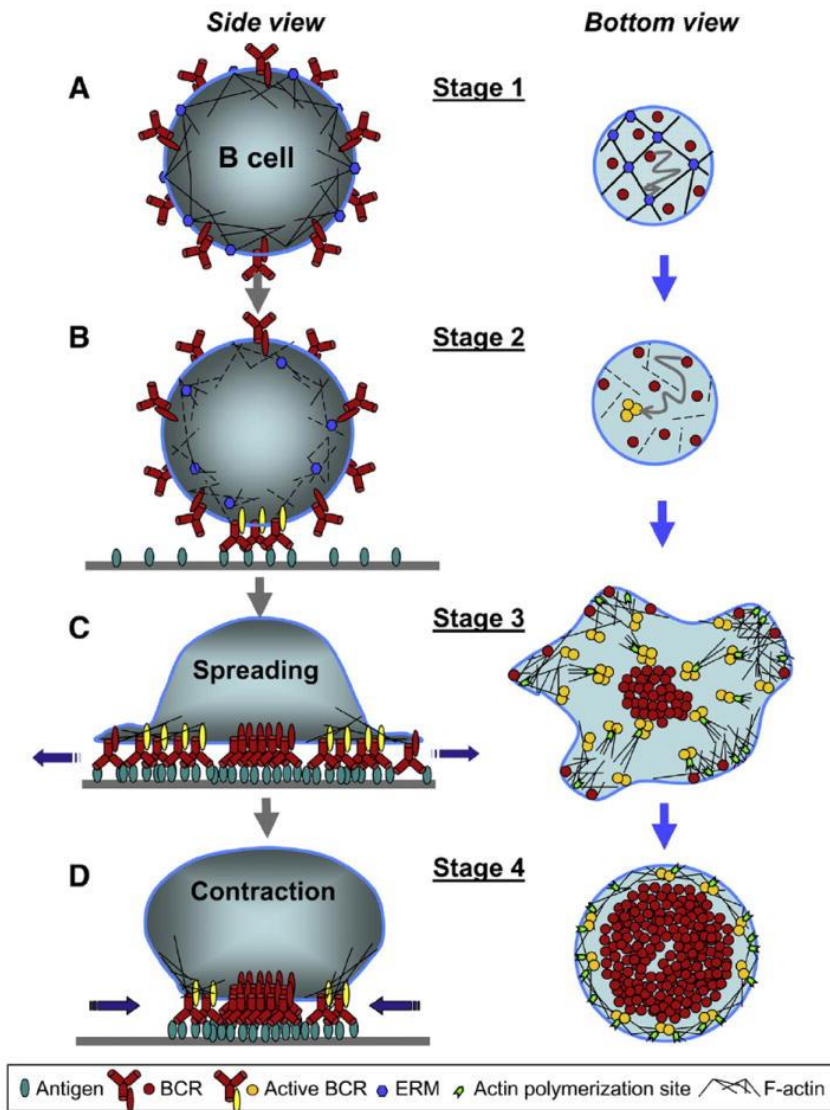


**Figure 1.11: Stages of B cell spreading, BCR clustering and actin reorganization.**

(a) The B cell is initially roughly spherical, with BCR corralled by a cross-linked actin network. (b) Upon antigen contact, a rapid depolymerization of the actin network allows for transiently increased BCR mobility. Small BCR clusters begin to form. (c) The B cell spreads rapidly on the activating surface, contacting maximal amounts of BCR. Clusters begin to merge and translocate toward the center of the contact zone. (d) The B cell contracts, drawing in all BCR clusters and the formation of the immune synapse is completed. Image is from [54].

Following the formation of the immune synapse, actin-associated clathrin pits begin to form, resulting in the endocytosis of BCR clusters [54]. Antigenic proteins are fragmented in the endosomes and then assembled with MHC class II molecules, which are later presented on the surface of the B cell for recognition by T cells [55].

### 1.4.3 The role of actin associated proteins in B cell activation

One connection between membrane-proximal signaling proteins and the actin cytoskeleton is effected by the membrane bound Bruton's tyrosine kinase (Btk). Btk regulates actin dynamics via phosphorylation of Vav and phosphatidylinositides, which activates the actin nucleation promoting factor Wiskott-Aldrich syndrome protein (WASp) and N-WASp [56]. WASp is only expressed in cells of the hematopoietic system and certain mutations of this protein lead to an illness of the same name. Wiskott-Aldrich syndrome is characterized by dysfunction of the actin cytoskeleton in B and T lymphocytes, resulting in a pronounced mis-regulation of the immune system. In its active state, WASp binds to the ARP2/3 complex and activates it. ARP2/3 is a well-known actin nucleating protein and pivotal for forming filamentous actin networks with a characteristic 70° branching angle and for promoting actin polymerization, which is essential for B cell spreading and activation [56].

A broadly expressed WASp homologue, N-WASp, has been found to perform a similar role in other cell types, but has a specific importance in the actin dynamics of B cells. Both WASp and N-WASp knockouts have been shown to have profound

negative effects on B cell function. WASp has been shown to promote B cell signaling and antibody production and N-WASp plays a role in the attenuation of B cell signaling. Interestingly, the presence of N-WASp has been shown to decrease the amount of filamentous actin accumulation in the B cell contact zone, whereas WASp has the opposite effect [57].

Another actin binding protein of direct importance to B cell activation is the motor protein myosin. The myosin family of proteins is large, with diverse functions in many cells and tissues and is most well known for its role in muscle contraction. While different types of myosin have different molecular architectures, the central function of this protein is achieved by the presence of one or two heavy chains in which the N-terminal domain has a catalytic domain that hydrolyses ATP and binds actin filaments. Coupled through a neck to a light chain which functions as a lever arm, this allows myosin to exert force on actin filaments [58]. In B cells the critical role of myosin in migration and antigen has been studied to some extent [59, 60] and in T cells it has been demonstrated that non-muscle myosin II is involved in cell signaling and the formation of an immune synapse [61].

## 1.5 The Importance of Ligand Mobility

### 1.5.1 Factors in plasma membrane mobility

The ability of proteins to diffuse within the planar geometry of the plasma membrane is known as mobility. There are many factors that can limit or alter the mobility of proteins embedded in the cell membrane, some of which were discussed in section

1.3.3. Furthermore, the lipid composition of the membrane, which is highly cell dependent, alters the mobility as well. The mobility of the ligand (as bound to the membrane of an APC) controls the rate at which ligand-bound BCRs may encounter each other and form signaling competent clusters.

## 1.5.2 Ligand mobility in hematopoietic cells

The extent to which ligand mobility regulates immune synapse formation in mast cells was examined by Amanda Carroll-Portillo et al. Mast cells were allowed to contact and spread on either mobile (supported lipid bilayer) or immobile (glass) ligand-presenting substrates, and the formation of the synapse was observed with TIRF and TEM. When contacting immobile ligand, the mast cell failed to form the central supramolecular activation cluster (cSMAC), which is the most cell-central portion of the immune synapse, and instead exhibited numerous smaller receptor clusters. The characteristic actin ring surrounding the cSMAC also failed to form on the immobile ligand substrates. While degranulation (a measure of mast cell activation) occurred on both substrates, it occurred to a much greater extent on mobile ligand-presenting substrates [62].

A more systematic investigation of ligand mobility was carried out by Hsu et. al in which the apparent ligand mobility was varied based on the composition of the supported lipid bilayer [63]. Multicomponent lipid mixtures with different ratios of SOPC/DMPC) were used to form supported lipid bilayers. The mixtures resulted in different apparent diffusion coefficients of lipids, measured between  $0.09 \mu\text{m}^2/\text{sec}$

and  $0.86 \mu\text{m}^2/\text{sec}$ . Antibodies against the T cell CD3 $\zeta$  was used to stimulate T cells and the spatial TCR distribution at the interface was observed with TIRF imaging. The kinetics of cSMAC assembly was markedly slowed on bilayers with limited diffusion coefficients, and the relative amount of receptors clustered at the cell-bilayer interface was reduced (Figure 1.12). These changes in TCR distribution were also found to affect TCR signaling, with higher levels of pY staining and calcium influx occurring on substrates presenting ligand with higher mobility [63].

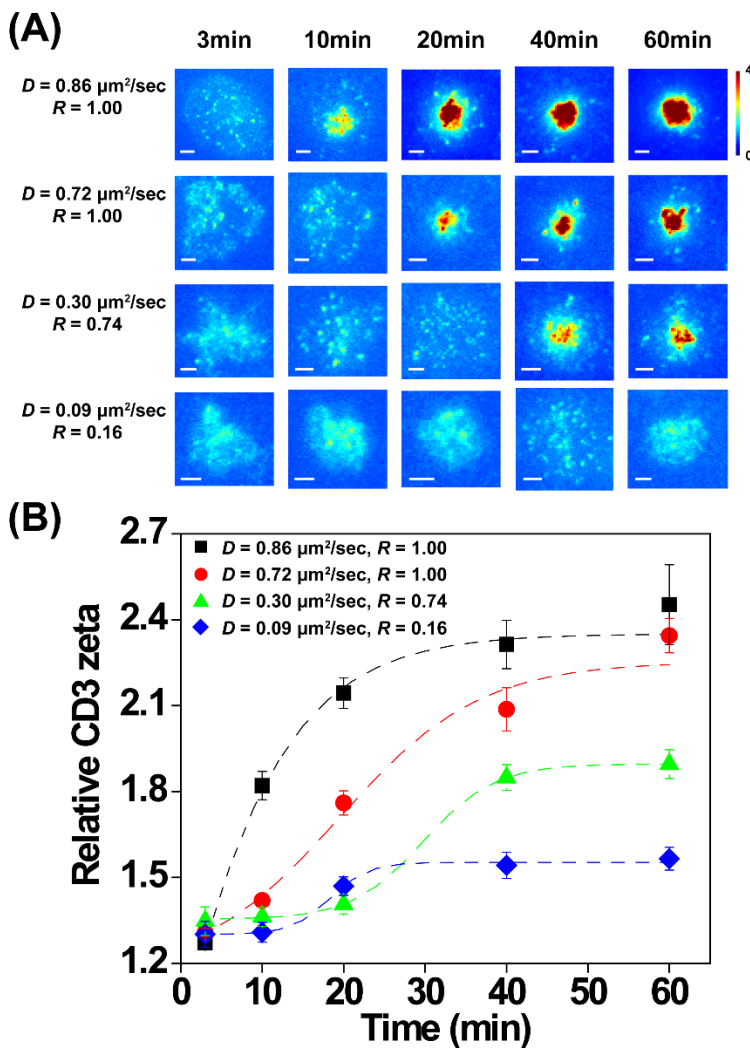


**Figure 1.12: The influence of ligand mobility on cSMAC formation.** (a) TIRF imaging of CD3 $\zeta$  receptor accumulation relative to ligand mobility. (b) Relative

amount of CD3 $\zeta$  accumulated over time for four different diffusion coefficients. Images are from [63].

A different probe into the effects of ligand mobility in T cells was employed by Groves and colleagues. Mossman et al. [64] constrained the mobility of surface bound ligands by introducing a 5 nm high chromium grid to interrupt the supported lipid bilayer. Addition of glycosylphosphatidylinositol (GPI) linked MHC-peptides into the supported bilayers rendered the membrane competent to stimulate T cells. Although the TCRs formed microclusters similar to stimulation on unpatterned lipid bilayers, the microclusters were prevented from migrating from the cell periphery to the interior. This large-scale restriction in ligand mobility interrupted the formation of a classic immune synapse and resulted in a dramatic reduction in T cell activation. DeMond et al. [65] further demonstrated that these microclusters were actively transported by the centripetal actin flows that are set up in the lamellipodia. Finally, Smoligovets et al. [66] introduced lattice grids using the chromium line fabrication to partition the lipid bilayers into discrete compartments and used these patterned lipid bilayers to stimulate T cells. The typical pattern of TCR clusters showed a tendency to cluster toward the inner corners of each chromium box (Fig. 1.13). Importantly, they were able to demonstrate that TCR clusters actively patterned the local actin dynamics, suggesting an intimate relationship between immune cell receptor signaling, spatial reorganization and the dynamic actin cytoskeleton.

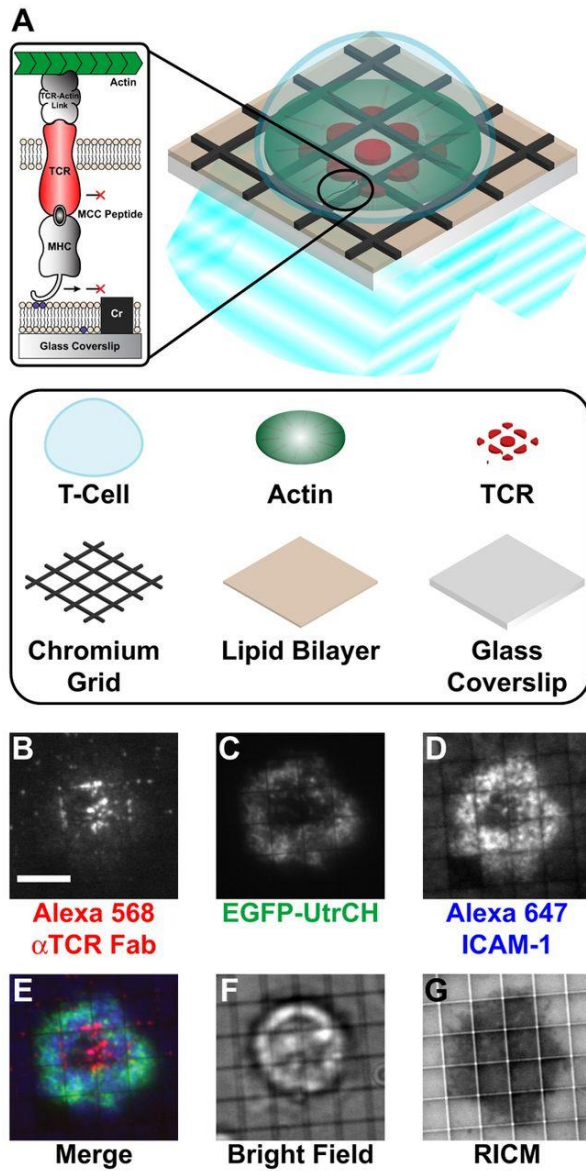


**Figure 1.13: Physical effects of a ligand mobility limiting substrate.** The combination of the chromium grid and bilayer provides limited areas of mobility, resulting in the TCR collecting in the inner corners of a frustrated bull's eye pattern. Image is from [66].

In B cells a wide range of BCR mobilities have been observed. Before activation BCRs are found to have a relatively restricted mobility of  $\sim 0.03 \mu\text{m}^2/\text{s}$  in naïve B cells [30, 67]. During transient actin depolymerization this value increases to  $\sim 0.05 \mu\text{m}^2/\text{s}$  which assists in the formation of BCR clusters [26, 27, 67]. Once inside a cluster the BCR mobility decreases to near zero [68, 69]. These results support a diffusion-trapping model of BCR signaling, wherein the initial events in BCR activation lead to diffusion of engaged BCRs, formation and growth of microclusters and macroscopic movement of microclusters into a central cluster. Within the framework of this model, the actin cytoskeleton appears to serve to limit diffusion and microcluster growth at early stages, with an additional role ascribed to retrograde actin flows in transporting the microclusters. However, Liu et al. [57, 70, 71] suggest a more active role for the actin cytoskeleton and the possible existence of a feedback loop between BCR signaling and actin cytoskeleton [28] that actively patterns the spatial distribution of microclusters and early B cell signaling. Taken together, these observations point to an important role for the mobility of BCRs in the cell membrane and will be the subject of investigation in Chapter 2. In B cells the role of ligand mobility remains an open question. Ligand mobility has the potential to influence many different aspects of B cell function by aiding or precluding BCR cluster formation and influencing actin dynamics. The modulation of these B cell aspects may then affect B cell signaling and eventually antibody production. Therefore, it is important to understand the role ligand mobility plays in the binding of B cells with antigen presenting cells and how this affects B cell function.

## 1.6 Topography and Cell Biology

### 1.6.1 Topography influences a variety of cell types

The environment a cell experiences can vary markedly based on the location of the cell within the body. Brain tissue provides a vastly different physical environment than bone tissue, including factors such as stiffness, geometry, and heterogeneity of cells. One important aspect of the cellular environment that may affect motile cells is the topography of the extracellular matrix. Collagen bundles and connective tissues present linear parallel but non-planar structures within the matrix that cells have to navigate [72]. For cells that come into close contact with a variety of other cells, such as immune cells, the geometry of other cells becomes important. These features may include the general cell shape, lamellipodial and filopodial protrusions, and other membrane convolutions.

There is an abundance of locations and conditions under which the B cell may encounter antigen *in vivo*. Although B cells can respond to pathogenic stimuli anywhere throughout the body, the majority of antigen contact takes place in specialized locations such as the lymph node and spleen, which are collectively known as secondary lymphoid organs (SLOs). The advantage of antigen contact within SLOs is that they provide a highly structured architecture, optimized for antigen presentation to lymphocytes [73]. Lymph nodes are located at strategic branching points of the lymphatic system that allow for maximum collection and sampling of antigenic content. The spleen, while possessing a similar architecture,

specializes in the monitoring of blood-borne antigens. Whether inside of an SLO or in circulation, B cells generally migrate constantly, surveying tissues for signs of infection. It has been shown that within SLOs B cells most often encounter antigen on the surface of antigen presenting cells (APCs) such as follicular dendritic cells and marginal zone macrophages [74]. Cellular membranes general present a variety of topographical features, but APCs have especially convoluted membrane features. Dendritic cells are named for their long, thin dendrite protrusions, and macrophages present significant membrane ruffles and invaginations [7]. Therefore, it is evident that B cells encounter a variety of different surface topographies in their binding of antigens. Whether and how these topographic features affect antigen gathering, BCR activation and B cell spreading remain unknown.

### 1.6.2 Techniques for studying the role of topography

Scientists have been actively studying the effect of surface topography on cell behavior for the last two decades. Surface topography has been found to alter proliferation, polarization, and migration in certain cell types [75-78]. As technological advances make the fabrication of micro- and nano-patterned surfaces easier, the diversity and complexity of topographically patterned substrates continues to increase. Many different topographies have been explored to examine their effects on various cell types. Some of the substrates that are being used by researchers include arrays of nanoposts [79], or arrays of nanopits [80]. One specific example of topography a cell might encounter is the extra cellular matrix (ECM), which has a range of topographic features, scaling from nanometers to micrometers. Some of these features have been mimicked by micro-fabricated or nano-fabricated substrates

of either ridges or grooves. As the most commonly studied topographical substrate, arrays of parallel nanoridges generally vary the width between two neighboring ridges [81-84]. These long, linear features can mimic how a cell might encounter bundles of collagen micro-fibrils in the ECM that run beside each other in parallel, with different types of cells attached to them [85]. It has been shown that these ridged and grooved arrays usually induce cells to elongate and align along them. Peripheral nervous system neurons, which generally take on a very narrow, elongated form, have been shown to extend along nanogrooved features designed to mimic the effects of neurite bundles [86]. Specially fabricated nanotopographies have even been shown to aid in the regrowth of severed peripheral neurons, providing a possible solution to nerve-damage [87, 88].

The degree of alignment of cells on ridged and grooved surfaces has been shown to depend on spatial parameters of the nanoridges [82]. Furthermore, intracellular structures, like actin stress fibers or focal adhesions prefer to align along the direction of these topographical features [84]. For example, lamellipodia, lamella, and filopodia usually elongate along the direction of the ridges (Fig. 1.14). Interestingly, the degree of alignment of these actin-based features has been shown to depend on the widths of underlying structures [89, 90].

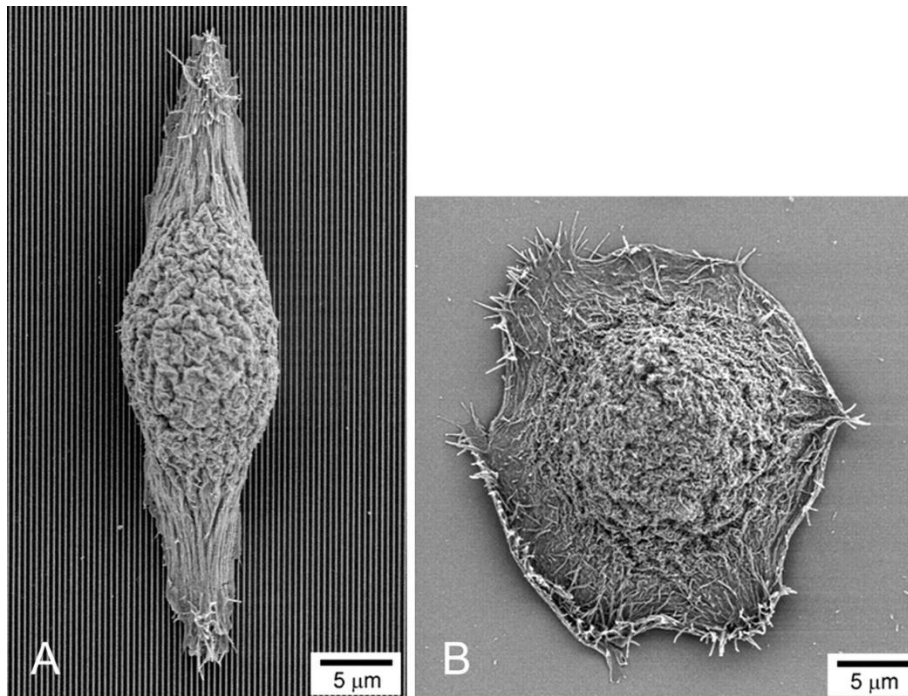


**Figure 1.14: Epithelial cell alignment along topographically patterned substrate.**

(A) A fibroblast cell plated on nanopatterned ridges exhibits an elongated, highly polarized structure. (b) Fibroblast plated on a smooth surface exhibits radial symmetry. Images are from [89].

The effect of topography on migratory cells is profound. The direction and speed of osteoblasts and fibroblasts can be controlled by the topography of the substrate [84]. Metastatic tumor cells have been shown to migrate preferentially along one dimensional channels [2]. Both stem cell migration and stem cell fate are influenced by local topography [91, 92]. The actin cytoskeleton is the cellular powerhouse enabling cell shape change and migration. Furthermore, the actin cytoskeleton has been shown to respond actively to topographical substrates. In a study by Sun et al. Dictyostelium discoideum cells and neutrophils were found to be guided on parallel ridges and asymmetrically patterned substrates through modulation of actin wave

dynamics [78, 93]. Cell guidance by these topographies indicates that the actin cytoskeleton itself and its regulatory proteins may be important for the sensing of topographical changes. These studies have shown that even small changes in surface topography can lead to drastic changes in cell morphology and function thus reinforcing the important role of topography on cell behavior. However, the details of the molecular mechanisms underlying topography sensing are not well understood. What makes a cell elongate in the presence of the ridges? How do local changes in surface topography affect global cytoskeletal properties of the cell?

### 1.6.3 Topography and immune cells

Lymphocytes, as well as other hematopoietic cells, such as mast cells and macrophages, are of particular interest in the study of mechanotransduction. These cells are highly motile as they circulate in the blood stream and migrate through tissues to infection sites. Furthermore, these cells form cell-cell junctions with antigen presenting cells during the immune response. These processes all involve physical interactions between the cell and other tissue and cell surfaces, therefore the physical features of the surface may have a significant effect on immune cell function.

Studies have shown that T cell morphology, as well as migration direction and velocity are strongly influenced by the nature of the topography the cell encounters. In a study conducted by Doh et al. fabricated ridges of 350 nm width, 700 nm gaps, and 500 nm height were used to probe these actin-mediated migration properties [94]. T cells in contact with nanostructured topographies were found to form narrower

lamellipodial protrusions, which were most often directed along the ridges (Fig. 1.15). Furthermore, the direction of migration was biased along the direction of the ridges. These differences were found to be actin-mediated, as the presence of the actin dynamics inhibitor Latrunculin-A above 25 nM abolished protrusions and halted cell motility. An interesting feature of these migrating T cells was that the cells rarely extended protrusions down into the ridge gaps and almost exclusively formed contacts with the ridge surfaces.

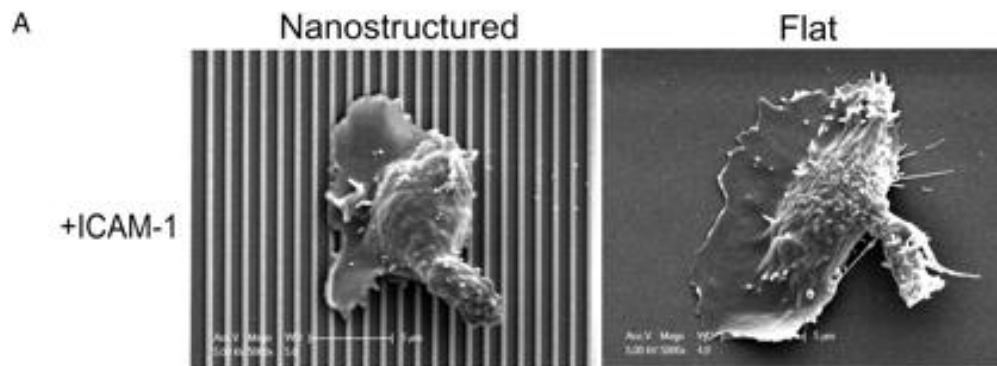


**Figure 1.15: Migratory T cells on topographically patterned substrates.** T cells on ICAM coated topographically patterned substrates form narrower lamellipodial protrusions oriented along the patterns. Images are from [94].

The role of topography has also been explored to some extent for macrophages by Saino et al. Macrophages were plated on substrates with either a non-orientated film, or electrospun poly(l-lactic) fiber scaffolds of either micro or nano diameter. Proinflammatory cytokines secretion and macrophage activation were found to be modulated by the surface topography where nano fibers resulted in the lowest inflammatory response, and the non-oriented film in the highest [95].

B cells, similarly as T cells and macrophages, interact with a wide variety of topographical environments. B cells migrate through tissues and form junctions with antigen presenting cells. However, the role of topography in B cell actin dynamics and signaling has not been explored. Known topographical features, such as membrane ruffles and protrusions, can be mimicked with topographically patterned substrates and would thereby provide a key avenue for the exploration of these effects. Given the coupling between the B cell receptor, the actin cytoskeleton and the downstream signaling of the B cell, the exploration of topographical features would provide fundamental knowledge of the interaction of B cells with their environment. A complete picture of the factors influencing B cell function, including the physical features of ligand mobility and topography can aid in the future manipulation of these effects that may lead to better prevention of disease through vaccination and treatment of disease through immunotherapies.

# Chapter 2: Ligand Mobility Regulates B Cell Receptor Clustering and Signaling Activation

The contents of the chapter have been published in the Biophysical Journal [96].

## 2.1 Introduction

Cellular sensing of the environment is mediated by surface receptors that bind to specific ligands and initiate signaling pathways. In many cases, the ligands are confined on a surface, and receptor-ligand interaction requires the direct contact of cells with the activating surface. Genetic and biochemical approaches have elucidated the molecular mechanisms of receptor signal transduction. However, recent studies have revealed that the spatial organization and physical presentation of surface ligands can regulate signaling [64, 97-101]. Despite its importance for the regulation of signaling, the role of physical factors of ligands that control the distribution of receptors is not well understood. The cells of the immune system require the contact between two cell surfaces for communication [102]. As a critical part of the humoral immune response, B-lymphocytes are activated by the binding of antigens (Ag) to clonally specific B cell receptors (BCR) [23]. B cells commonly encounter two forms of antigens in lymphoid organs, soluble and membrane-associated [103-106]. Although multivalent, soluble antigens induce BCR clustering and B cell activation [107], recent studies have shown that surface-anchored antigens are more efficient in triggering B cell activation [24, 74]. The binding of antigen to the BCR results in

receptor cross-linking as well as conformational changes in the BCR, facilitating the aggregation of BCRs into microclusters (~ 300 to 600 nm diam.) [24, 68, 103]. BCR microclusters recruit a number of signaling intermediaries, which initiate activation of downstream biochemical pathways [23, 108].

Initiation of signaling drives the rapid spreading of B cells on the surface of the antigen-presenting cell. This is induced by the reorganization of the actin cytoskeleton and can further amplify the signaling response [27, 53, 71]. In the lymph nodes and spleen, B cells encounter antigen commonly presented by antigen presenting cells, such as marginal zone macrophages [103] and follicular dendritic cells (DC) [69, 106, 109]. Antigen is commonly presented as large complexes such as viral aggregates, antibody-antigen, and complement-opsonized antigen aggregates, as well as antigen-coated microspheres and complexed with aluminum hydroxide gel injected as vaccines [108]. These vaccines are capable of triggering B cell activation. The most common adjuvant and vehicle of FDA-approved vaccines, antigen absorbed by aluminum hydroxide gel, would present immobile antigen. However, antigen in immune complexes presented by Fc receptors on the surface of antigen presenting cells will have varying degrees of mobility depending on the size of immune complexes and the cytoskeletal architecture of the APC. However, whether antigen mobility affects BCR clustering and signaling is an open question. BCR signaling is dependent on signaling-induced actin reorganization [27, 71]. BCR stimulation induces a rapid depolymerization of actin followed by repolymerization [51]. Perturbing the cortical actin network, which increases the lateral mobility of surface

BCRs, can facilitate BCR aggregation and signaling activation [27, 67]. Although actin is known to be important for maintaining cortical integrity, and the depolymerization of actin has been shown to increase receptor mobility potentially by removing the cortical barriers to movement, whether the actin cytoskeleton plays an active role in BCR microcluster formation and coalescence has not been fully examined. In this study, we investigate the impact of ligand lateral mobility on BCR dynamics and signaling activation. Using high-resolution time-lapse imaging of live cells, we compare the morphology and BCR clustering of B cells when interacting with mobile ligands tethered on planar lipid bilayer and immobile ligand on glass surfaces. We show that ligand mobility significantly modulates B cell spreading dynamics, formation and movement of receptor clusters, actin organization, as well as the level of signaling activation. Our data reveal a potential role for the actin cytoskeleton in regulating the sensitivity of BCR clustering to ligand mobility. Our results indicate that the physical properties of the ligand regulate the level of BCR signaling by modulating B cell morphology, receptors, and actin organization.

## 2.2 Ligand lateral mobility modulates B cell spreading and BCR aggregation

### 2.2.1 Cell spread area is larger on immobile ligand presenting surfaces

To examine the effect of ligand mobility on BCR signaling and activation, we labeled surface BCRs on A20 lymphoma B cells with monovalent, biotinylated, fluorescently

labeled Fab' fragment of antibody (AF546-mB-Fab'-anti-Ig). This labels the BCR without cross-linking and ensures that BCR clustering was entirely attributable to the streptavidin coated on a glass cover slip or planar lipid bilayer. This model system has been shown to induce spreading of B cells [70] and actin reorganization, recapitulating many aspects of early cellular events of BCR signaling [108]. We analyzed the spreading response of B cells using interference reflection microscopy (IRM). Within a few seconds of incubation, cells established contact with the streptavidin-coated substrate and formed small adhesive patches. Following this, the cells spread on the surface, increasing their contact area, reaching a plateau at 6 min (Fig. 2.1 A, B). The cell spread area at 8 min was larger on glass ( $98.1 \pm 11.3 \text{ mm}^2$ , mean  $\pm$  SD) than that on bilayer substrates ( $66.8 \pm 7.4 \text{ mm}^2$ ) (Fig. 2.1 C). To test whether the observed cell spreading results from stimulation drive changes in morphology, we measured the spread areas at 8 min of B cells on glass or bilayer under nonstimulating conditions using biotinylated transferrin (biotin-Tf). The binding of biotin-Tf labeled receptor to coated streptavidin enables cells to interact with glass and bilayer surfaces without cross-linking and stimulating BCRs. We found that B cells under this non-stimulatory condition, on both streptavidin coated glass and lipid bilayers did not show significant spreading (Fig. 2.1 D), suggesting that the spreading of B cells requires BCR signaling.

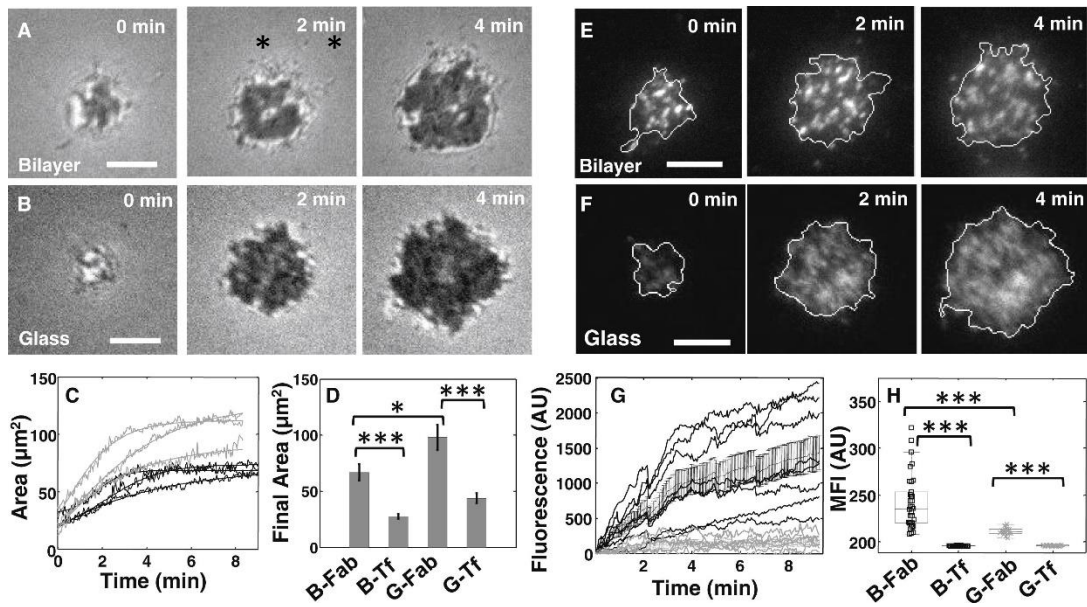


**Figure 2.1: Effect of ligand mobility on spreading and BCR accumulation of A20**

**B cells.** (A) Time-lapse IRM images showing the increasing contact zone of a cell spreading on an activating bilayer substrate. (B) Time-lapse IRM images of a cell spreading on an activating glass substrate. (C) Contact area as a function of time for representative cells spreading on a bilayer (dark gray) and glass (light gray) surface. (D) Average final spread areas (with SE) for cells on glass (N = 23) and bilayer (N = 22). The spread area at 8 min for cells on a glass surface (G-Fab) was greater than that on a bilayer (B-Fab) ( $p < 0.05$ ; t-test). Spread areas of cells on both the glass (G-Fab) and bilayer (B-Fab) surface were significantly larger than for control conditions of transferrin mediated spreading for glass (G-Tf) ( $p < 0.001$ , t-test) and bilayer (B-Tf) ( $p < 0.001$ , t-test). (E) Time-lapse TIRF images of AF546 labeled BCR clusters in an A20 cell spreading on a supported lipid bilayer. Cell contour obtained from IRM is shown in white. (F) Time-lapse TIRF images of BCR clusters for a cell spreading on a glass surface. The cell contour is drawn in white. (G) Increase in total BCR fluorescence intensity in the contact zone as a function of time on supported lipid

bilayer (dark gray) and glass (light gray) substrates (mean and SE) (H) Mean fluorescence intensity of labeled BCR at the contact zone at 8 minutes for cells on bilayer (B-Fab) (N = 34) and glass (G-Fab) (N = 18) substrates. MFI was significantly larger for cells on bilayer surfaces ( $p < 0.001$ , t-test). MFI for bilayer and glass was also significantly higher than for cells spreading under control conditions on bilayer (B-Tf) (N=16) ( $p < 0.001$ ) and glass (G-Tf) (N=24) ( $p < 0.001$ ). All scale bars are 5  $\mu\text{m}$ .

### 2.2.2 BCR accumulation is greater on a bilayer substrate

As B cells spread on a stimulating surface, BCRs accumulate in the contact zone [23, 53]. We examined the effect of ligand mobility on the accumulation of BCR during spreading using TIRF microscopy. BCR clusters formed upon initial contact and continued to increase in number and intensity as the cell contact area increased (Fig. 2.1, E and F). The total fluorescence intensity of BCR staining, indicative of BCR accumulation in the contact zone, increased over time until saturation on surfaces with either immobile or mobile ligands (Fig. 2.1 G). However, there were significant differences between cells on the two types of surfaces. Cells on glass achieved maximum BCR fluorescence at  $\sim 2$  min, but on lipid bilayers, the BCR fluorescence intensity continued to increase for at least 6 min. Cells on glass substrates showed smaller increases in BCR fluorescence and lower fluorescence intensity at all time points compared with cells on lipid bilayers. Since both cell contract area and BCR fluorescence reach their plateau by 8 min, we used this as the nominal end point for all our subsequent analyses. The mean fluorescence intensity (MFI) of BCRs at 8 min

was also significantly higher on lipid bilayer than on glass substrates (Fig. 2.1 H). Cells spreading under non-stimulating conditions (as described before) made limited contact with the surface and showed significantly lower MFI than their stimulated counterparts on both bilayer and glass (Fig. 2.1 H). To ensure that the greater BCR accumulation observed on the bilayer surface was not because of increased coating of streptavidin on bilayer compared with glass, we verified that the coating density of streptavidin was similar for glass and bilayer substrates using ELISA (See Section 5.2.2). To test whether the increase in BCR clustering on bilayers was because of increased accumulation of mobile streptavidin in the contact zone, we stimulated cells using AF546-mB-Fab'-anti-Ig to coat the bilayer. This system is also known to induce robust BCR activation and signaling [70]. Although streptavidin again formed distinct clusters in the center of the B cell contact region, the MFI in the contact region did not show as large an increase (See Section A.3), indicating that the accumulation of mobile streptavidin alone is not sufficient for the increase in BCR clustering. Further, we verified that photobleaching was minimal during our timelapse imaging and similar on both glass and bilayer (See Section A.2). Taken together, these results suggest that the increase in BCR fluorescence intensity, corresponding to BCR accumulation and the formation of receptor clusters, is a specific response to interactions of the BCR with stimulating ligand, and that the level of BCR clustering is regulated by ligand mobility.

### 2.2.3 Syk-mediated B cell signaling is greater with mobile ligand

We next asked whether the differences in receptor accumulation on lipid bilayer and glass influenced BCR signaling activation. We examined the differences in the levels of signaling by measuring the phosphotyrosine (pY) levels. We allowed A20 B cells to interact with ligand on glass and lipid bilayer substrates for various lengths of time, immuno-stained for pY after fixation, and analyzed the spatial pattern of tyrosine phosphorylation at the cell contact zone. pY staining of B cells rapidly arose at 2 min in a similar manner on both the lipid bilayer (Fig. 2.2 A) and the glass (Fig. 2.2 B) forming loci that became more numerous over time. However, on bilayer substrates, pY loci became brighter and larger than those on the glass. The MFI of pY was greater in the contact zone of B cells on the bilayer than those on glass at all time points, but both reached their peaks at 6 min. BCR clusters on the bilayer appear to organize into a recognizable immune synapse (Fig. 2.2 C) and began to decrease at 8 min. We further quantified the signaling levels in individual clusters using an intensity threshold. Consistent with the pY levels in the B cell contact zone, the MFI of individual pY clusters for B cells on bilayer surfaces was higher than that on glass substrates (Fig. 2.2 D).

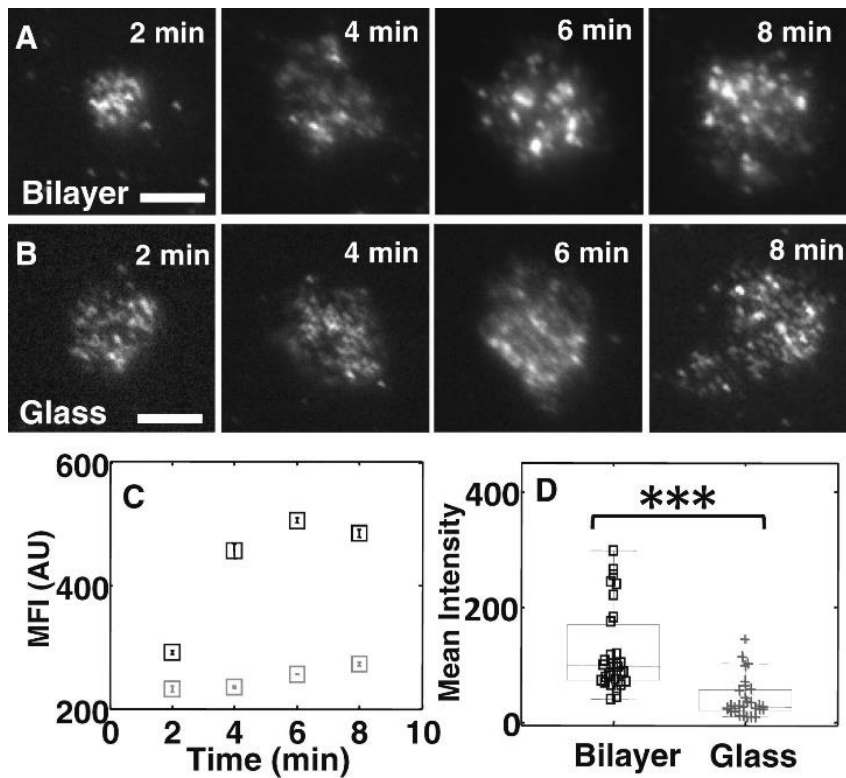


**Figure 2.2: Signaling levels are affected by ligand mobility.** (A, B) TIRF images of phosphotyrosine (pY) staining for cells spreading on supported lipid bilayer (A) or glass (B) substrates and fixed at the indicated times after surface engagement. (C) Mean fluorescence intensity (MFI) of pY staining of cells (Bilayer N>21; Glass N>15) spread on a supported lipid bilayer (dark gray) and glass (light gray) surface at the indicated time points, plotted with standard error. The differences were statistically significant for all time points except at 2 min ( $p<0.001$ ; t-test). (D) Comparison of mean fluorescence intensity (per pixel of cell contact area) of pY labeled clusters for cells fixed at 6 minutes (N = 32 bilayer and N = 29 glass) activated on bilayer and glass surfaces. Mean intensities were significantly higher for cells on the bilayer surface ( $p<0.001$ ; t- test).

## 2.3 Effect of ligand mobility on BCR microcluster formation, dynamics, and signaling

### 2.3.1 BCR cluster formation is less efficient when bound to immobile ligand

BCR signaling proceeds by the aggregation of BCRs within the contact zone into microclusters and the subsequent induction of downstream signaling pathways [23, 110]. The enhanced levels of BCR signaling in response to mobile ligands compared with immobile ones may arise because of differences in BCR clustering. To test whether ligand mobility influenced microcluster formation, we performed a detailed analysis of BCR cluster dynamics. We identified BCR clusters with custom software (see Methods) by fitting a Gaussian profile to an intensity distribution above a predefined threshold. The peak of the Gaussian corresponds to the brightness of the cluster and is proportional to the amount of receptors accumulated in the cluster (See Section A.3), whereas the location of the cluster corresponds to the position of the peak. We show representative TIRF images of clusters on the bilayer and glass surface respectively in Fig. 2.3, A and B and the spatial maps of the fluorescence intensity at each pixel and the corresponding Gaussian fits to the three-dimensional intensity map in Fig. 2.3, C–F. The peak intensity is higher for clusters in B cells on bilayer than for those on glass. Accordingly, the average peak intensity of BCR clusters on bilayers was significantly larger than those on glass substrates (Fig. 2.3 G). Further, the ratio of the peak intensity of clusters to the MFI over the cell contact

area was significantly higher for B cells on the bilayer surface than for those on glass (Fig. 2.3 H). We also found that the number of BCR clusters tracked during 8 min time-lapse movies to be significantly lower on the glass than on the bilayer substrate (Fig. 2.3 I). Taken together, these results suggest that BCR accumulation and cluster formation is more efficient when cells interact with mobile ligands than with immobilized ligands.

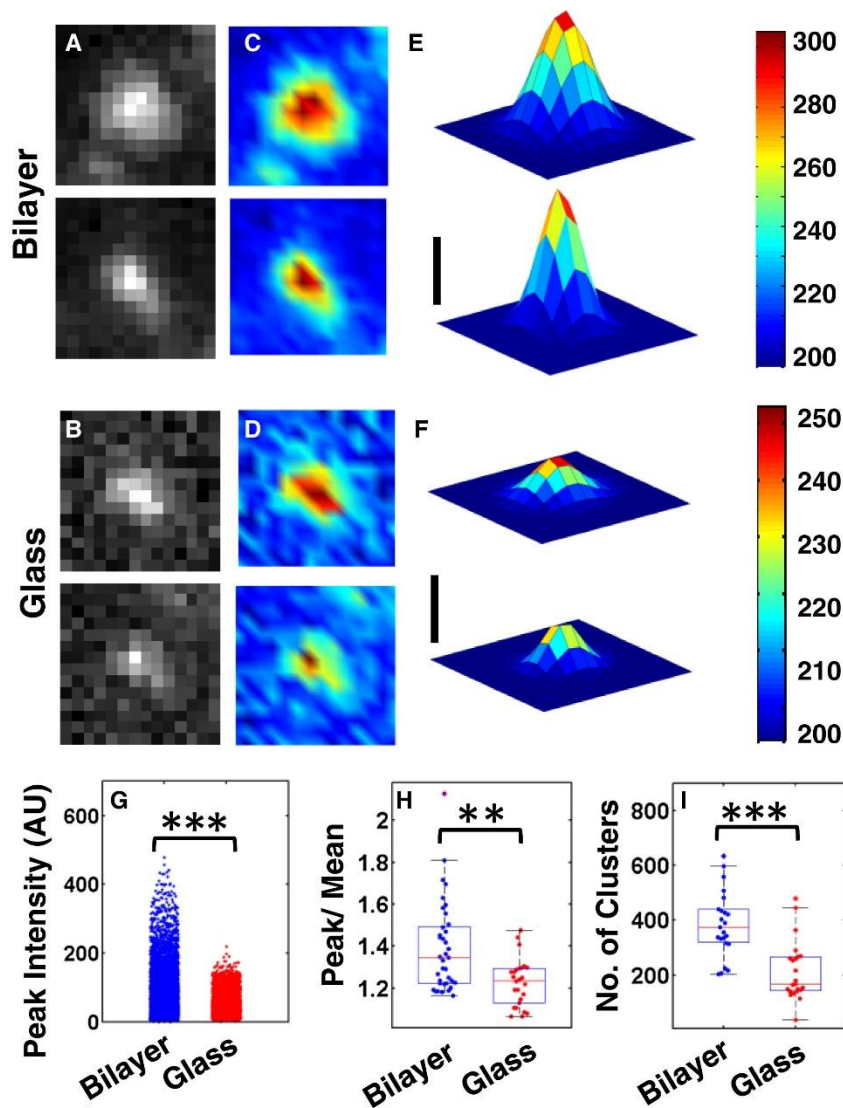


**Figure 2.3: BCR cluster formation is distinct on bilayer and glass surfaces.** (A, B) Representative TIRF images of two clusters in a cell spreading on a bilayer surface (A) and a glass surface (B). (C, D) Color maps with the color corresponding to the pixelwise fluorescence intensity of each of the clusters on bilayer (C) and glass (D). (E, F) Gaussian fits to the pixelwise intensity data in C and D. Scale bars denote 50 AU. (G) Comparison of the peak intensity of BCR clusters on glass versus bilayer substrates. Peak intensities on bilayer were significantly larger than on glass (N=8850

clusters, bilayer; N=4917 clusters, glass;  $p < 0.001$ ; KS-test). (H) The ratio of peak fluorescence intensity of clusters to the mean intensity over the cell contact area was significantly larger for bilayer as compared to glass substrates (N=37 cells, bilayer; N=26 cells, glass;  $p < 0.01$ ; t-test). (I) Average number of clusters detected and tracked per cell on glass versus bilayer substrates. The bilayer surface had significantly higher number of clusters (N=23 for both;  $p < 0.001$ , t-test).

### 2.3.2 BCR cluster motion is dependent on ligand mobility

The formation of BCR clusters is critical for the initiation of signaling and antigen gathering [24, 27, 67, 102]. To quantitatively compare the dynamics of BCR clusters on the different surfaces, we identified and tracked individual BCR clusters from time-lapse images, and calculated ensemble statistics of BCR cluster behavior. We categorized these tracks into three groups, “short” (less than 0.6 mm), “medium” (less than 1.2 mm), or “long distance” (greater than 1.2 mm). Fig. 2.4, A–C show time-lapse TIRF images of three representative clusters, long, medium, and short, with the calculated track coordinates superimposed on the images. To obtain a wider view of the cluster tracks, a representative selection of BCR cluster tracks are superimposed on a TIRF image of B cells on lipid bilayer (Fig. 2.4 D) and glass substrates (Fig. 2.4 E), respectively. Representative medium- and long-distance tracks of each type are plotted with the cell contour at 8 min for a cell on bilayer (Fig. 2.4 F) and glass (Fig. 2.4 G). The fraction of mobile clusters (medium and long distance) was larger in B cells on the bilayer surface (30%) than that in B cells on the glass surface (10%). The ligand on glass surface generated a higher percentage (> 90%) of short distance clusters as compared to the bilayer surface (70%). The distribution of

the track lengths of BCR clusters show a heavier tailed distribution for tracks on the supported lipid bilayer surface than on glass (Fig. 2.4 H), indicating a preponderance of longer cluster tracks on the bilayer substrate. These data suggest that BCR clusters induced by mobile ligand traverse longer distances than those induced by immobile ligand. We found an inverse correlation between peak intensity of clusters and their average velocity (defined as the total distance traveled divided by the total time taken, Fig. 2.4 I), indicating that highly mobile clusters are likely to contain less BCR than the slower-moving ones. We next quantified the fate of BCR clusters on the two substrates. Cluster tracks may end in one of two ways: ceasing to be tracked by disappearing from the field or by reaching the end of the movie (“end”), or joining another cluster (“merge”). On the bilayer substrate, BCR clusters had a significantly higher probability of merging with one another as compared with the glass substrate (Fig. 2.4 J; N = 23 cells). These results are consistent with earlier studies that postulate a diffusion-trap model of BCR microcluster growth, wherein microclusters form and enlarge by binding diffusing receptors [30, 111]. To examine how BCR accumulation within clusters was affected by ligand mobility, we quantified the ratio of the peak intensity at the end of a track to the peak at the start of the track (representing the change in BCR density over time). This ratio was also significantly higher for clusters induced by mobile ligand as compared to those by immobile ligand (Fig. 2.4 K). These results indicate that mobile ligands presented on membranes enable more efficient recruitment of BCRs into preexisting clusters.

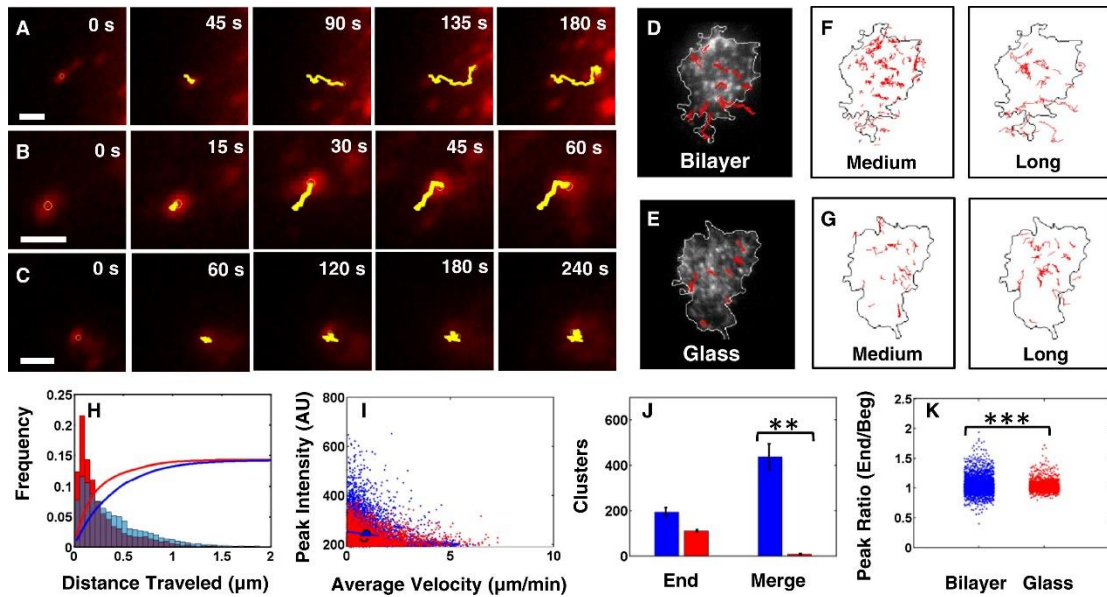


**Figure 2.4: BCR cluster dynamics depends on ligand mobility.** (A, B, C) Time-lapse TIRF images of representative BCR clusters in cells spread on bilayer substrates. The calculated track is overlaid at each time point and corresponds to a “long” (A), medium (B), and a short track (C). Scale bars: 1 μm. (D, E) Representative selection of cluster tracks (red) superimposed on TIRF images of fluorescently labeled BCR taken at 6 minutes after the initiation of spreading on bilayer (D) and on glass (E). (F, G) Example medium distance and long distance cluster tracks from eight minutes of imaging (red) superimposed on the outline of a representative cell on bilayer (F) and glass (G). (H) Histograms of the total distance traveled by tracked clusters on bilayer (blue) and glass (red), superimposed for comparison. Smooth curves represent the cumulative distribution of distances traveled on the two types of substrates, bilayer (blue) and glass (red). The difference between the two distributions is statistically significant ( $p < 0.001$ ; KS test). (I) Peak intensity of each cluster plotted against its average velocity (total distance traveled divided by the total time taken) for all tracked clusters on bilayer (blue) and glass substrates (red). (J) Comparison of the

different types of cluster events, i.e. number of clusters that end or merge on bilayer (blue) versus glass (red) (Merge:  $p < 0.01$ ; t-test). (K) The ratio of peak intensities from the end to the beginning of each cluster track for clusters moving on bilayer (blue) versus a glass (red) surface ( $p < 0.001$ ; t-test). The number of clusters examined were  $N = 8850$  bilayer;  $N = 4917$  glass.

### 2.3.3 Primary B cells recapitulate mobile and immobile cluster behavior

To ensure that the differences shown above were not specific to the A20 B cell line, we examined cell spreading and BCR clustering of mouse splenic B cells. These were labeled with AF546-mB-Fab'-anti-Ig and activated by streptavidin-coated glass and lipid bilayers in the same way as the A20 cells. Time-lapse TIRF images of spreading primary B cells show the formation of BCR clusters on both glass and bilayer surfaces (Fig. 2.5, A and B). Primary B cells spread to a greater extent on glass as compared with bilayer, (Fig. 2.5 C) similar to the A20 cells. The MFI of labeled BCR at the contact zone was significantly higher for cells on the bilayer as compared with the glass surface (Fig. 2.5 D). The average peak intensity of clusters was significantly higher for clusters induced by the bilayer surface as compared with those induced by the glass surface (Fig. 2.5 E), demonstrating that ligand mobility enabled clusters to recruit a larger amount of receptor/antigen pairs.

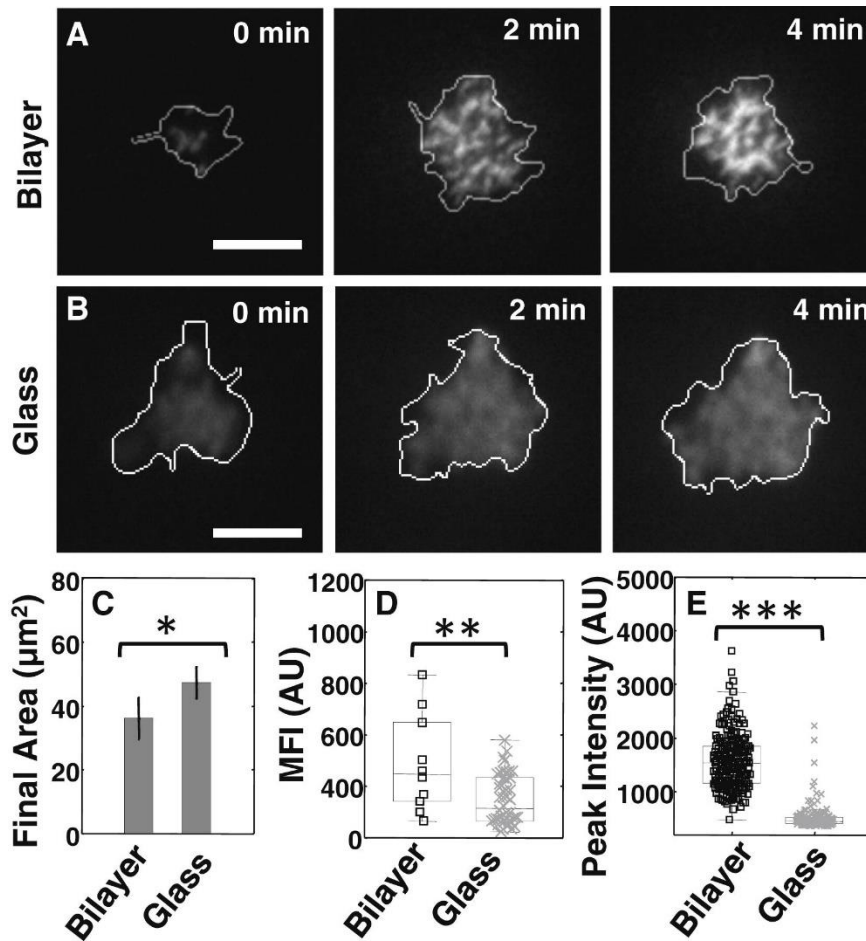


**Figure 2.5: Spreading and BCR clustering in mouse primary B cells.** (A) Time-lapse TIRF images of AF546 labeled BCR clusters in a primary B cell on a supported lipid bilayer. Cell contour obtained from IRM imaging is shown in white. (B) Time-lapse TIRF images of BCR clusters in a primary B cell spreading on glass. Scale bars are 5µm. (C) Final spread areas (mean ± s.e.) for cells spreading on glass (N=27) and bilayer (N=17). The final area on glass surfaces was significantly larger than those on bilayer surfaces ( $p < 0.05$ ; T-test). (D) Comparison of mean fluorescence intensity (MFI) of labeled BCR at the cell surface contact zone at 8 minutes for bilayer (N=10) and glass (N=48). MFI on bilayer surfaces was found to be significantly greater than that on glass ( $p < 0.01$ ; t-test). (E) Comparison of peak intensities of BCR clusters on

bilayer versus glass substrates. Peak intensities were significantly higher on bilayer surfaces (N=928 bilayer; N=2463 glass;  $p < 0.001$ ; KS-test).

## 2.4 Actin organization with respect to BCR and receptor cluster formation and signaling

### 2.4.1 Actin patches are colocalized with BCR clusters

The actin cytoskeleton is known to play an important role in BCR organization and activation at the B cell surface [51, 71, 112]. To test the effect of ligand mobility on actin dynamics and organization with respect to BCR clusters, we used dual color time-lapse imaging of A20 cells expressing EGFP-actin and labeled surface BCRs. As the cell spread, actin formed localized patches throughout the contact zone and distinct lamellipodia with retrograde actin flow during the later stages of spreading. We analyzed the relationship between the dynamics of BCR clusters and local actin patches. Actin patches often formed in close proximity to BCR clusters. On glass surfaces, these patches remained near the BCR clusters but were typically immobile (Fig. 2.6 A), as shown by the peaks of the intensity profiles of actin and BCR cluster (representing their location), which do not move over time (Fig. 2.6 B). On the other hand, actin patches associated with BCR clusters induced by ligand on lipid bilayer moved concurrently with BCR clusters as shown by the movement of the two intensity peaks (Fig. 2.6, C and D). Quantitative analysis showed that they moved with similar average speeds ( $4.2 \mu\text{m}/\text{min}$ ,  $n = 10$  cells,  $p > 0.1$ ). These results suggest

that actin dynamics coordinate with the movement of BCR clusters induced by mobile ligands.

To further elucidate the relationship between actin patches and BCR cluster dynamics, we tracked a large number of moving actin patches and BCR clusters. We generated the histograms of distances traveled by actin patches and BCR clusters induced by mobile and immobile ligands (Fig. 2.6, E and F), and quantified the distributions using the Kullback-Leibler distance (KLD) (31), a measure of similarity of two probability distributions. On bilayer substrates, the actin patches and BCR clusters had very similar distributions, indicating that they moved similar amounts (KLD = 0.0232), whereas the actin patches were considerably more mobile than BCR clusters on glass substrates (KLD = 0.2034). Taken together, our results suggest that on bilayer surfaces, actin and BCR movements are coupled, whereas on glass surfaces they are not.

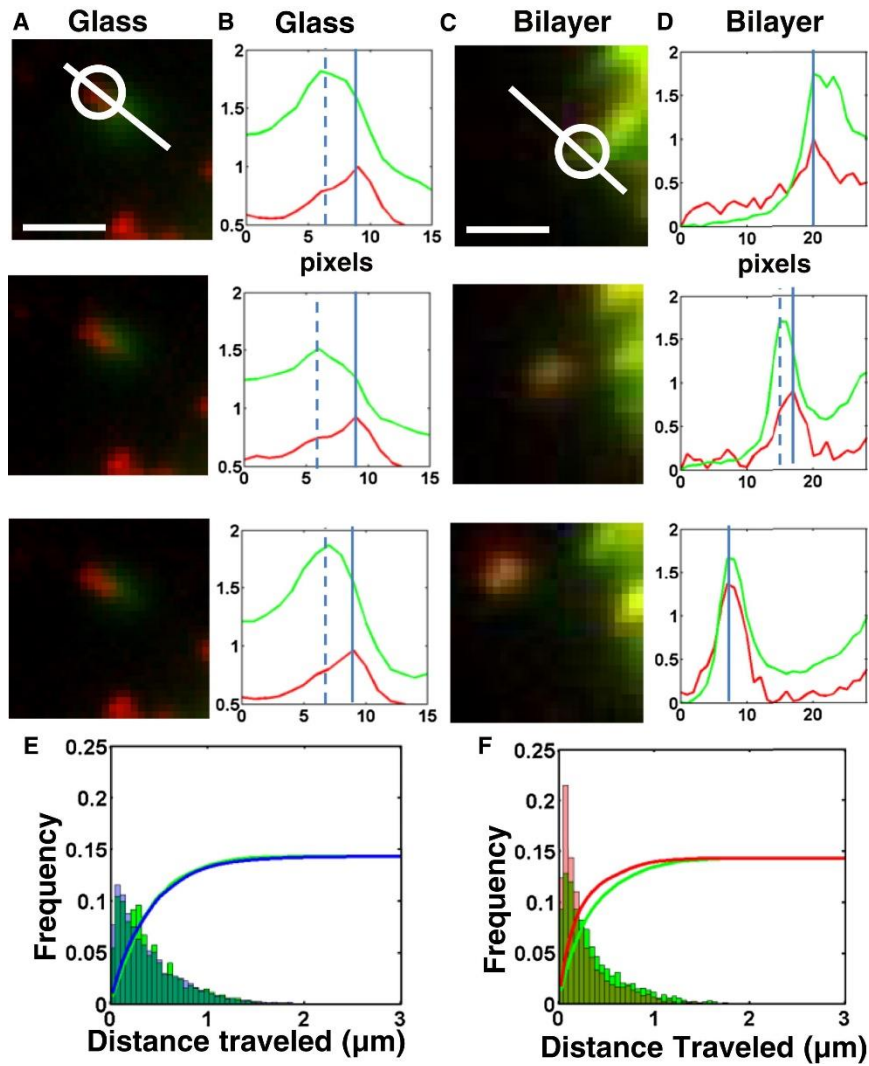


**Figure 2.6: Actin dynamics are distinct on bilayer and glass substrates.** (A) Time lapse dual wavelength TIRF images of a representative BCR cluster (red) and an EGFP-actin patch (green) on a glass surface. Images are separated in time by 3 sec intervals. Scale bar is 1  $\mu\text{m}$ . (B) Intensity profiles measured along the line drawn on the top panel. The peaks corresponding to the center of the BCR cluster (solid line) and actin patch (dashed line) show no net movement. (C) Time lapse dual wavelength TIRF images of a representative BCR cluster (red) and an EGFP-actin patch (green) on a bilayer surface. Images are separated by 6 sec intervals. Scale bar is 1  $\mu\text{m}$ . (D) Intensity profiles measured along the line drawn on the top panel. The peaks

corresponding to the center of the BCR cluster (solid line) and actin patch (dashed line) show a net movement ( $1.5 \mu\text{m}$ ) away from the cell center. (E) Histograms of the total distance traveled by tracked BCR clusters (blue) and actin patches (green) on a bilayer surface, superimposed for comparison. Smooth curves represent the cumulative distribution of distances traveled by BCR clusters (blue;  $N=8850$ ) and actin patches (green;  $N=1610$ ). (F) Histograms of the total distance traveled by tracked BCR clusters (red;  $N=4917$ ) and actin patches (green;  $N=2843$ ) on a glass surface, superimposed for comparison. Smooth curves represent the cumulative distribution of distances traveled by BCR clusters (red) and actin patches (green).

## 2.4.2 Actin modulates BCR signaling by controlling cluster conformations

We next examined whether the differences that we observed on the localized movement of BCR and actin resulted in global differences in spatial organization of actin. In the early stages of activation and spreading, actin patches were interspersed with early BCR clusters in the B cell contact zone on both bilayer and glass surfaces (Fig. 2.7, A and B, 2 min). As cells spread on the bilayer surface and BCR clusters merged into larger clusters, the actin was observed to surround larger aggregates of BCR clusters (Fig. 2.7 A, 8 min). In contrast, on the glass surface, actin patches remained interspersed randomly with BCR clusters (Fig. 2.7 B, time 8 min). To correlate actin distribution with receptor signaling, we analyzed the spatial relationship between actin and pY staining. On the bilayer substrate, actin patches appeared to surround the pY rich regions (Fig. 2.7, C and D), whereas on the glass

substrate pY signaling loci were largely colocalized with actin patches (Fig. 2.7, E and F). We quantified the pixelwise Pearson's correlation coefficient for localization of actin and pY in B cells on glass (N = 16) and bilayer (N = 21) at 6 min (Fig. 2.7 G). There was a significantly higher degree ( $p < 0.05$ ) of anticorrelation between the actin and pY in cells on the bilayer surface than those on glass. On bilayer surfaces, the localization pattern of pY in relation to actin (Fig. 2.7 C) was qualitatively similar to the pattern of BCR with relation to actin (Fig. 2.7 A). This is consistent with previous studies showing that pY staining strongly colocalizes with BCR fluorescence [67]. These results indicate that the dynamic actin cytoskeleton may regulate BCR signaling capability by modulating the mesoscale movement and spatial organization of BCR clustering.

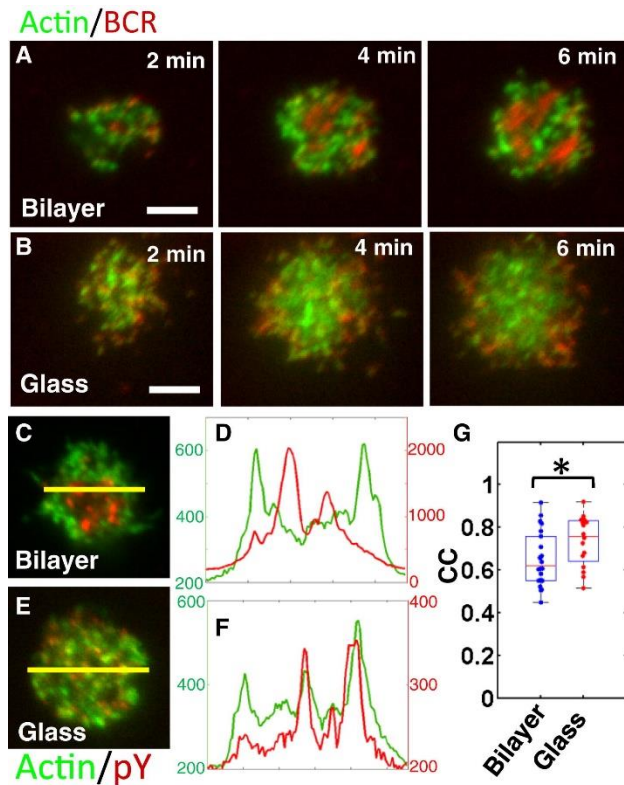


**Figure 2.7: Actin organization is distinct on bilayer and glass substrates.** (A) Time-lapse images using dual wavelength TIRF of EGFP-actin (green) cells where BCR were labeled with AF546-Ab (red) spreading on a supported lipid bilayer substrate show formation of BCR clusters and actin organization around the clusters. (B) Dual wavelength TIRF images of cells spreading on a glass substrate show the formation of clusters but a lack coordination of the actin cytoskeleton with BCR clusters. Scale bars are 5  $\mu\text{m}$ . (C, E) Images of cells spread on bilayer (C) and glass (E) at 6 minutes with EGFP-actin (green) and pY staining (red). Intensity profiles along the lines drawn in yellow for bilayer (D) and glass (F) respectively. pY and actin are plotted on different scales. (G) Pearson's correlation coefficient for two color images (GFP- actin and pY) on glass (N=16) and bilayer (N=21) for the area of

cell contact at 6 min. The distributions were found to be significantly different ( $p < 0.05$ , t-test).

### 2.4.3 Actin cytoskeleton integrity is essential for BCR cluster formation and translocation

Given our observations that the movement of BCR clusters on the bilayer surface was coordinated with movement of actin patches, we hypothesized that actin polymerization may provide the driving force for these movements. To test this hypothesis, we treated cells with Latrunculin-A (Lat-A), a drug that sequesters actin monomers and promotes actin depolymerization, after the initial formation of BCR microclusters. We allowed A20 cells to spread for 2 to 3 min and form mobile clusters. We then added Lat-A to the imaging well at a final concentration of 100 nM, whereupon we found that the movement of BCR clusters decreased dramatically on the bilayer surface. The tracks of cluster movements were much shorter in the presence of Lat-A as compared to the control (Fig. 2.8, A and B). Quantitative analysis of cluster tracks revealed that movement of BCR clusters on bilayer substrates was affected to a greater degree by Lat-A as compared to the movement on glass substrates. This is shown by the larger difference (KLD) between the distance distributions of tracks with and without Lat-A on the bilayer surface (KLD = 1.0732) (Fig. 2.8 C) compared with that on glass substrates (KLD = 0.0575) (Fig. 2.8 D). Consistent with this, BCR clusters in B cells on bilayers moved significantly smaller distances upon Lat-A application, as compared with those in untreated cells (Fig. S6

A). In contrast, the mean distance moved by BCR clusters in cells on glass substrates were much less affected by LatA application (Fig. S6 A). Furthermore, the average velocity of BCR clusters on bilayer surfaces was significantly lowered by Lat-A application, whereas the average velocity of clusters on glass increased in the presence of Lat-A (Fig. 2.8 E). These data indicate that actin polymerization plays a more active role in the movement of BCR clusters on the bilayer surface than those on the glass. Further, we observed that upon Lat-A addition, the MFI of the BCR in the cell substrate contact zone (a measure of receptor accumulation) significantly decreased in cells on bilayer, but not in cells on glass surfaces (Fig. 2.8 F), suggesting that receptor accumulation on the glass substrate occurred independently of actin coordination. To examine whether actin polymerization was required for clustering efficiency, we compared the end-to-beginning ratio of the peak cluster intensities for cluster tracks in the presence and absence of Lat-A on the two surfaces. The end/begin ratio of peak intensities was significantly decreased upon Lat-A addition for clusters on bilayer surface, but much less affected for clusters on glass surface (Section A.4). This indicates that inhibition of actin polymerization reduced the efficiency of cluster formation in cells interacting with mobile ligand. Our results indicate that cluster growth and mobility in response to mobile ligands, but not to immobile ligands, are driven by active polymerization of actin.

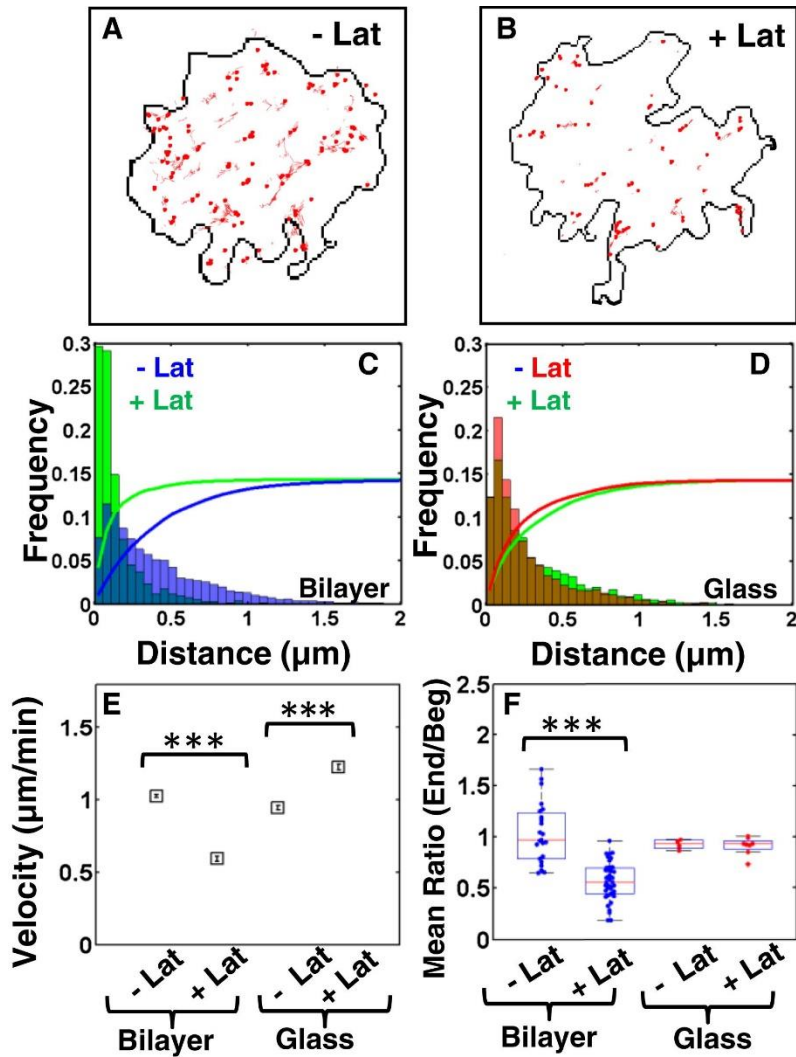


**Figure 2.8: Role of actin polymerization in BCR movement.** (A) Representative cluster tracks superimposed on a cell contour for a cell spreading on bilayer in the absence of Lat-A. (B) Representative cluster tracks superimposed on a cell contour for a cell spreading on bilayer in the presence of 100 nM Lat-A. (C) Histograms of the total distance traveled by BCR clusters in the absence of Lat-A (blue) and in the presence of 100 nM Lat-A (green) on a bilayer surface. Smooth curves represent the corresponding cumulative distributions. (D) Histograms of the total distance traveled by BCR clusters in the absence of Lat-A (red) and in the presence of 100 nM Lat-A (green) on a glass surface. Smooth curves represent the corresponding cumulative

distributions. (E) Mean of the average velocity of BCR clusters on a bilayer surface in the absence of Lat-A (- Lat) is significantly higher than the velocity in the presence of Lat-A (+ Lat) ( $p < 0.001$ ; KS-test). Average velocity of BCR clusters on a glass surface is lower in the absence (- Lat) than in the presence of 100 nM Lat-A (+Lat). (F) The ratio of mean fluorescence intensity (over the entire contact area) from the end to the beginning of time lapse movies (ranging from 2– 5 min in duration) for glass and bilayer surfaces in the absence and presence of Lat-A. The mean ratio is significantly lower in Lat-A for cells spreading on bilayer surface ( $N=23$ , -Lat;  $N=38$  +Lat;  $p < 0.001$ ; t-test).

## 2.5 Discussion

The clustering of surface BCRs has been shown to initiate signaling upon contact with surface-bound antigens [113, 114]. BCR proximal signaling, in turn, activates actin reorganization and further cell spreading, providing a positive feedback by promoting BCR clustering. These discrete receptor clusters appear to be a common feature of lymphocyte activation and thus may represent the basic unit of signaling. How these signaling assemblies are organized is critical for understanding lymphocyte signaling and activation. We have investigated the role of antigen mobility in regulating BCR signaling activation. We find that physical constraints on the mobility of the activating cross-linking agent not only alters spreading behavior of B cells, but also clustering dynamics of surface BCRs, and signaling activation. When interacting with the mobile ligand on lipid bilayer substrates, BCR microclusters are

mobile and prefer to grow and merge with each other, forming larger clusters with enhanced pY signaling. In contrast, BCR clusters induced by the immobile ligand on glass remain small, unstable, and dispersed, leading to inefficient signaling. These results indicate that BCR signaling is promoted by the formation of relatively large and stable supramolecular clusters, and ligand mobility regulates BCR signaling by modulating dynamic reorganization of BCRs at the cell surface.

In B cells stimulated by immobile ligands, most BCR clusters were immobile but a smaller fraction of clusters appear to be highly mobile. Since ligands are immobile on glass, these mobile clusters are unlikely to be engaged with ligands during their movement, suggesting that unbound BCR can self-cluster. Such ligand-free BCR clusters have been shown to form in B cells treated with Latrunculin [30, 71], but grow to a limited extent and are less signaling competent than those induced by ligand binding. In response to ligand binding, the early BCR signaling induces a transient depolymerization of cortical actin and detachment of the membrane from the cortical actin [67]. This actin disassembly releases membrane proteins from lateral mobility barriers and allows BCR movement and organization into clusters [27]. The transient depolymerization of actin potentially leads to the formation of the mobile clusters that we observed in B cells on glass.

The actin cytoskeleton is well known to play an important role in B cell signaling [112]. Previous studies have shown that perturbing the cortical actin network interferes with BCR aggregation, cell spreading, and signaling [27, 51, 71]. Although

the importance of an intact actin cytoskeleton in BCR signaling is well known, the role of actin polymerization on BCR dynamics has not been explored. In this study, we found that mobile and immobile ligands induce actin remodeling in distinct ways. Actin patches colocalize and move laterally for relatively long distances with BCR clusters formed in response to mobile ligands. However, in response to immobile ligands, the actin patches are uncorrelated with BCR and move shorter distances. These results suggest that actin dynamics may facilitate the long-range movement and coalescence of BCR clusters. Further, the movement and intensity of BCR clusters on bilayer surfaces is reduced by inhibition of actin polymerization indicating a role for actin polymerization in cluster movement. Our results together suggest an active role for actin cytoskeleton dynamics in driving BCR movement, leading to further growth of BCR microclusters. BCR signaling is known to activate key activators of actin nucleation factors, which, in turn, may allow actin polymerization to actively drive the surface BCRs and facilitate their clustering. Recent modeling studies using stochastic simulations of the dynamics of BCR and LFA1 molecules suggest that the formation of the synapse occurs only if BCR mobility is enhanced by directed movement as might occur because of actin polymerization [62]. These models and our observations together suggest that local BCR signaling to actin regulators lead to actin polymerization and directed motility of clusters, which facilitates BCR aggregation into larger clusters, enhancing signaling [70]. Whether the activation of actin regulators differs with ligand mobility remains to be explored.

In summary, our results show that ligand mobility influences the cell spreading behavior and BCR organization and signaling on the surface of B cells. Several recent studies have emphasized the role of ligand mobility on intracellular signaling in immune cells including FcεRI signaling in mast cells [62] and TCR signaling in T cells [63, 64]. Our results suggest that the spatial reorganization of microclusters may be a general theme of immunoreceptor signaling. Furthermore, in addition to tuning the diffusion dynamics of BCRs during early signaling [27, 67], the actin cytoskeleton plays an active role in the fusion and translocation of receptor clusters, amplifying signaling. The clinical implication of our findings is that vaccine design with mobile antigens, such as viral proteins on liposomes, is likely to be more effective than immobile antigens where the viral proteins immobilized on hydrogels to activate B cells for antibody response. Our results thus provide the knowledge basis for improving immunogenicity of vaccines by manipulating the physical form of antigen.

# Chapter 3: Substrate Topography Guides Actin dynamics and Calcium Oscillations in B Cells

## 3.1 Introduction

The interaction between antigen presenting cells and B cells is a complex spatiotemporal evolution beginning with the recognition of antigen by B cell receptors and resulting in the formation of an immunological synapse. B cells encounter activating antigens most often within the secondary lymphoid organs, such as the spleen and lymph nodes [73]. Within these organs, antigen can be presented to B cells either in soluble [115] or membrane bound form on the surface of antigen presenting cells such as marginal zone macrophages and follicular dendritic cells [74]. While both means of encounter will elicit B cell response, recent studies have indicated that membrane bound antigen is more effective at triggering B cell activation [24, 74]. This discovery is important information in the study of B cell activation, which may one day help provide better vaccinations and immunotherapies. The question, however, remains: why is membrane bound antigen so much better at activating B cells and which aspects of this cell-cell interaction can we then reconstitute?

In our previous work, we explored the role of ligand mobility in B cell actin dynamics and activation and found that mobile ligand results in higher B cell signaling [96].

However, many other features of membrane bound antigen still require investigation, one of which is the role of surface topography of antigen presenting cells encountered by B cells. Topography has been shown to affect cell behavior and gene expression changes for many cell types, and especially for migratory cells. Human keratinocytes were found to have increased motility on PCL/collagen nanofibrous matrices coated with collagen gels [116]. Fibroblasts and myofibroblasts were found to migrate parallel to ridged structures of greater than 1  $\mu\text{m}$  separation [117]. Immune cells have also been found to be responsive to topography. Migratory T cells can be guided by patterned substrates and macrophages excrete higher levels of cytokines on topographically patterned substrates as opposed to flat substrates [94, 95]. The amoeboid migration of *Dictyostelium discoideum* and the lamellipod-driven migration of human neutrophils were found to be guided by both symmetrically and asymmetrically patterned substrates [93]. This behavior was found to be accomplished through the topographic modulation of the actin network, which is responsible for cell migration.

Upon encountering antigen, B cells undergo actin mediated changes in morphology, with an initial depolymerization phase, a lamellipodial spreading phase, and then a contractile phase. This canonical picture has been established either on antibody labeled glass or on supported bilayer substrates. While both systems are sufficient for activating the B cell and represent key aspects of the B cell-antigen presenting cell interaction, these substrates provide an artificially smooth and featureless surface of contact. The topographical complexity of the antigen presenting cell is a completely

unexplored feature of this system. While all cells have a topographically featured plasma membrane, the surfaces of antigen presenting cells are especially convoluted as has been observed in live cell microscopy and with SEM. Dendritic cells not only present long extensions, but significant membrane ruffles and invaginations. These ruffles or membranes sheets present a radius of curvature around 200 – 300 nm [118], while the dendrites of follicular dendritic cells are micrometers long with a width of 100 – 300 nm [119], therefore providing a surface of contact which is topographically complex, as can be seen in Figure 3.1. Such obstacles demand a significant reassessment of B cell spreading as the actin features observed can be precluded or dramatically altered.

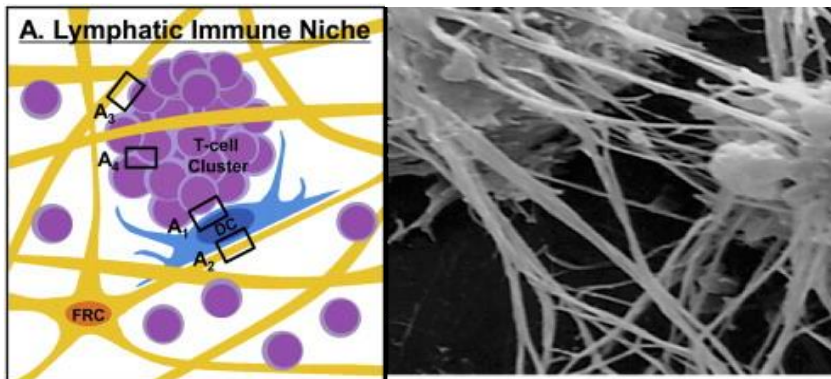


**Figure 3.1: Example images of nanostructures encountered by B cells in vivo.**

(A). Schematic of the lymphatic immune niche (adapted from [120]). (B). SEM image of the FDC dendrites and networks (adapted from [121]).

Actin and its binding proteins allow for the formation of a variety of cellular structures, such as filopodia and lamellipodia depending on the stoichiometry and organization of these various components. The current understanding of B cell -

antigen presenting cell contact focuses on a roughly uniform lamellar spreading of the B cell. Lamellipodia and the actin associated proteins that drive them are necessarily disrupted by the presence of topographical features which force a certain geometry to the spreading process, but further actin structure can arise as an active response to the topography of the substrate [122]. There exists an intimate connection between the dynamics of the actin network and the intracellular distribution and configuration of BCRs [28, 56, 57, 71, 123]. Alterations in the organization of BCR aggregates have been shown to affect receptor signaling intensity and dynamics as was demonstrated in Chapter 2. Modulation of the actin network can define the diffusion and oligomerization of BCR on the nano scale and the translocation and cluster formation of BCR on the meso scale, which may down or upregulate BCR signaling. The signaling of the BCR, in turn, encourages actin polymerization through Btk, WASp and N-WASp, which allows for more dramatic changes in the actin cytoskeleton upon BCR engagement. Thus, the feedback between BCR activation and organization and the dynamics of the actin cytoskeleton may be sensitive to topographic features, which can influence both aspects of B cell behavior. Therefore, we hypothesized that the modulation of actin reorganization in response to surface topography would have profound effects on the activation of the B cell.

In order to explore this possibility systematically, we have used topographically patterned surfaces created with nanofabrication techniques that allow systematic variation of geometric parameters of surface topography. These surfaces permit live cell fluorescence imaging of the B-cell/substrate interface to examine the dynamics of

cell spreading, actin dynamics and B cell activation. We found that cell morphology, the dynamics of the actin cytoskeleton and B cell signaling were modulated by surface topography. Our observations show that ridges with 3  $\mu\text{m}$  and 5  $\mu\text{m}$  separations induce recurring actin contractions in B cells. These contractions are dependent on Syk signaling downstream of BCR engagement as well as by non-muscle myosin II activity. BCR antigen binding and cross-linking result in the phosphorylation of the cytosolic ITAM regions of BCR by SRC kinases.

Phosphorylated ITAMS then recruit and activate Syk, where disruption of Syk function precludes signaling propagation [16]. Syk then phosphorylates and recruits the adaptor proteins Grb2 and BLNK, as well as PI3K, and Bruton's tyrosine kinase (Btk) to form a signaling platform on the cytosolic side of the plasma membrane.

Further, Btk and Syk activate PLC $\gamma$ 2, which by cleaving PIP2 creates IP3, which then moves to the ER and releases calcium stores [19-21]. We also found that calcium oscillations exhibit lower frequencies on patterned substrates than is observed in B cells stimulated on flat substrates. Finally, small separations of the ridges (between 0.8  $\mu\text{m}$  and 1.8  $\mu\text{m}$ ) promote the formation of BCR-tipped actin protrusions. Our results indicate that substrate topography regulates B cell actin dynamics and signaling, motivating the search for a mechanistic basis for topography sensing.

## 3.2 Recurring actin contractions are induced on patterned substrates

### 3.2.1 Nanotopographic substrates alter B cell morphology and spreading

Extensive studies on a diverse cell types have demonstrated that substrate topography has a profound influence on cell shape [76]. In order to test how B cells respond to topographic features of the substrate, we first quantified B cell morphology on arrays of parallel nanoridges 200 nm wide and 600 nm in height, but with different spacings between ridges (ranging from 0.8  $\mu\text{m}$  to 5  $\mu\text{m}$ ). Cells were allowed to spread on ridges of uniform height and width (Fig 3.2A-D), but with variable spacing coated with activating F(ab)<sub>2</sub> antimouse IgM+G antibody. We observed that peak B cell spread area and signaling was normally achieved six minutes after contact with the activating substrate on both ridged and flat substrates. Therefore, cells were evaluated for size and shape after six minutes of contact with the patterned surface once they had achieved a semi-stable state and BCR clusters had formed. We found that A20 B cells had significantly larger median spread size of  $448 \pm 174 \mu\text{m}^2$  (Median  $\pm$  SD) on the 1.2  $\mu\text{m}$  spacing than B cells on both smaller and larger spacings, which resulted in smaller spread sizes (Fig. 3.2E). In general, B cells on larger ridge spacing (1.5 - 5  $\mu\text{m}$ ) achieved greater spread areas than on smaller spacing (0.8 - 1.2  $\mu\text{m}$ ). A similar bimodal distribution was found for spread B cell elongation, which was characterized using the eccentricity value for an ellipse  $e = \sqrt{1 - \frac{b^2}{a^2}}$  where a is the semi-major axis and b is the semi-minor axis. Cells exhibited the greatest median eccentricity of  $0.85 \pm 0.1$  on substrates with the 1.8  $\mu\text{m}$  spacing (Fig. 3.2F). The effects on spread area and eccentricity of ridge spacing demonstrates that B cell spreading morphology is influenced by the topography of the substrate.



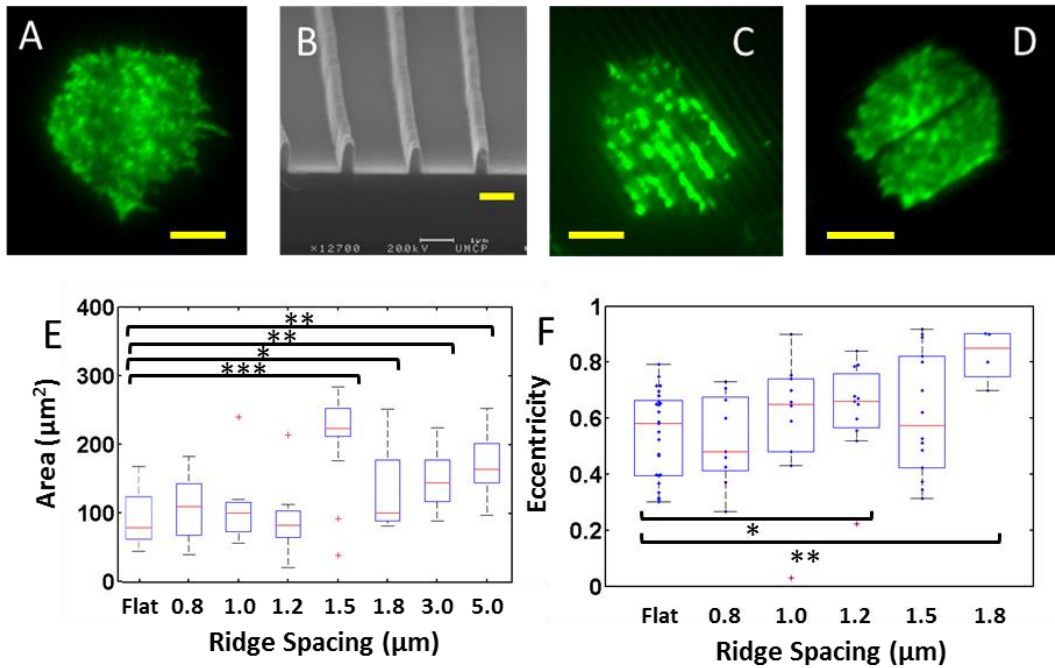


**Figure 3.2: A20 B cells spreading dynamics on patterned substrates.** A) EGFP-actin expressing A20 cell spread on a flat glass substrate. Scale bar 5μm. B) SEM image of nanopatterned substrate. Scale bar 1μm. C) EGFP-actin A20 cell spread on a nanopatterned substrate with a 1.0 μm ridge spacing. Scale bar 5μm. D) EGFP-actin A20 cell spread on a nanopatterned substrate with 5.0 μm ridge spacing. E) Contact area of A20 B cells spread on nanopatterns with ridge spacings between 0.8 and 5.0 μm. F) Eccentricity of A20 B cells spread on nanopatterns with ridge spacings between 0.8 and 1.8 μm.

### 3.2.2 Contact with multiple ridges cause repeated actin enrichments

To investigate the influence of substrate topography on the actin dynamics and signaling of B cells, EGFP-actin expressing A20 lymphoma B cells were allowed to spread on these antibody coated substrates as above and imaged using TIRF

microscopy to observe the distribution and dynamics of actin. Ridge spacings of 3  $\mu\text{m}$  and 5  $\mu\text{m}$  induced cells to exhibit repeated actin enrichment and depletion over large portions of the cell area as observed in TIRF (Fig. 3.3 A-B). These enrichments were quantified using an ROI centered over the enrichment area, which was sized to fit between the ridges (3 and 5 $\mu\text{m}$  accordingly). The integrated fluorescence intensity of the ROI was found to be roughly periodic in nature (Fig. 3.3 C). The time intervals between intensity peaks were measured by first smoothing the integrated intensity track with a span of 10 seconds and then using a custom Matlab function to identify peaks. These time intervals were found to have an average of  $33 \pm 11$  seconds on the 3  $\mu\text{m}$  ridges (n=25) and  $35 \pm 13$  seconds on the 5  $\mu\text{m}$  ridges (n=30). On flat surfaces the actin distribution was evaluated using similarly sized ROIs. Actin intensity was found to vary over time, but did not undergo large scale actin intensity oscillations (Fig. 3.3 B,D). In order to quantify the actin intensity variability over time that arises from these actin intensity oscillations, the coefficient of variation was used, which is defined as:  $c_v = \frac{\sigma}{\mu}$ , where  $\sigma$  is the standard deviation and  $\mu$  is the mean. ROIs, as previously described, were used to find the integrated actin intensity over time. The coefficient of variation was then found for this time trace, wherein a larger value indicates greater deviations from the mean intensity value. On patterned substrates  $c_v$  values were similar on 3  $\mu\text{m}$  and 5  $\mu\text{m}$  substrates, with a combined mean value of  $0.61 \pm 0.12$ , whereas on flat substrates this  $c_v = 0.45 \pm 0.08$ . This drop in the coefficient of variation indicates that there is much greater variability in actin intensity over time on patterned substrates (Fig. 3.3E). These same intensity time traces were then evaluated with a fast Fourier transform (FFT). Time intensity traces

were standardized by local detrending in order to compensate for low frequency drifts, and then mean subtraction and dividing by the standard deviation. From the FFT the composite spectral density of both patterned substrates were evaluated, wherein the spectra for ridges show peaks at 0.02 Hz (50 s) on the 3  $\mu\text{m}$  ridge (Fig. 3.3F) and 0.025 Hz (40 s) on the 5  $\mu\text{m}$  (Fig. 3.3G) ridge spacing, respectively.

We also observed an increase in actin intensity directly adjacent to the ridges for B cells adhered to the patterned surface. The enrichment changed in size and intensity but remained static in space. One way to characterize this feature is a peak-to-mean intensity measure, wherein the peak actin intensity pixel and the mean actin intensity are both taken from the entire spread area of the cell. Dividing the peak by the mean gives a measure of the degree of local actin enrichment compared to the background actin levels of the cell spread area. This measure indicated a higher than normal amount of actin proximal to the contact surface, which was evident when the peak to mean actin intensity was evaluated for cells on flat and ridged surfaces. For a B cell spread on a flat surface, this ratio had a median value of  $1.57 \pm 0.14$  (mean  $\pm$  std). This value was significantly higher on ridges with the 5  $\mu\text{m}$  spacing at  $2.29 \pm 0.54$ , and even higher on the 3  $\mu\text{m}$  spacing at  $2.52 \pm 0.65$  (Fig. 3.3H) ( $p < 0.001$  KS Test). These observations indicate that both temporal dynamics of actin oscillations and local spatial enrichment of actin are consistent features of B cells spread on patterned substrates.

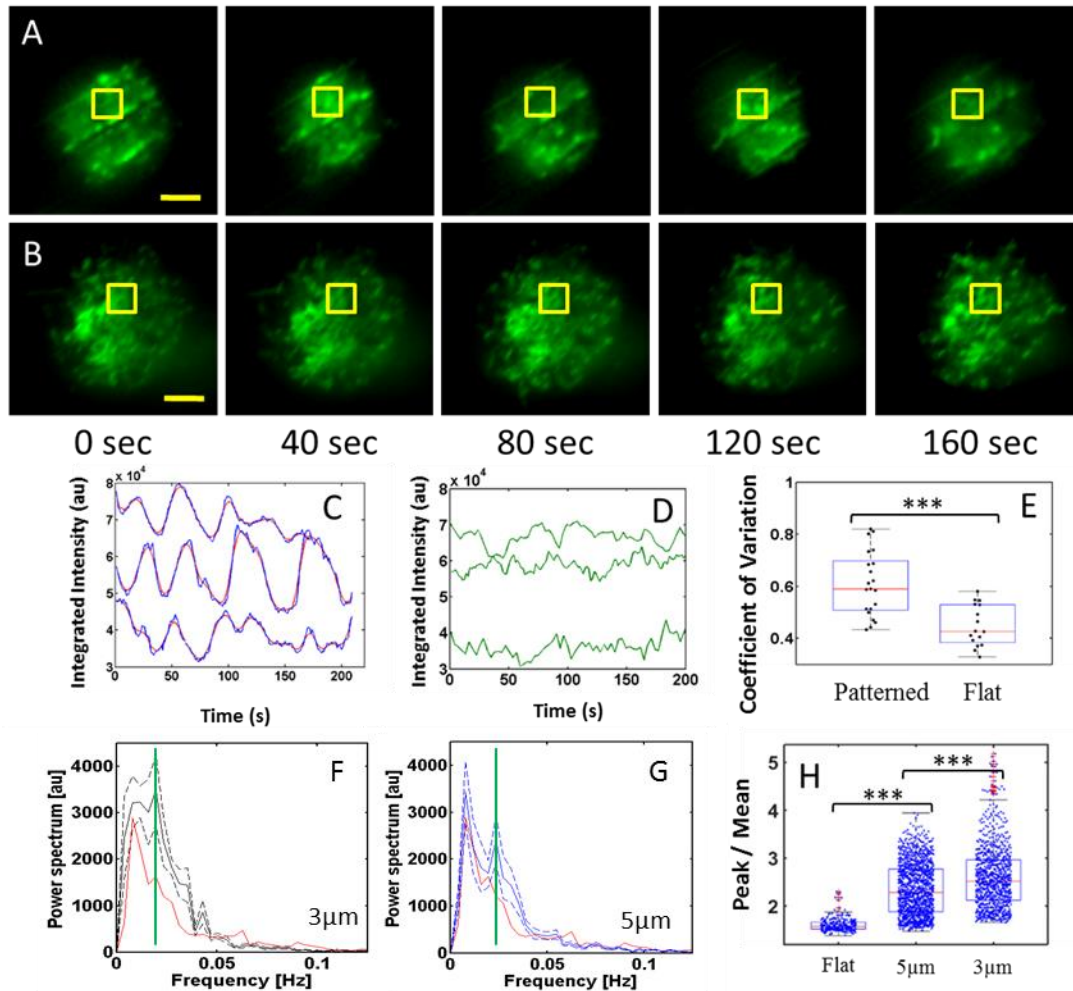


**Figure 3.3: Effect of topographically patterned substrates of 3  $\mu\text{m}$  and 5  $\mu\text{m}$  spacings on B cells.** (A) EGFP-actin A20 B cell on patterned substrate with 5  $\mu\text{m}$  spacing exhibiting actin oscillations. Scale bars are 5  $\mu\text{m}$ . Yellow ROI is centered over oscillation zone (B) EGFP-actin A20 B cell on flat substrate exhibiting no actin contractions with similar ROI. (C) Examples of actin intensity dynamics on patterned substrates of ROIs of 5  $\mu\text{m}$  diagonals. (D) Examples of actin intensity dynamics on flat substrates for ROIs of 5  $\mu\text{m}$  diagonals. (E) Coefficient of variation of actin dynamics on patterned and flat substrate (5  $\mu\text{m}$  and 3  $\mu\text{m}$  values were not significantly different). (F) Composite power spectrum of actin intensity oscillations

for a cell exhibiting actin oscillations on 3  $\mu\text{m}$  patterned substrates. Peak is at 0.02 Hz indicated by green line. Dotted line indicates 99% confidence interval. Red line indicates B cell on flat substrate. (G) Composite power spectrum of actin intensity oscillations for a cell exhibiting actin oscillations on 5  $\mu\text{m}$  patterned substrates. Peak is at 0.025 Hz indicated by green line. Dotted line indicates 99% confidence interval. Red line indicates B cell on flat substrate. (H) Whole cell peak to mean actin intensity for all frames (N=9 flat, N=16 5  $\mu\text{m}$ , and N=15 3  $\mu\text{m}$  cells) ( $p \ll 0.001$  KSTest).

Periodic actin oscillations and actin enrichment along ridges can be more readily observed when actin intensity is processed using pixel-wise intensity autocorrelations. The fluctuations of intensity away from the time-average value was computed using

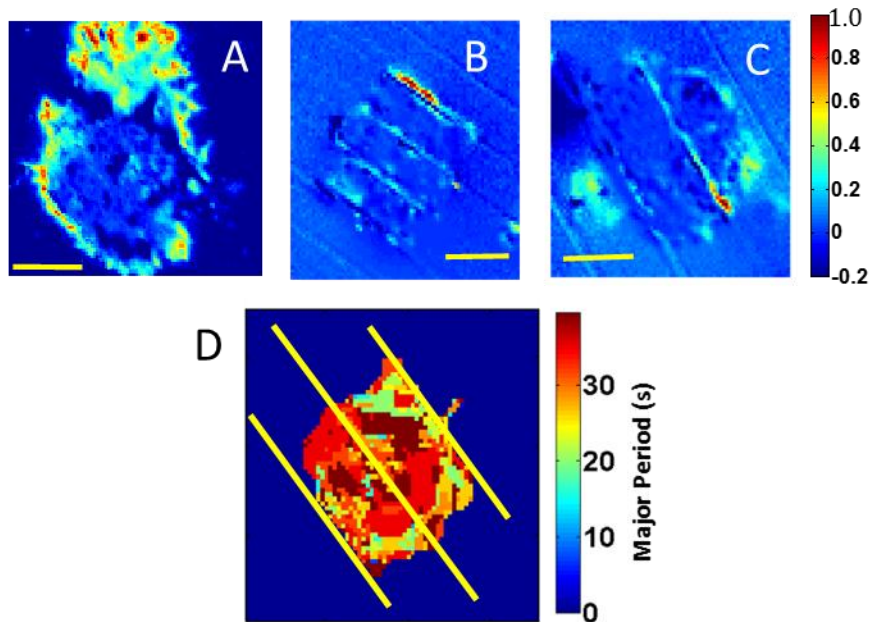
$$\delta I_{xy}(t) = I_{xy}(t) - \frac{1}{T} \int I_{xy}(t) dt \quad (1)$$

The pixel-wise autocorrelation was the computed using

$$G_{xy}(\tau) = \frac{\langle \delta I_{xy}(t) \cdot \delta I_{xy}(t + \tau) \rangle}{\left[ \frac{1}{T} \int I_{xy}(t) dt \right] \left[ \frac{1}{T} \int I_{xy}(t) dt \right]} \quad (2)$$

An autocorrelation sum heatmap was made by summing each pixel over all autocorrelation values. The semi-static buildup of actin along ridges can be observed in the autocorrelation sum heatmap, where the most correlated regions are along the ridges instead of in the lamella as seen on the flat substrate (Fig. 3.4A-C). The major period from each pixel's power spectrum was then plotted as a heat map (Fig. 3.4D) for a clear picture of the size and spatial correlation of actin oscillation zones. The central ring in dark red, surrounding the ridge indicates the extent of the actin

contraction



zone.

**Figure 3.4: Actin oscillation and ridge-adjacent accumulation analysis.** A) Autocorrelation heat map of an EGFPactin A20 cell on a flat substrate. B) Autocorrelation heat map of an EGFPactin A20 cell on 3  $\mu\text{m}$  ridged substrate. C) Autocorrelation heat map of an EGFPactin A20 cell on 5  $\mu\text{m}$  ridged substrate. D) Heatmap of major periods of single pixels within a cell after application of high pass filter (width 100s). Central region shows a spatially correlated region of the actin contraction zone.

### 3.2.3 Signaling downstream of BCR cross-linking is necessary for actin-based contractions

In order to test whether the observed actin intensity dynamics and ridge-adjacent enrichment were specific to BCR stimulation, we coated the nanoridges with the

protein transferrin, which allows B cells to bind via transferrin receptor but does not induce BCR activation.. EGFP-actin expressing A20 B cells adhered to the surface but failed to exhibit any actin oscillations or enrichment along the ridges, as can be seen in Figure 3.5A. Peak to mean analysis, to evaluate whether non-activating ligand also induces actin enrichment along ridges, was performed. While activating antibody results in a peak to mean value of  $2.47 \pm 0.37$  while peak to mean values of B cells on non-activating ligand resulted in a median value of  $1.59 \pm 0.13$  as seen in Figure 3.5B. These values indicate that actin enrichment along ridges requires contact with activating antigen.

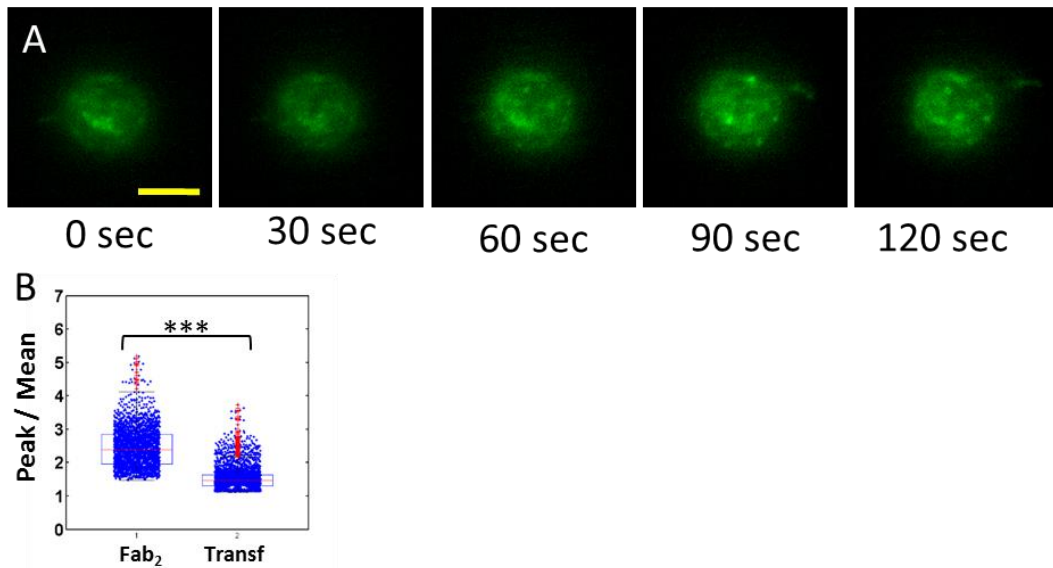


**Figure 3.5: Transferrin controls.** A) TIRF image of EGFP-actin A20 B cell spread on 5  $\mu\text{m}$  spaced ridges coated with transferrin. B) Peak to mean actin intensity ratio of B cells spread on antibody coated and transferrin coated patterned substrates ( $p < 0.001$ ).

Although it is clear that the actin enrichment along ridges and actin contractions require B cell activation and not simply adhesion to the surface, it is still necessary to identify which components of the BCR signaling cascade are responsible for driving this phenomenon.

In order to test whether Syk inhibition precludes these actin dynamics, we used the inhibitor piceatannol, which is a phenolic stilbenoid that competes for the tyrosine containing substrate binding site [124]. At concentrations as low as 10  $\mu\text{M}$  [125], piceatannol is known to be an effective inhibitor of B cell Syk activity, while a concentrations of 50  $\mu\text{M}$  have been shown to inhibit cytokine release in mast cells [126] .

B cells were allowed to spread on surfaces with 3  $\mu\text{m}$  and 5  $\mu\text{m}$  ridge spacings and observed as they initiated characteristic periodic actin enrichments. Six minutes after initiation of spreading, when the cells had reached their greatest spread area, 50  $\mu\text{M}$  piceatannol was added to the medium and imaging was continued (Fig. 3.6A-B). Within seconds of inhibitor addition, the periodic actin enrichment ceased (Figs. 3.6C). This reduction in actin dynamics was quantified by calculating the coefficient of variation of actin intensity over time as previously described, which is dramatically reduced in the presence of piceatannol (Fig. 3.6D). Traces were detrended for loss of intensity due to photobleaching before processing. Further, actin enrichment along the ridge base was significantly reduced, which is reflected in the dramatic reduction of the measured peak to mean values of actin intensity (Fig. 3.6E). This reduction

indicates that both repeated actin enrichments and semi-static actin enrichments are not simply induced by the geometry of the substrate, but are dependent on competent signaling of the BCR.

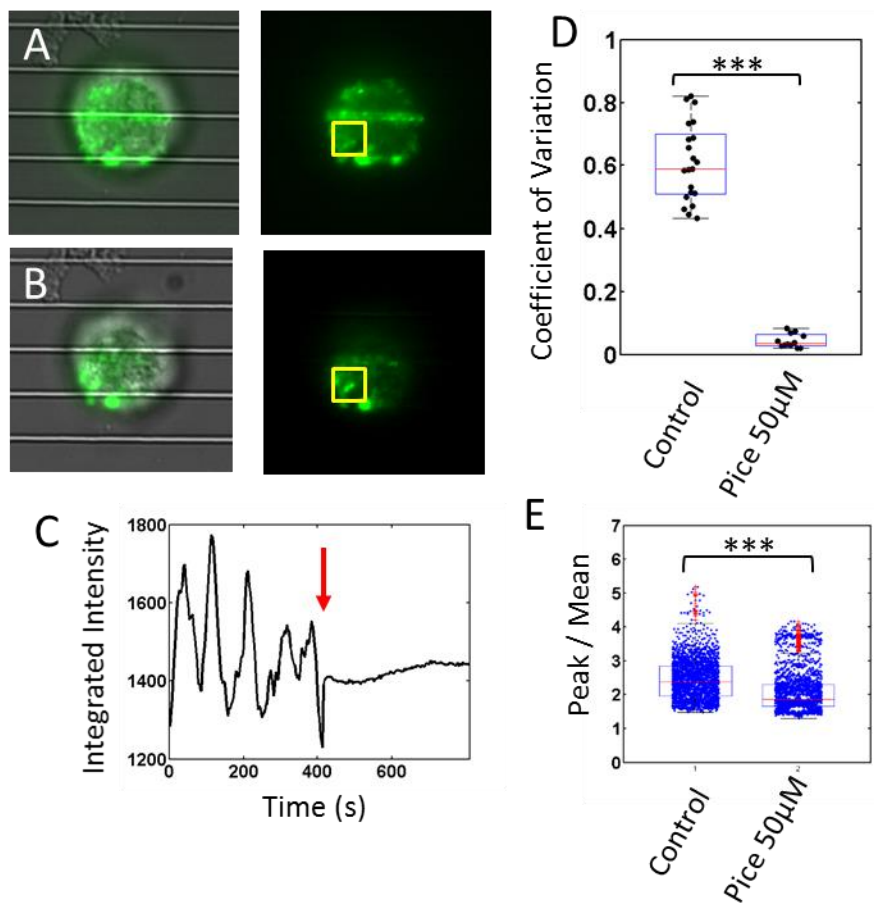


**Figure 3.6: Actin oscillations are mediated by Syk.** A) GFPactin A20 cell spread on a 5µm ridge separation. B) The same GFPactin A20 cell on a 5µm ridge separation two minutes after the addition of 50 µM piceatannol. C) Actin intensity within the ROI (shown in yellow in panels A and B) before and after the addition of piceatannol, where the red arrow indicates the time of inhibitor addition. D) Coefficient of variation before and after piceatannol addition (n=21, n=12 respectively, p<0.001 KS test). E) Peak to mean ratio of actin intensity for cells on 3 and 5 µm ridges before and after piceatannol addition (p<<0.001 KS test).

### 3.2.4 Myosin IIA regulates actin oscillations

The molecular motor myosin can provide contractility within a cell by binding two actin filaments and walking along both of them in opposite directions forcing filaments to slide past each other. In a cross-linked network, actin filaments are unable to slide freely, and instead the network buckles and contracts [58, 127]. Additionally, this myosin based contractility often takes on an oscillatory form [128-130]. Thus, we suspect that myosin II may drive the actin oscillations observed on the ridged substrates. In order to test the role of non-muscle myosin IIA in periodic actin contractions, cells were again allowed to spread on large patterned ridges and the inhibitor Y-27632 was added after 6 minutes. The selective Rho-associated protein kinase (ROCK) inhibitor Y-27632 has been shown to be an effective inhibitor of non-muscle myosin IIA activity by preventing the phosphorylation of myosin light chain kinase (MLCK) by ROCK [131]. We found that addition of 10  $\mu$ M Y-27632 after spreading abolished actin oscillations, as shown in time lapse images of EGFP-actin cells (Fig. 3.7A-B) and time series of integrated actin intensity within an ROI (Fig. 3.7C). The actin intensity within the contact zone remained consistent with the baseline actin intensity during periodic enrichment. The coefficient of variation of the intensity time series was significantly reduced after addition of Y-27632 (Fig. 3.7D). The actin dynamics were similar to those seen on flat substrates, but repeated actin contractions ceased. Our results indicate that actin accumulation is not dependent on non-muscle myosin IIA activity, but that its activity is necessary for maintaining

repeated cycles of actin oscillations.

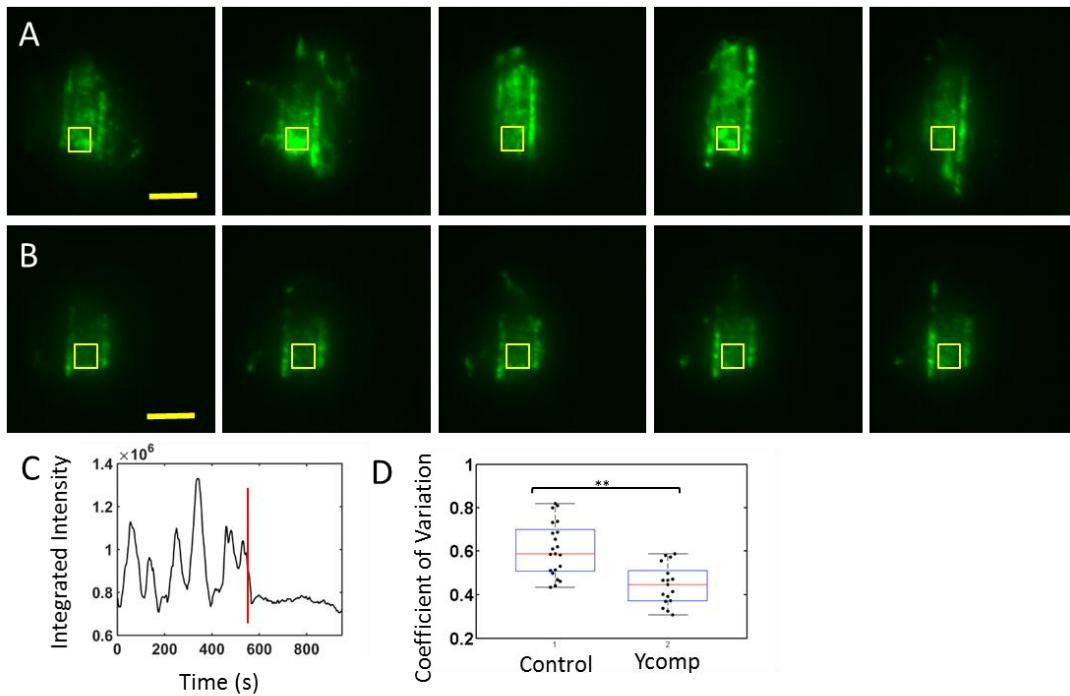


**Figure 3.7: Actin oscillations are mediated by myosin.** A) EGFP-actin B cell spread on a 5 μm patterned substrate exhibiting actin contractions. Scale bars are 5 μm. B) EGFP-actin B cell spread on a 5 μm patterned substrate after Y-27632 10 μM addition at 6 minutes after spreading. C) Integrated intensity of the ROI region before and after Y-27632 addition. D) Coefficient of variation for whole cell integrated intensity before and after Y-27632 addition (N=21, N=17 respectively p=0.004 KS test).

### 3.2.5 Role of topography on BCR clustering

Given the demonstrable coupling between the actin cytoskeleton and BCR cluster motions, we investigated the location and dynamics of BCR clusters for B cells

spread on patterned substrates. Using custom Matlab programs, which identify clusters based on a predetermined threshold and find their distance from ridges, the distribution of BCR clusters was determined. On the larger set of ridge spacings (3 and 5  $\mu\text{m}$ ) we found the distribution of BCR clusters to be non-homogeneous, as compared to how they appear on glass substrates (Figs. 3.8A-C). Further analysis showed that the individual clusters were brighter on ridged substrates than on flat substrates as evidenced by the Peak / Mean ratio as defined in section 3.2.2 (Fig. 3.8D). These results indicate that in the presence of ridges BCR form clusters with higher BCR density, which are hence brighter relative to the mean. The distribution of clusters showed preferential groupings of clusters at  $\sim 0.8 \mu\text{m}$  from the ridge. The least likely position for BCR clusters was in between the two ridges (Fig. 3.8E-F), whereas on a flat substrate BCR clusters were to be randomly distributed (Fig 3.8G) when measured with respect to a virtual ridge bisecting the cell. Histogram distribution BCR distances on 3  $\mu\text{m}$  and 5  $\mu\text{m}$  ridged substrates were found to be significantly different from BCR distributions on flat substrates using the KStest. We hypothesized that a greater density of BCR clusters in between the two ridges might result from the accumulation of actin near the ridges that the topography induces. To compare these two distributions we evaluated actin intensity line profiles perpendicular to the direction of the ridges (3.8H-J). Peaks were identified in Matlab using a minimum threshold of  $(2/3)$  greater than the difference between the mean intensity and the minimum intensity. These peaks were then measured for width at half height and plotted in a similar histogram (Fig. 3.8 K). This figure shows an extinction of actin enrichment at the 0.8  $\mu\text{m}$  distance, indicating that these

phenomena may be related. As we have previously shown, dense accumulation of polymerized actin can exclude large BCR clusters.

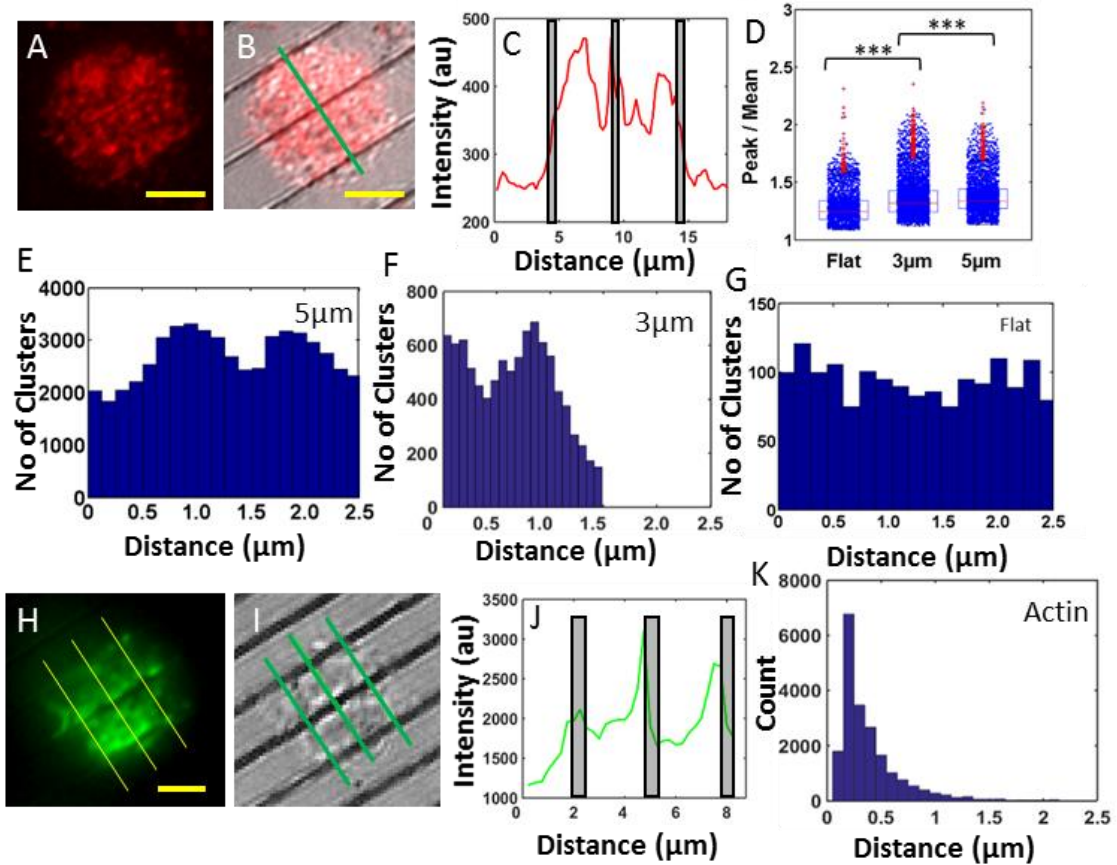


**Figure 3.8: BCR analysis on patterned substrates.** BCR-tag labeled A20 cell on 5µm ridge spacing shown in TIRF (A) and with IRM to emphasize location of ridges (B). Green line indicates line profile. Scale bars are 5 µm. C) AF546-labeled BCR intensity line profile. Grey bars indicate ridges. D) Peak to mean ratios of AF546 labeled BCR on flat and patterned substrates ( $p < 0.001$  KStest). E) Histogram of BCR cluster locations with respect to the nearest ridge for 5 µm ridged patterns. F) Histogram of BCR cluster locations with respect to the nearest ridge for 3 µm ridged patterns. G) Histogram of BCR cluster distribution on a flat substrate. Distances are measured from a virtual “ridge” bisecting the cell. H) GFPactin A20 B cell on patterned substrate. Yellow lines indicate perpendicular actin profiles. Scale bar is 3 µm. I) Cell from A shown in IRM to emphasize location of ridges. J) Single actin line

profile indicating enrichment peaks near ridges. Ridges shown in gray boxes. K)  
Histogram of actin enrichment widths.

### 3.3 Small ridge spacings induce actin protrusions

#### 3.3.1 Protrusion velocity and length are modulated by pattern width

Given the notable effects of large ridge spacings on B cell actin dynamics, we next sought to examine how smaller ridge spacings affect B cell behavior. On smaller ridge spacings (ranging from 0.8 to 1.5  $\mu\text{m}$ ) we observed traveling waves or fronts of actin along the ridges in both directions. At the cell periphery, these resemble filopodia-like protrusions and retractions along the base of the ridges. By comparing kymographs from adjacent ridges it was observed that protrusions were transient and not correlated from ridge to ridge. Both the length and the rates of these actin-based protrusions and retractions were further influenced by the spacing of the ridges.

Protrusion lengths were measured using kymography as shown in Figure 3.9. The base of the protrusion was defined as the region exhibiting stable actin fluorescence intensity for at least thirty seconds and the tip of the protrusion was defined at the furthest maximum point the actin protrusion reached, as shown in Figure 3.9C-D. We found that actin protrusion dynamics were regulated by the width of the ridges.

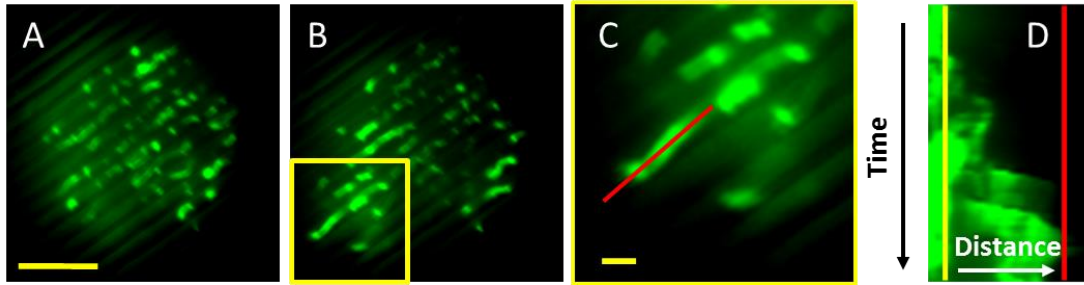


**Figure 3.9: Technique for measuring protrusion length.** (A) B cell spread on patterned ridges with 1.2  $\mu\text{m}$  ridge spacing before exhibiting protrusion. Scale bar is 5  $\mu\text{m}$ . (B) Same B cell exhibiting actin protrusion. (C) Magnification of the yellow box in panel B showing kymograph line drawn on actin protrusion. Scale bar is 1  $\mu\text{m}$ . (D) Kymograph of actin protrusion where the protrusion base is marked in yellow and the protrusion tip is marked in red.

Examples of protrusions along different ridge spacings are shown Figure 3.10A. These actin based protrusions occur most often on the 1.0  $\mu\text{m}$  ridge spacing in 87% of cells (Fig. 3.10B), which is in contrast with B cells spreading on flat substrates, on which  $\sim 25\%$  of cells showed similar narrow protrusions. The longest protrusions were formed on the 1.0  $\mu\text{m}$  ridge spacings with a median value of  $1.89 \pm 0.26 \mu\text{m}$  (Fig. 3.10C). The speed of protrusions as they extended along ridges was measured using kymography (Fig. 3.10D). Protrusion speeds achieved the highest median value of  $5.18 \pm 0.51 \mu\text{m}/\text{min}$  on ridges with 1.2  $\mu\text{m}$  spacing (Fig. 3.10E). When actin protrusions are imaged concurrently with the location of BCRs it becomes clear that each protrusion is tipped with a group of tightly clustered BCRs (Fig. 3.10F). As the protrusion extends the BCR cluster moves along the groove ahead of the actin extension (Fig. 3.10G).

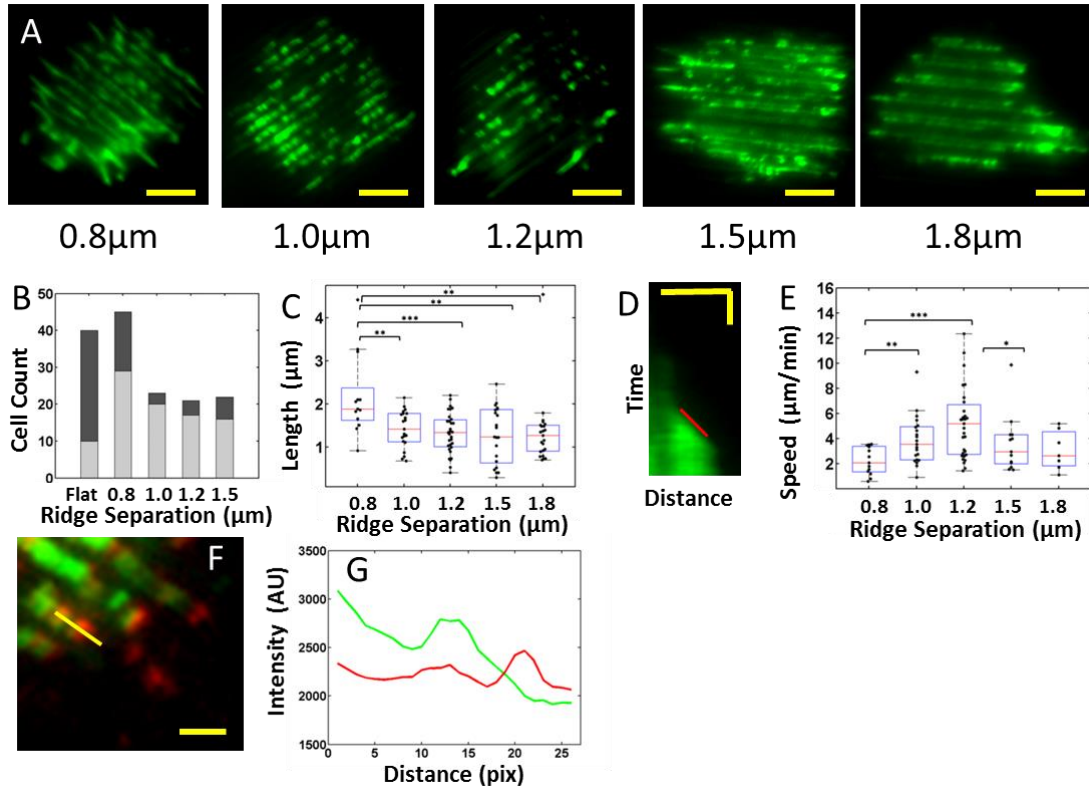


**Figure 3.10: Patterned substrates induce actin-based protrusions on ridge separations less than 2 microns.** A) Examples of EGFP-actin A20 cells spread on patterns of different ridge spacings (0.8 $\mu\text{m}$  – 1.8 $\mu\text{m}$ ). Images obtained with TIRF imaging, revealing the actin in spaces between ridges. Scale bars are 5 $\mu\text{m}$ . B) Number of cells exhibiting protrusions (light grey) and number not exhibiting protrusion (dark grey) on different ridge spacings. C) Length of actin based protrusions on ridges of various spacings. D) Kymograph of an EGFP-actin protrusion along the base of a 1.0  $\mu\text{m}$  ridge. Scale bars are 1  $\mu\text{m}$  and 30 seconds. E) Speed of actin based protrusions on patterns of various spacings. F) Example image of BCR tipped actin protrusions. Scale bar is 1.0  $\mu\text{m}$ . G) Line profile of EGFP-actin (green) and AF546 BCR (red) from image in (f).

### 3.3.2 N-WASP and ARP2/3 branching are necessary for actin based protrusions

We next tested the role of the actin branching protein Arp2/3 in the formation and maintenance of actin based protrusions along narrowly spaced ridges. We used CK666, a small molecule inhibitor of the Arp2/3 complex, which stabilizes the inactive state of the complex. Similar spreading experiments were performed as before, but with the addition of 50  $\mu$ M CK666 upon six minutes of cell spreading, after protrusions had been observed. After the addition of CK666, we observed that no new protrusions were formed in spreading cells, but those that were already formed did not disappear (Fig. 3.11 A-B). This result indicates that Arp2/3 is required in part to generate the actin wave dynamics along ridges via the nucleation of new actin branches, resulting in actin based protrusions at the cell edge.

In previous studies the role of N-WASP in B cell activation and clustering has been established. N-WASP assists in the down-regulation of B cell signaling, and its inhibition is associated with an increased amount of surface proximal actin in B cells spread on supported lipid bilayers [57]. To test the effects of N-WASP on actin-based protrusions on patterned substrates, cells were incubated in 10  $\mu$ M wiskostatin, a selective inhibitor, and allowed to spread on patterned substrates. Although cells were able to spread effectively (Fig. 3.11C), actin-based filopodia-like protrusions were precluded. Of N = 11 observed cells, none formed protrusions. This implies that actin based protrusion formation is dependent on the function of N-WASP.

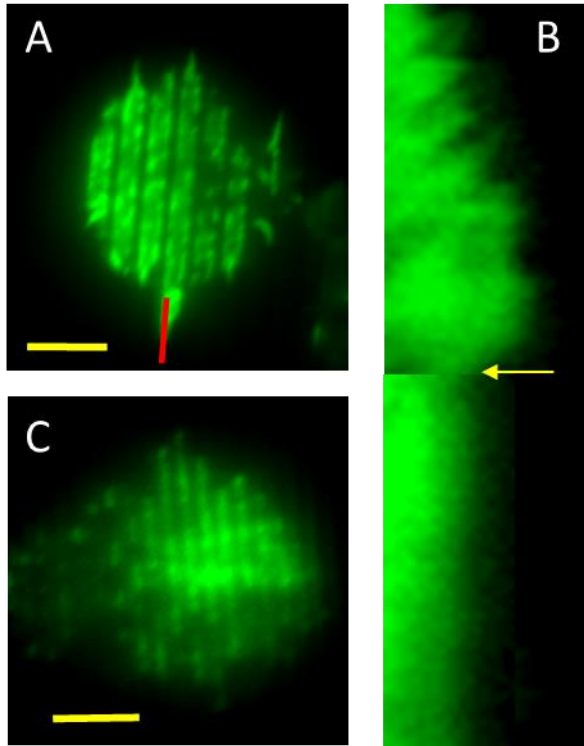


**Figure 3.11: Actin protrusions on small ridge spacings (0.8  $\mu\text{m}$  – 1.5  $\mu\text{m}$ ) are stalled by Arp2/3 and N-WASP inhibition.** A) EGFP-actin A20 B cell exhibiting characteristic protrusions along 1.5  $\mu\text{m}$  ridge spacings. B) Kymograph of protrusion on 1.5  $\mu\text{m}$  ridge spacing. The inhibitor CK666 (50  $\mu\text{M}$ ) is added at the arrow. The kymograph shows that the protrusions freeze. C) EGFP-actin A20 B cell on 1.0  $\mu\text{m}$  ridge spacing incubated in 10  $\mu\text{M}$  wiskostatin showing the lack of actin protrusions.

### 3.3.3 Patterned substrates induce waves and oscillations in primary B cells

The biphasic actin behavior of B cells spread on ridged substrates was also observed with primary B cells. Transient actin enrichment was observed for primary B cells spread on 5  $\mu\text{m}$  ridge spacings (Fig. 3.12A), which exhibited a recurring oscillatory

nature similar to that found in A20 B cells (Fig. 3.12C). Furthermore, actin-based protrusions similar to those seen on the smaller spacings were observed for primary cells on 1.5  $\mu\text{m}$  spacing (Fig. 3.12B). This indicates that the observed biphasic actin dynamics is not only a feature of the A20 B cell line, but an intrinsic feature of B cells and their response to topographically patterned surfaces. When actin based contractions were quantified with the coefficient of variation, as previously performed, the median value for primary cells was  $0.43 \pm 0.08$  on patterned substrates and  $0.33 \pm 0.08$  on flat substrates (Fig. 3.12D). Thus we have demonstrated that transient actin enrichments are induced on patterned substrates in primary B cells as well.

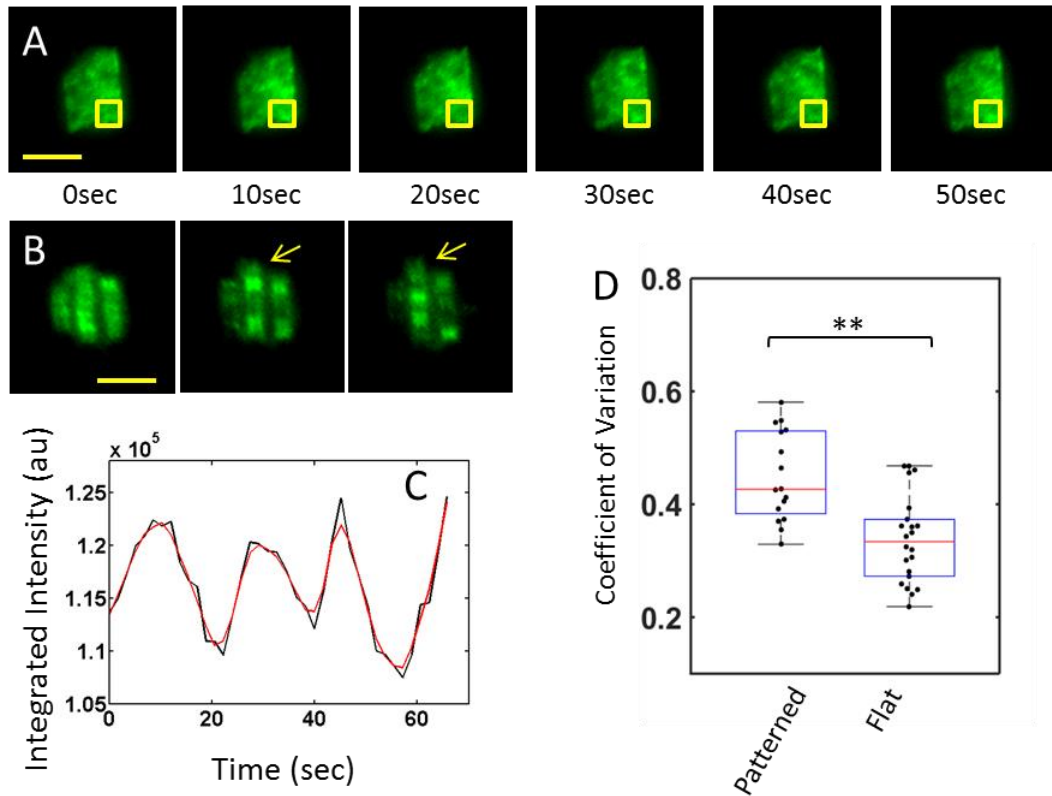


**Figure 3.12: Primary B Cells exhibit actin on patterned substrates.** A) LifeAct primary B cell exhibiting actin contractions on a 5 μm ridge spacing. Scale bars are 5 μm. B) LifeAct primary B cell exhibiting a protrusion and retraction along a 1.5 μm ridge spacing. C) ROI integrated actin intensity for a primary cell exhibiting actin contractions on a 5 μm ridge spacing. D) Coefficient of variation for LifeAct Primary B cells on patterned substrates (3 and 5 μm) and on flat substrates (p= 0.0012 KStest).

## 3.4 B cell signaling is modulated by ridge spacing

### 3.4.1 Calcium oscillation frequency dependent on ridge spacing

A prominent characteristic of B cell activation is the release of intracellular calcium stores from the endoplasmic reticulum to the cytoplasm, which then subsequently triggers the opening of CRAC channels in the plasma membrane, allowing more calcium influx, which can result in intracellular calcium oscillations.

Calcium oscillations have been observed in numerous cell types, such as cardiac and neuronal cells. While a single sustained calcium influx in some regimes can be thought of as the flipping of a switch which sets into action a series of expression changes, calcium oscillations can be related to that of a radio signal, whereby the frequency and amplitude of oscillations encodes information for the cell. The decoding of  $\text{Ca}^{2+}$  oscillations is carried out by frequency-sensitive transcriptional factors. This molecular mechanism of oscillation decoding is thought to take place in the on/off kinetics of calcium binding with certain kinases and phosphatases. Three of these transcription factors play major roles in the activation of B lymphocytes. NF- $\kappa$ B, MAPK and NFAT are sensitive to calcium oscillations with a period of between 10 and 1000 seconds [132]. This is also the range of periods within which B lymphocytes have been observed to undergo oscillations under a variety of conditions.

Calcium has many other cellular effects, including a highly regulatory effect on the dynamics of the actin network. Calcium availability controls the contractile dynamics

of actin networks through myosin regulation, which was first found to be true for myosin rich muscle cells, but is also seen in many other cell types.

The relation between calcium oscillations and the actin cortex has been investigated in more detail in mast cells. Upon antigenic stimulation of the mast cell FC $\epsilon$ RI receptor, cell-wide calcium oscillations commence. These oscillations, having a period of ~30s, have then been observed to drive oscillations of N-WASP [133]. Furthermore, the concentration of calcium in mast cells has been found to be markedly increased by depolymerization of the actin cytoskeleton using cytochalasin D [134]. This effect was precluded when cells were incubated in the actin-stabilizing drug jasplakinolide, demonstrating the coupling of intracellular calcium levels with the integrity of the actin cortex.

The intracellular concentration of calcium can be used to understand better the effects of ridged substrates on B cell signaling. To observe intracellular calcium concentrations the non-ratiometric calcium sensitive dye Oregon Green 488 BAPTA-1 (OGB1) was loaded into A20 B cells (see Methods 5.3.1). OGB1 has a relatively high affinity ( $K_d \sim 170$  nm) for  $Ca^{2+}$  and low phototoxic effects [135]. OGB1 loaded A20 cells were imaged on either flat substrates or ridged substrates in TIRF after 6 minutes of spreading. TIRF imaging of OGB-1 intensity allowed for the measurement of cell integrated intensity over time, revealing calcium pulses. Calcium oscillations were observed in all B cells which were fully spread on activating substrates including flat surfaces (Fig. 3.13A). Calcium oscillations were also

observed in cells on ridged substrates, but with varying periods (Fig. 3.13B). The frequency of calcium pulses was quantified by peak to peak measurements in Matlab taken after a 6 second rolling average. B cells spread on flat substrates have the shortest calcium oscillation periods, with a median value of  $13.9 \pm 0.6$  seconds. Cells spread on the 5  $\mu\text{m}$  and 3  $\mu\text{m}$  ridge spacings had similar periods, where oscillations on 5  $\mu\text{m}$  exhibit markedly slower calcium oscillations with a period of  $55.6 \pm 4.0$  seconds. Oscillations were even slower on 1.5  $\mu\text{m}$  spacing with an average period of  $94.3 \pm 10.6$  seconds (Fig. 3.13C). These results indicate that the effects of a topographically patterned substrate extend beyond affecting the actin distribution and behavior: it is further communicated through the signaling machinery to affect the calcium feedback within the cell.

To test whether the modulation of calcium frequency can be transmitted through the actin cytoskeleton for B cells, we used the inhibitor Latrunculin-A (LatA), which is a potent inhibitor of actin polymerization. LatA at 100nM was added after the establishment of calcium oscillations (~ 8 minutes) on flat substrates. Peak to peak calcium measurements were made as before and it was found that LatA does indeed slow calcium pulses (Fig. 3.13D). While control cells on the flat substrate had a median value of  $13.9 \pm 0.6$  seconds, the addition of LatA results in a median peak to peak value of  $24.9 \pm 0.4$  seconds. The slowing of these oscillations points toward a system in which actin dynamics can influence B cell calcium signaling. In many systems oscillatory behavior can result from a delayed feedback loop. Therefore, we hypothesized that such a feedback loop may exist between the actin cytoskeleton and

calcium influx. To explore this possibility, we inhibited the release of calcium using 1 $\mu$ M Thapsigargin. Thapsigargin is a non-competitive inhibitor of the endoplasmic reticulum Ca<sup>2+</sup> ATPase. Upon addition of Thapsigargin in cells plated on ridged substrates, actin oscillatory behavior ceased (Fig. 3.13E). This change was reflected in a drop in the coefficient of variation (Fig. 3.13F). Taken together, these results indicate the existence of a feedback loop between the actin cytoskeletal dynamics and the influx of calcium. The observation that both of these oscillatory events take place on the same time scale ( $\sim$ 50s for 3 $\mu$ m and 5 $\mu$ m spacings) further supports this argument.

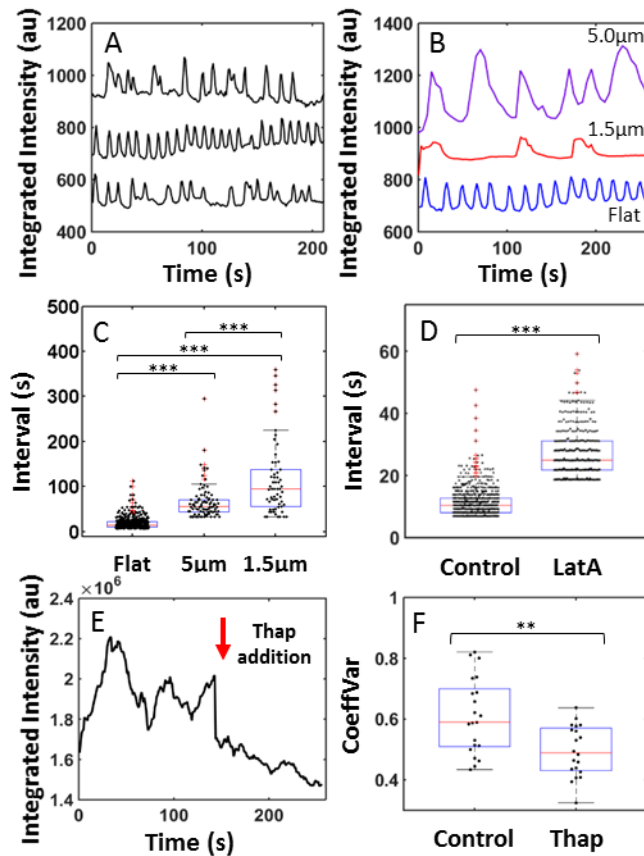


**Figure 3.13: Patterned substrates influence the distribution of BCR clusters and intracellular calcium signaling.** A) Representative OGB-1 integrated A20 cell

intensities on flat substrates. B) Integrated whole cell intensity of calcium dye OGB-1 of representative cells on flat and patterned substrates. Flat (blue), 5  $\mu\text{m}$  (purple), 1.5  $\mu\text{m}$  (red). C) Peak to peak time intervals of OGB-1 intensity for cells on three substrate patterns: flat (n=27), 5  $\mu\text{m}$  (n=17), 1.5  $\mu\text{m}$  (n=15). All intervals are significantly different ( $p \ll 0.001$  KStest). (D) Peak to peak time intervals of OGB-1 intensity for cells on a flat substrate with and without the addition of 100nM Latrunculin-A: control (n=27) and LatA (n=20) ( $p \ll 0.001$  KStest). (E) Representative trace of EGFP-actin A20 cell ROI integrated intensity before and after 1 $\mu\text{M}$  Thapsigargin addition. Red arrow indicates time of addition. (F) Coefficient of variation for whole cell integrated EGFP-actin intensity before (control) and after 1 $\mu\text{M}$  Thapsigargin addition (N=21, N=20 respectively  $p=0.0046$  KS test).

### 3.5 Discussion

The presentation of antigen to B cells occurs mainly within SLOs by antigen presenting cells. APCs such as follicular dendritic cells and marginal zone macrophages have convoluted membranes with many topographical features such as dendrites, membrane ruffles and invaginations. As other physical factors, such as ligand mobility, substrate stiffness, and antigen density have profound effects on B cell actin dynamics and activation, it is clear that the role of substrate topography on these factors requires investigation. Using a set of variably spaced patterned ridges, we have demonstrated that B cells respond to substrate topography with a modulated BCR distribution patterns, oscillatory actin dynamics and calcium signaling. We have

demonstrated that B cells on 3  $\mu\text{m}$  and 5  $\mu\text{m}$  ridge separations undergo periodic actin contractions after achieving a final spread area. These contractions were shown to be non-muscle myosin II mediated and dependent on competent BCR signaling. As a measure of B cell signaling, robust calcium oscillations were measured on ridged substrates. Ridged substrates were found to slow down the calcium oscillations, indicating that B cell signaling responds to the topography of the antigen presenting substrate. A second regime of actin behavior was found for B cells on ridged substrates with 0.8 to 1.8  $\mu\text{m}$  separations. On these smaller ridge spacings actin formed protrusions along the base of ridges, which was modulated both in speed of growth and length by the spacing of the ridges. Finally, the modulation of actin dynamics by ridged substrates was also confirmed in LifeAct primary murine B cells.

The standard view of B cell –antigen contact shows a B cell undergoing rapid lamellipodial spreading on a flat or smooth substrate. This conceptualization clearly requires rethinking, given our results. The actin cytoskeleton actively responds to the presence of topographical features. Furthermore, as Syk is known to regulate the actin meshwork in mast cells [136] and B cells [137], following its autocatalytic activation downstream of BCR activation [138], it may provide a link between BCR activation and local patterning of the actin cytoskeleton. A consistently higher actin concentration around ridges, as evidenced by higher peak to mean values indicates that topographical features promote enhanced actin polymerization in their vicinity, which can lead to cell edge protrusions (mediated by bidirectional actin waves) under some conditions and actin intensity oscillations (potentially mediated by large scale

contractions of the actin network) under others. In the context of B cell spreading on the surface of an antigen presenting cell, this behavior may be advantageous as different actin modules can be employed upon encountering variable membrane features, which then allow the B cell to encounter as much antigen as possible and therefore maximize activation. Modulated calcium influx frequency indicates that the configuration of the membrane and actin network influence the operation of calcium channels and may therefore lead to feedback of continued actin dynamics. Further evaluation of comparative levels of B cell activation on ridged substrates could help to determine the role of topography during signaling activation, which occurs during the first six minutes after contact. Evaluation of eventual B cell antibody production could help to determine total cell activation levels. This information is critical for a complete picture of B cell immune function and could further aid in the development of better vaccines and immunotherapies, by provoking topographically specific responses.

# Chapter 4: Conclusions and Future Directions

## 4.1 Conclusions

B cells, as a part of the adaptive immune system continually circulate throughout the body, performing immune surveillance. When responding to sites of infection B cells often gather activating antigen from the surface of other cells. These antigen presenting cells possess complex membrane topographies and variable membrane fluidity, depending on the type of cell and its location within the body. Thus it is important that the role these physical factors play in B cell dynamics and activation is well studied. In this thesis we focused on the morphology, actin dynamics and signaling of B cells when presented with physical constraints. In Chapter 2 we examined the morphology, actin dynamics and signaling of B cells upon encountering either mobile or immobile ligand. We found that presentation of mobile ligand resulted in smaller final spread areas, but larger BCR clusters which propagated higher levels of signaling. Furthermore, actin was found to colocalize with BCR clusters on both immobile and mobile ligand substrates. Importantly, we identified that efficient growth of B cell receptor clusters was driven by active dynamics of the actin cytoskeleton. In Chapter 3 we explored the relationship between substrate topography and B cell actin dynamics and signaling. On topographically patterned substrates with large ridge spacings B cells exhibited large scale actin intensity oscillations. Furthermore, these ridged surfaces modulated the frequency of calcium

oscillations.. On smaller ridge spacings, actin waves traveling along the ridges resulted in protrusions and retractions, which were found to be tipped with BCR clusters.

These results point to the conclusion that B cells are mechanosensitive to the mobility of ligand and to topographical features of the antigen presenting surface. Both physical factors induced not only actin and morphological changes, but also affected signaling – as measured with phosphotyrosine staining and calcium imaging. It is therefore clear that B cells can sense and actively respond to the presence of topographical ridges. Future measurements of comparative antibody production levels may reveal whether these cell changes are profound enough to influence overall B cell function, which would be critical for potential medical applications. Given that the degree to which B cell signaling propagates has a direct relation to antibody production and health of an organism, it is therefore imperative to understand which physical factors may influence these outcomes. This may have applications in vaccine development and immune therapies for cancer as the physical properties of B cells stimulation could potentially be tuned for more effective B cell activation.

While the work presented here answers some important questions about the mechanosensitivity of B cells, other questions naturally arise. Given the variety of actin dynamics demonstrated in Chapter 3, it would be of interest to further explore the boundaries of B cell sensitivity to topography. What, if any, limits exist to the lower and upper bounds of topographical feature size that a B cell can detect? It

would be of interest to explore B cell sensitivity to different types of topographical features as well. Ligand mobility can also be further explored with a more systematic varying of membrane fluidity by varying lipid composition. While the connection between B cell actin dynamics, BCR-dependent signaling and physical environmental factors has been established, the precise molecular mechanisms enacting these changes have yet to be elucidated. Further investigation is required to help expound on these connections and to further our understanding of B cell function.

## 4.2 Future Directions

### 4.2.1 Other topographically patterned geometries

The topographically patterned substrates we utilized in Chapter 3 provided meaningful insights into B cell mechosensitive response. There are, however, many other patterned geometries, which can be explored for their effects on B cell function. The pattern fabrication process employed in the lab of Dr. John Fourkas enables the production of pattern geometries of arbitrary complexity with features as small as 100nm. Currently our lab is exploring the interaction of B cells with patterned features known as nano-posts, which are of 300nm diameter and 200nm in height (Fig. 4.1) which present an analogous physical barrier as that of microvilli or similar protrusive membrane structures. These dots can be varied in diameter, height and separation.

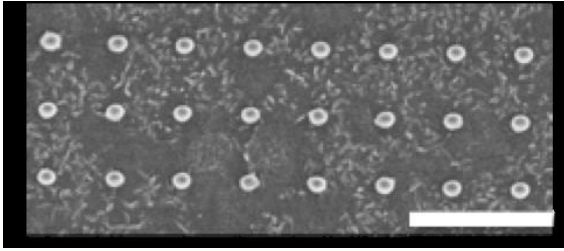


**Figure 4.1: Scanning electron micrographs showing nano-posts fabricated using MAP/RAPID lithography.** Scale bar is 5  $\mu\text{m}$ . Features are  $\sim 200$  nm in height.

Further topographical structures, such as spirals and concentric rings may be helpful in exploring the formation of the cSMAC.

#### 4.2.2 Curvature sensing proteins

A class of proteins, known as curvature sensing proteins, has recently been of interest in their ability to detect and bind to regions of high curvature in the plasma membrane. These proteins possess a characteristic BAR domain which binds to curvatures between  $1/100$  and  $1/300$   $\text{nm}^{-1}$ , which would be present on the tops of the ridges we have examined in Chapter 3. Two such proteins, Bin3 and Mtss (metastasis suppressor 1), are known to be enriched in B cells and both serve as upstream regulators of actin. Dendrites and membrane ruffles as are present on follicular dendritic cells would present positive curvatures well within this range. The effects of curvature sensing proteins on actin dynamics, BCR organization, and B cell signaling would provide further insight into the mechanisms of topography sensing by B cells.

### 4.2.3 Substrate stiffness and B cell activation

Both during migration and while forming contact with antigen presenting cells, B cells encounter physical tissues of a variety of different stiffness. Throughout the body, tissues have a variety of different stiffnesses from muscle (~12kPa) to brain (~50Pa). In many different cell types the stiffness of the substrate can influence migration, the dynamics of the actin cytoskeleton and gene expression changes [139]. T cells have been shown to be mechanosensitive and exert variable forces based on the stiffness of the substrate. These changes were found to be directed by changes in the actin cytoskeleton [140]. Using a technique called traction force microscopy, where fluorescent beads are embedded in gels presenting a variety of Young's Moduli (Fig. 4.2A), not only can the effects of stiffness on B cells be quantified, but also the forces the cell exerts on the substrate (Fig. 4.2B).

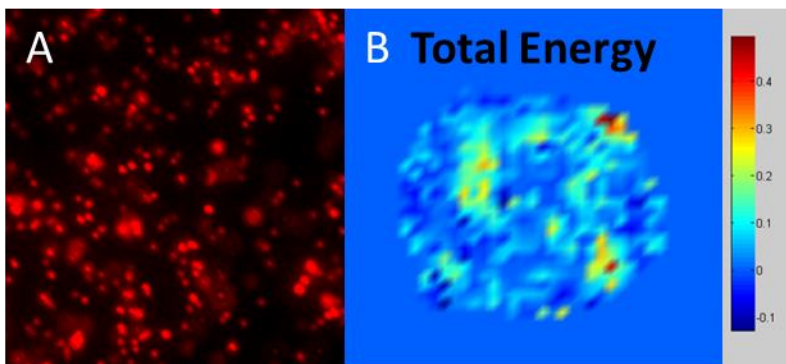


**Figure 4.2: Traction force microscopy.** (A) Field of fluorescent beads embedded in a polyacrylamide gel. (B) Total energy heatmap of a B cell exerting forces on the gel substrate.

Although some preliminary results on the effects of substrate stiffness on B cells have been quantified [141], the forces the B cell exert have not yet been quantified and may prove another important physical parameter influencing B cell behavior.

# Chapter 5: Materials and Methods

## 5.1 Cells and Reagents

### 5.1.1 Reagents

Piceatannol (5mg stock) was procured from Cayman Chemical.

Y-27632 was procured from SelleckChem.

CK666 was procured from Sigma Aldrich.

Wiskostatin was procured from Calbiochem.

LatrunculinA (100 $\mu$ g stock) was procured from Sigma Aldrich.

### 5.1.2 Cell culture

A20 cells or enhanced green fluorescent protein (EGFP)-actin expressing A20 cells were cultured as described previously (19,25). Cells were used at a density  $7 \times 10^5$  cells/mL for imaging. Surface BCRs were labeled with Alexa Fluor 546 labeled mono-biotinylated Fab' fragment of antimouse IgM+G antibody (AF546-mB-Fab'-anti-Ig, 2.5  $\mu$ g/mL, Jackson ImmunoResearch, West Grove, PA), generated as described previously (25) at 4°C before incubating with streptavidin (SA) coated glass and planar lipid bilayers. As a control, cells were incubated with Cy3-labeled

Fab' fragment of goat antimouse IgG (2.88  $\mu\text{g}/\text{mL}$ ) to label surface BCRs and biotinylated transferrin (3.5  $\mu\text{g}/\text{mL}$ ) to label surface transferrin receptor at 4°C before incubating with substrates at 37°C.

## 5.2 Substrate Preparation

### 5.2.1 Glass substrates

Immobile ligand substrate: eight-well glass bottom LabTek (155411, Thermo Scientific, Waltham, MA) dishes were coated with 0.01% PLL for 10 min and dried for 1 h, washed 3  $\times$  with PBS and then coated with 1  $\mu\text{g}/\text{mL}$  SA for 1 h and finally blocked for 10 min at 37°C.

### 5.2.2 Bilayer substrates

Mobile ligand substrate: glass cover slips were cleaned with NanoStrip (539200, Cyantek, Fremont, CA). A lipid mixture of 5 mM and a DOPC/DOPE-cap-biotin ratio of 100:1 was created by vesicle extrusion (610000, Avanti Polar Lipids, Alabaster, AL). Wells were incubated for 10 min with lipids at 4  $\mu\text{M}$ , washed with excess PBS, then incubated for 10 min with 2  $\mu\text{g}/\text{mL}$  SA and washed thoroughly. Lipid mobility was verified using a fluorescence recovery after photobleaching (FRAP) assay. Only substrates with at least 70% recovery (Fig. 5.1) were used for experiments.

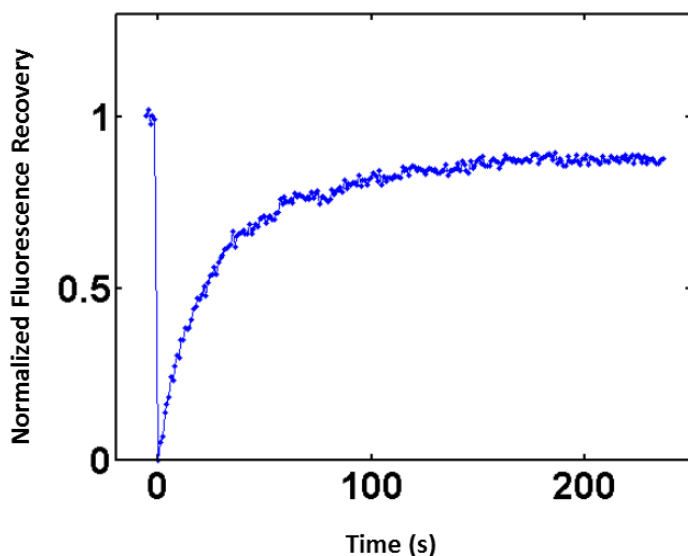


**Figure 5.1: FRAP evaluation of planar lipid bilayer mobility.** Streptavidin coated lipid bilayer substrates were coated with biotinylated antibody (mono-biotinylated Fab'-anti-mouse IgM+G antibody (AF546-mB-Fab'-anti-Ig) generated from the F(ab')<sub>2</sub> fragment) . An area of  $\sim 10 \mu\text{m}^2$  was photobleached using a 561nm laser. The integrated fluorescence intensity of that area, prior to photobleaching, was recorded and normalized to 1. The recovery of integrated fluorescence intensity was measured following photobleaching and the mobile fraction of lipids was recorded (as indicated by the percentage recovery, in this case 87.2%).

After coating, surfaces were washed thoroughly to remove unbound SA. Based on previously published measurements, typical SA densities on bilayer surfaces were estimated to be  $\sim 1500$  per  $\mu\text{m}^2$  (4). Enzyme-linked immunosorbent assay (ELISA) assays were used to confirm similar densities of SA on glass and bilayer substrates (Fig. 5.2).

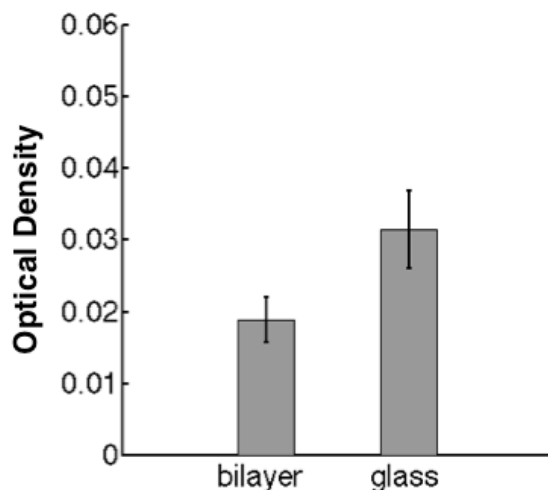


**Figure 5.2: ELISA assay showing levels of streptavidin density on bilayer and glass substrates.** Both glass and bilayer substrates were evaluated for streptavidin density using an ELISA protocol. Values for optical density of the reaction mix after quenching are shown on both substrates (N = 7 trials). Mean values were found to be  $0.02 \pm .003$  and  $0.03 \pm .005$  on bilayer and glass surfaces respectively.

### 5.2.3 Topographically patterned substrates

Topographically patterned substrates were provided by the group of Dr. John Fourkas (University of Maryland, Department of Chemistry and Biochemistry). Nanoscale surface features were created on optically clear substrates using multiphoton absorption polymerization [142]. On the substrate surface a negative-tone photoresist was exposed to a tightly focused, ultrafast laser beam, which causes selective cross-linking within the focal volume. After the initial production of a master surface using this technique, subsequent patterned surfaces were replicated using the soft-lithographic technique called microtransfer molding, wherein the master surface is immersed in polydimethyl siloxane (PDMS) which is then peeled off and cured [143].

The mold is then filled with photocurable acrylic resin and then cured. After curing and separation from the mold, the surface is chemically functionalized using surface acrylate groups via Michael addition for biocompatibility [93]. Surfaces were then coated with 0.01% poly-L-lysine for 10 min and dried for 1 h and then coated with 1.3  $\mu\text{g}/\text{mL}$  Fab2-anti-IgG+IgM overnight, then rinsed 3x with PBS. Before use substrates were blocked with BSA for 10 min at 37°C.

## 5.3 Microscopy

### 5.3.1 Microscopy of live cells

Cells were seeded onto chambers for imaging and maintained at 37°C using an airstream incubator (ASI400 Nevtek, Williamsville, VA). Images were collected using an inverted microscope (TE2000 PFS, Nikon, Melville, NY) with a cooled CCD camera (Coolsnap HQ2, Photometrics, Tucson, AZ) at a frame interval of 3 s. EGFP-actin and fluorescent receptors were imaged with total internal reflection fluorescence (TIRF) using a  $60 \times 1.49$  NA objective lens, a 491 nm laser (100 mW, Andor, South Windsor, CT) for EGFP excitation, and a 561 nm laser (75 mW, Andor) for AF546 excitation.

Calcium imaging was performed by resuspending A20 B cells in HBSS containing 1% FBS, 2  $\mu\text{M}$  OGB1 dye, and 0.02 % F-127. Cells were incubated for 30 min at room temperature. Cells were then washed and maintained in fresh L-15 medium for 15 min at RT to permit intracellular enzymatic hydrolysis of the AM ester to proceed

to completion. Then the calcium loaded A20 B cells were seeded into the chamber and imaged using TIRF and  $60 \times 1.49$  NA objective lens and the 491 nm laser.

### 5.3.2 Immunofluorescence imaging

For intracellular staining, cells were fixed with 4% paraformaldehyde in phosphate buffered saline (PBS) at various time points after incubation, and then labeled with antiphosphotyrosine antibody (4G10, Millipore, Billerica, MA), followed by Cy2-goat antimouse IgG2b (Millipore). For inhibition of actin polymerization, cells were incubated with Latrunculin A (100 nM, L5163, Sigma, St. Louis, MO).

## 5.4 Image Analysis

### 5.4.1 Cluster identification and tracking

BCR cluster tracking was performed using the MATLAB (Mathworks, Natick, MA) image analysis package uTrack (<http://lccb.hms.harvard.edu/software.html>) (26).

Postprocessing of tracked data was performed with custom programs in MATLAB.

The same settings were applied to a field of nonmoving particles of similar size and average cluster displacement was calculated. Three times this value was set as a lower threshold for meaningful cluster motion.

### 5.4.2 Autocorrelation analysis

Actin intensity is processed using pixel-wise intensity autocorrelations. The fluctuations of intensity away from the time-average value was computed using

$$\delta I_{xy}(t) = I_{xy}(t) - \frac{1}{T} \int I_{xy}(t) dt.$$

The pixel-wise autocorrelation was the computed using

$$G_{xy}(\tau) = \frac{\langle \delta I_{xy}(t) \cdot \delta I_{xy}(t + \tau) \rangle}{\left[ \frac{1}{T} \int I_{xy}(t) dt \right] \left[ \frac{1}{T} \int I_{xy}(t) dt \right]}$$

An autocorrelation sum heatmap was made by summing each pixel over all autocorrelation values and then normalizing positive correlation values and negative correlation values.

# Appendices

## A: Additional Ligand Mobility Data

### A.1 Streptavidin accumulation in the B cell contact zone

To test whether the increase in BCR clustering on bilayers was because of increased accumulation of mobile streptavidin in the contact zone, we stimulated cells using AF546-mB-Fab'-anti-Ig to coat the bilayer. This system is also known to induce robust BCR activation and signaling [70]. Although streptavidin again formed distinct clusters in the center of the B cell contact region, the MFI in the contact region did not show as large an increase (Section A.1), indicating that the accumulation of mobile streptavidin alone is not sufficient for the increase in BCR clustering.

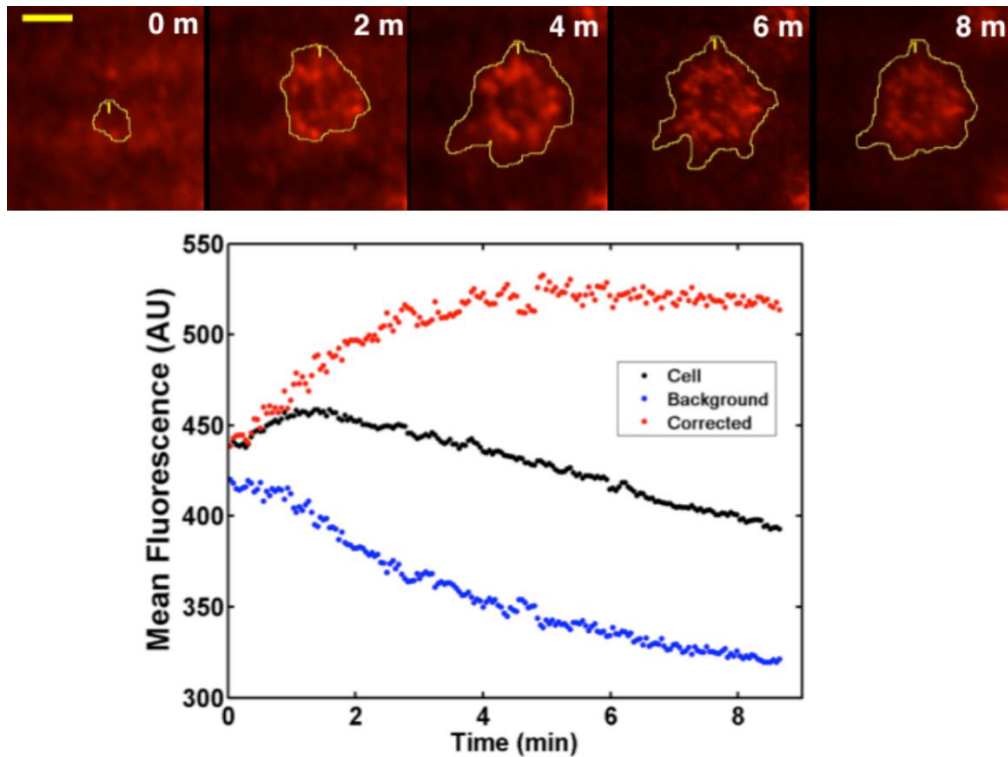


**Figure A.1: Labeled bilayer shows that streptavidin does not accumulate within the contact zone.** Top panels: TIRF image of an A-20 B cell spreading on a streptavidin conjugated lipid bilayer labeled with biotin-AF-456 Fab'. The cell contours were extracted from the IRM image and superimposed on the fluorescent image. Scale bar is 5 μm. Bottom panel: Mean fluorescence intensity of labeled streptavidin within the contact region in a bilayer shows a limited increase over time. An adjacent cell free region is used to correct for photobleaching.

## A.2 Photobleaching correction of fluorescence intensity

Photobleaching during ligand mobility experiments was verified to be minimal during our time-lapse imaging and similar on both glass and bilayer (Fig. A.2).

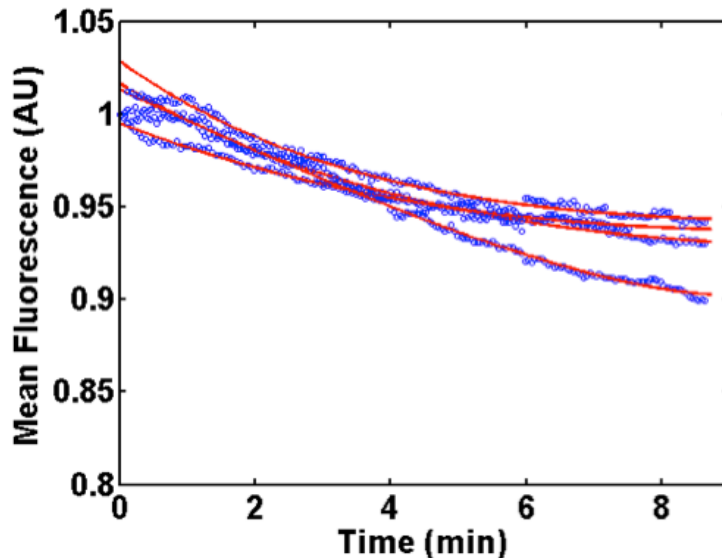


**Figure A.2: Fluorescence intensity curves to assess photobleaching rates.** Glass and bilayer substrates labeled with AF546-mB-Fab'-anti-Ig were exposed to the same laser intensity at the same exposure time and frame rates. Plots of mean fluorescence (normalized to the initial fluorescence values) versus time are shown for 4 representative imaging areas (blue circles). The fluorescence decay over time was fit with biexponential functions and the corresponding fits are shown (red curves).

### A.3 BCR peak cluster intensity is proportional to total cluster intensity

The BCR clusters identified using custom Matlab software were fit to a Gaussian profile. The peak of the Gaussian is proportional to the brightness of the cluster and is proportional to the amount of receptors accumulated in the cluster (Fig. A.3).

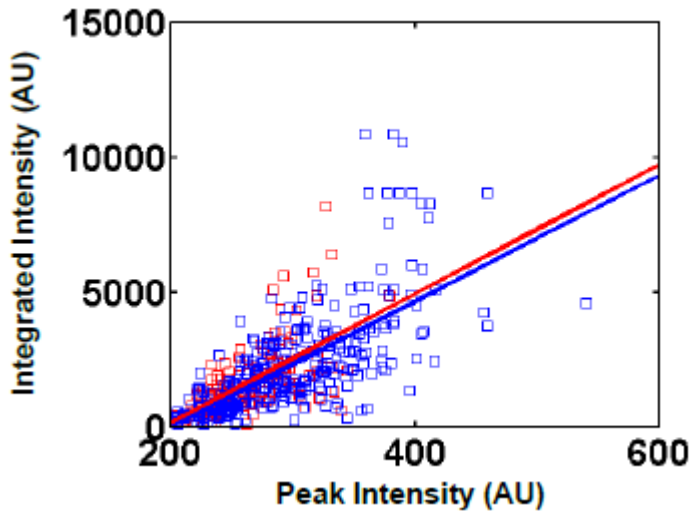


**Figure A.3: BCR cluster peak intensity and integrated cluster intensity are correlated.** BCR cluster peak intensities at a range of time points, between 0 and 8 minutes, plotted against the same clusters' integrated intensity as calculated by a sum of all pixels within the cluster for cells spreading on bilayer (blue) and glass (red). Integrated cluster intensity corresponds to the number of receptors in a cluster. Regression slopes were 23.23 and 23.89 for bilayer and glass respectively.

#### A.4 BCR cluster motion and intensity is actin dependent on mobile ligand substrates

BCR cluster motion was further evaluation with the application of Latrunculin A, which inhibits actin polymerization by sequestering actin monomers. Consistent with the hypothesis that BCR cluster motion on the supported lipid bilayer substrate is actin driven, BCR clusters in B cells on bilayers moved significantly smaller distances upon Lat-A application, as compared with those in untreated cells. In contrast, the mean distance translocated by BCR clusters in cells on glass substrates

were much less affected by application (Fig. A.4). Furthermore, the formation of competent BCR clusters was found to be actin dependent on supported bilayer substrates. Where the peak BCR cluster intensity ratio (end/beginning) was much higher for BCR clusters before the application of LatA on bilayer, while seemingly unaffected on the glass substrate (Fig. A.4B).

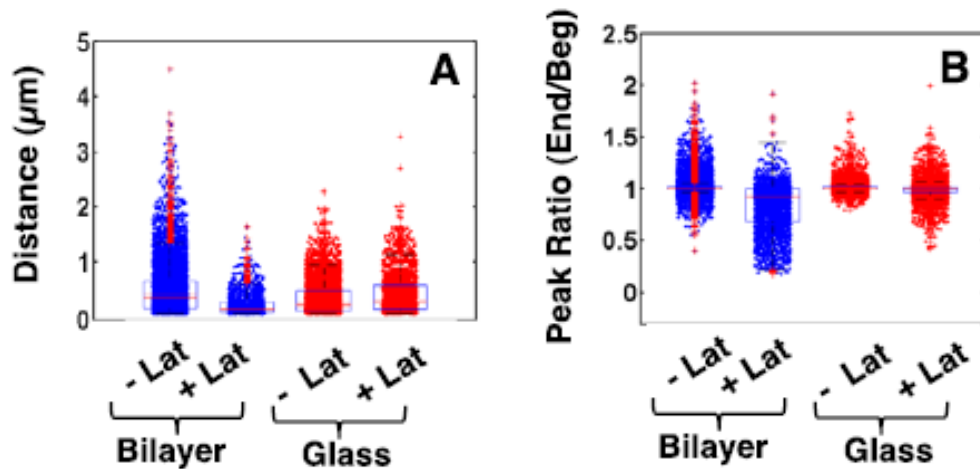


**Figure A.4: Disruption of actin polymerization inhibits BCR cluster movement and growth.** (A) Comparison of the distance traveled by BCR clusters on a bilayer surface in the absence (-Lat) and presence (+Lat) of 100 nM Lat-A on bilayer (blue) and glass (red) surface. (B) The ratio of peak intensities from the end to the beginning of each cluster track for clusters moving on bilayer (blue) versus a glass (red) surface in the presence of 100 nM Lat-A.

## B: Additional Patterned Substrate Data

### B.1 Photobleaching correction of calcium fluorescence

intensity

Photobleaching of OBG1 calcium intensity was corrected by using ImageJ Plugin CorrectBleach from EMBL Heidelberg [144]. The algorithm employed was the double exponential fitting method.

### B.2 Protrusion widths vary by ridge spacing

Actin protrusion lengths and protrusion speeds were markedly influenced by the ridge spacing of the patterns. But are these actin protrusion of a uniform width for all ridge spacings? In order to answer this question, the cross sectional profile of individual actin protrusions was taken (Fig. B.1A-C). The profile line was then fit with a Gaussian distribution where the width at half height was then recorded for EGFP-actin protrusions on each ridge spacing. These widths were found to be dependent on the spacing of the ridges, with the largest width on the smallest spacing (0.8  $\mu\text{m}$ ) and the smallest widths on the large spacing (1.5  $\mu\text{m}$ ) (Fig. B.1D).

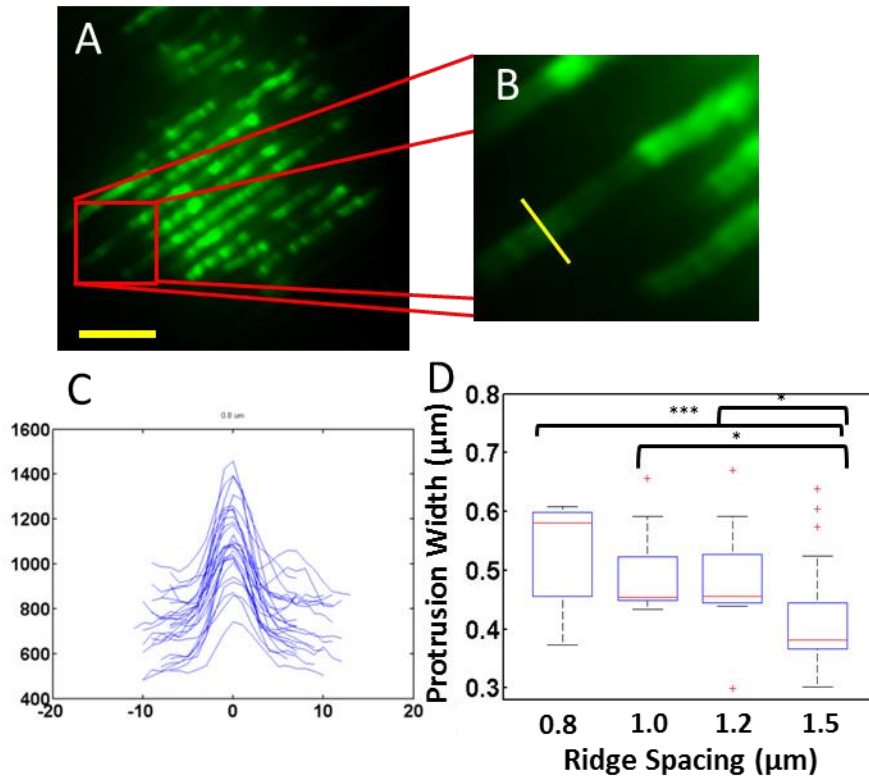


**Fig. B.1: Protrusions width is influenced by ridge spacing.** A) EGFP-actin B cell spread on 1  $\mu\text{m}$  ridge spacing exhibiting protrusions. Scale bar is 5  $\mu\text{m}$ . B) Inset of Protrusion where a demonstrative cross-sectional profile is taken. C) Multiple plots of protrusion widths measured on 1  $\mu\text{m}$  exhibiting a normal integrated intensity distribution. D) Gaussian fitted protrusion widths for ridge spacings between 0.8 and 1.5  $\mu\text{m}$ .

# Bibliography

1. Engler, A.J., et al., *Matrix Elasticity Directs Stem Cell Lineage Specification*. Cell, 2006. **126**(4): p. 677-689.
2. Bordeleau, F., L.N. Tang, and C.A. Reinhart-King, *Topographical guidance of 3D tumor cell migration at an interface of collagen densities*. Physical biology, 2013. **10**(6): p. 065004-065004.
3. Kraning-Rush, C.M., et al., *Microfabricated collagen tracks facilitate single cell metastatic invasion in 3D*. Integrative biology : quantitative biosciences from nano to macro, 2013. **5**(3): p. 606-616.
4. Pasare, C. and R. Medzhitov, *Toll-like receptors: linking innate and adaptive immunity*. Microbes and Infection, 2004. **6**(15): p. 1382-1387.
5. Alberts, B., A. Johnson, and J. Lewis, *Molecular Biology of the Cell*. 2002, New York: Garland Science.
6. Dranoff, G., *Cytokines in cancer pathogenesis and cancer therapy*. Nat Rev Cancer, 2004. **4**(1): p. 11-22.
7. Janeway, C.J., et al., *Immunobiology*. 2001, New York: Garland Science.
8. Oysteri, F.t., *B cell activation*.
9. Parham, P., *The Immune System*. 2005, New York: Garland Science.
10. Bonnerot C, L.D., Hanau D, Spehner D, Davoust J, Salamero J, Fridman WH, *Role of B cell receptor Ig alpha and Ig beta subunits in MHC class II-restricted antigen presentation*. Immunity, 1995. **3**(3): p. 335-47.
11. JC, C., *New nomenclature for the Reth motif (or ARH1/TAM/ARAM/YXXL)*. Immunology Today, 1995. **16**(2).

12. Sohn, H.W., P. Tolar, and S.K. Pierce, *Membrane heterogeneities in the formation of B cell receptor–Lyn kinase microclusters and the immune synapse*. The Journal of Cell Biology, 2008. **182**(2): p. 367-379.
13. Cheng, P.C., et al., *A Role for Lipid Rafts in B Cell Antigen Receptor Signaling and Antigen Targeting*. The Journal of Experimental Medicine, 1999. **190**(11): p. 1549-1560.
14. Dykstra, M., et al., *Location is Everything: Lipid Rafts and Immune Cell Signaling\**. Annual Review of Immunology, 2003. **21**(1): p. 457-481.
15. Sohn, H.W., S.K. Pierce, and S.-J. Tzeng, *Live Cell Imaging Reveals that the Inhibitory FcγRIIB Destabilizes B Cell Receptor Membrane-Lipid Interactions and Blocks Immune Synapse Formation*. The Journal of Immunology, 2008. **180**(2): p. 793-799.
16. Jiang, A., et al., *Different Protein Tyrosine Kinases Are Required for B Cell Antigen Receptor–mediated Activation of Extracellular Signal–Regulated kinase, c-Jun NH(2)-terminal Kinase 1, and p38 Mitogen-activated Protein Kinase*. The Journal of Experimental Medicine, 1998. **188**(7): p. 1297-1306.
17. Dal Porto, J.M., et al., *B cell antigen receptor signaling 101*. Molecular Immunology, 2004. **41**(6–7): p. 599-613.
18. Kurosaki, T., *Regulation of BCR signaling*. Molecular Immunology, 2011. **48**(11): p. 1287-1291.
19. Takata, M., et al., *Tyrosine kinases Lyn and Syk regulate B cell receptor-coupled Ca<sup>2+</sup> mobilization through distinct pathways*. The EMBO Journal, 1994. **13**(6): p. 1341-1349.
20. Fluckiger, A.C., et al., *Btk/Tec kinases regulate sustained increases in intracellular Ca<sup>2+</sup> following B-cell receptor activation*. The EMBO Journal, 1998. **17**(7): p. 1973-1985.
21. Kabak, S., et al., *The Direct Recruitment of BLNK to Immunoglobulin α Couples the B-Cell Antigen Receptor to Distal Signaling Pathways*. Molecular and Cellular Biology, 2002. **22**(8): p. 2524-2535.

22. Akimzhanov, A.M. and D. Boehning, *IP3R function in cells of the immune system*. Wiley Interdisciplinary Reviews: Membrane Transport and Signaling, 2012. **1**(3): p. 329-339.
23. Harwood, N.E. and F.D. Batista, *Early Events in B Cell Activation*. Annual Review of Immunology, 2010. **28**(1): p. 185-210.
24. Tolar, P., H.W. Sohn, and S.K. Pierce, *The initiation of antigen-induced B cell antigen receptor signaling viewed in living cells by fluorescence resonance energy transfer*. Nat Immunol, 2005. **6**(11): p. 1168-76.
25. Mongini, P.K., et al., *Membrane IgM-mediated signaling of human B cells. Effect of increased ligand binding site valency on the affinity and concentration requirements for inducing diverse stages of activation*. J Immunol, 1992. **148**(12): p. 3892-901.
26. Freeman, S.A., et al., *Cofilin-Mediated F-Actin Severing Is Regulated by the Rap GTPase and Controls the Cytoskeletal Dynamics That Drive Lymphocyte Spreading and BCR Microcluster Formation*. The Journal of Immunology, 2011. **187**(11): p. 5887-5900.
27. Treanor, B., et al., *Dynamic cortical actin remodeling by ERM proteins controls BCR microcluster organization and integrity*. The Journal of Experimental Medicine, 2011. **208**(5): p. 1055-1068.
28. Song, W., et al., *Actin-mediated feedback loops in B-cell receptor signaling*. Immunological Reviews, 2013. **256**(1): p. 177-189.
29. Tolar, P., H. Won Sohn, and S.K. Pierce, *Viewing the antigen-induced initiation of B-cell activation in living cells*. Immunological Reviews, 2008. **221**(1): p. 64-76.
30. Mattila, P.K., et al., *The actin and tetraspanin networks organize receptor nanoclusters to regulate B cell receptor-mediated signaling*. Immunity, 2013. **38**(3): p. 461-474.
31. Yang, J. and M. Reth, *Oligomeric organization of the B-cell antigen receptor on resting cells*. Nature, 2010. **467**(7314): p. 465-469.

32. Yang, J. and M. Reth, *The dissociation activation model of B cell antigen receptor triggering*. FEBS Letters, 2010. **584**(24): p. 4872-4877.
33. Woodruff, M.F.A., B. Reid, and K. James, *Effect of Antilymphocytic Antibody and Antibody Fragments on Human Lymphocytes in vitro*. Nature, 1967. **215**(5101): p. 591-594.
34. Pierce, S.K. and W. Liu, *The tipping points in the initiation of B cell signalling: how small changes make big differences*. Nature Reviews. Immunology, 2010. **10**(11): p. 767-777.
35. Treanor, B., *B-cell receptor: from resting state to activate*. Immunology, 2012. **136**(1): p. 21-27.
36. Singer, S.J. and G.L. Nicolson, *The Fluid Mosaic Model of the Structure of Cell Membranes*. Science, 1972. **175**(4023): p. 720-731.
37. Pike, L.J., *Lipid rafts: bringing order to chaos*. Journal of Lipid Research, 2003. **44**(4): p. 655-667.
38. Hao, M., S. Mukherjee, and F.R. Maxfield, *Cholesterol depletion induces large scale domain segregation in living cell membranes*. Proceedings of the National Academy of Sciences, 2001. **98**(23): p. 13072-13077.
39. Mayor, S. and F.R. Maxfield, *Insolubility and redistribution of GPI-anchored proteins at the cell surface after detergent treatment*. Molecular Biology of the Cell, 1995. **6**(7): p. 929-944.
40. Gupta, N. and A.L. DeFranco, *Visualizing Lipid Raft Dynamics and Early Signaling Events during Antigen Receptor-mediated B-Lymphocyte Activation*. Molecular Biology of the Cell, 2003. **14**(2): p. 432-444.
41. Kovářová, M., et al., *Structure-Function Analysis of Lyn Kinase Association with Lipid Rafts and Initiation of Early Signaling Events after Fcε Receptor I Aggregation*. Molecular and Cellular Biology, 2001. **21**(24): p. 8318-8328.
42. Young, R.M., D. Holowka, and B. Baird, *A Lipid Raft Environment Enhances Lyn Kinase Activity by Protecting the Active Site Tyrosine from Dephosphorylation*. Journal of Biological Chemistry, 2003. **278**(23): p. 20746-20752.

43. Kusumi, A., et al., *Paradigm Shift of the Plasma Membrane Concept from the Two-Dimensional Continuum Fluid to the Partitioned Fluid: High-Speed Single-Molecule Tracking of Membrane Molecules*. Annual Review of Biophysics and Biomolecular Structure, 2005. **34**(1): p. 351-378.
44. Suzuki, K., et al., *Rapid Hop Diffusion of a G-Protein-Coupled Receptor in the Plasma Membrane as Revealed by Single-Molecule Techniques*. Biophysical Journal, 2005. **88**(5): p. 3659-3680.
45. Oh-hora, M. and A. Rao, *Calcium signaling in lymphocytes*. Current opinion in immunology, 2008. **20**(3): p. 250-258.
46. Parekh, A.B. and J.W. Putney Jr., *Store-Operated Calcium Channels*. Physiol Rev, 2005(85): p. 757–810.
47. Furukawa, R., et al., *Calcium regulation of actin crosslinking is important for function of the actin cytoskeleton in Dictyostelium*. Journal of Cell Science, 2003. **116**(1): p. 187-196.
48. Wei, C., et al., *Calcium flickers steer cell migration*. Nature, 2009. **457**(7231): p. 901-905.
49. Gittes, F., et al., *Flexural rigidity of microtubules and actin filaments measured from thermal fluctuations in shape*. The Journal of Cell Biology, 1993. **120**(4): p. 923-934.
50. Cooper, G., *The Cell: A Molecular Approach*. 2nd Edition ed. 2000, Sunderland (MA): Sinauer Associates.
51. Hao, S. and A. August, *Actin Depolymerization Transduces the Strength of B-Cell Receptor Stimulation*. Molecular Biology of the Cell, 2005. **16**(5): p. 2275-2284.
52. Freeman, S.A., et al., *Toll-like receptor ligands sensitize B-cell receptor signalling by reducing actin-dependent spatial confinement of the receptor*. Nat Commun, 2015. **6**.
53. Fleire, S.J., et al., *B Cell Ligand Discrimination through a Spreading and Contraction Response*. Science, 2006. **312**(5774): p. 738-741.

54. Song, W., C. Liu, and A. Upadhyaya, *The pivotal position of the actin cytoskeleton in the initiation and regulation of B cell receptor activation*(). *Biochimica et biophysica acta*, 2014. **1838**(2): p. 10.1016/j.bbamem.2013.07.016.
55. Vascotto, F., et al., *Antigen presentation by B lymphocytes: how receptor signaling directs membrane trafficking*. *Current Opinion in Immunology*, 2007. **19**(1): p. 93-98.
56. Sharma, S., G. Orłowski, and W. Song, *Btk Regulates B Cell Receptor-Mediated Antigen Processing and Presentation by Controlling Actin Cytoskeleton Dynamics in B Cells*. *The Journal of Immunology*, 2009. **182**(1): p. 329-339.
57. Liu, C., et al., *N-WASP Is Essential for the Negative Regulation of B Cell Receptor Signaling*. *PLoS Biology*, 2013. **11**(11): p. e1001704.
58. Krendel, M. and M.S. Mooseker, *Myosins: Tails (and Heads) of Functional Diversity*. *Physiology*, 2005. **20**(4): p. 239-251.
59. Natkanski, E., et al., *B cells use mechanical energy to discriminate antigen affinities*. *Science (New York, N.Y.)*, 2013. **340**(6140): p. 1587-1590.
60. Santos-Argumedo, L., J.L. Maravillas-Montero, and O. López-Ortega, *Class I myosins in B-cell physiology: functions in spreading, immune synapses, motility, and vesicular traffic*. *Immunological Reviews*, 2013. **256**(1): p. 190-202.
61. Ilani, T., et al., *T cell antigen receptor signaling and immunological synapse stability require myosin IIA*. *Nat Immunol*, 2009. **10**(5): p. 531-539.
62. Carroll-Portillo, A., et al., *Formation of a Mast Cell Synapse: FcεRI Membrane Dynamics upon Binding Mobile or Immobilized Ligands on Surfaces*. *The Journal of Immunology*, 2010. **184**(3): p. 1328-1338.
63. Hsu, C.-J., et al., *Ligand Mobility Modulates Immunological Synapse Formation and T Cell Activation*. *PLOS One*, 2012. **7**(2): p. e32398.
64. Mossman, K.D., et al., *Altered TCR Signaling from Geometrically Repatterned Immunological Synapses*. *Science*, 2005. **310**(5751): p. 1191-1193.

65. DeMond, A.L., et al., *T Cell Receptor Microcluster Transport through Molecular Mazes Reveals Mechanism of Translocation*. Biophysical Journal, 2008. **94**(8): p. 3286-3292.
66. Smoligovets, A.A., et al., *Characterization of dynamic actin associations with T-cell receptor microclusters in primary T cells*. Journal of Cell Science, 2012. **125**(3): p. 735-742.
67. Treanor, B., et al., *The membrane skeleton controls diffusion dynamics and signaling through the B cell receptor*. Immunity, 2010. **32**(2): p. 187-199.
68. Tolar, P., et al., *The constant region of the membrane immunoglobulin mediates B-cell receptor clustering and signaling in response to membrane antigens*. Immunity, 2009. **30**(1): p. 44-55.
69. Bajénoff, M. and R.N. Germain, *B-cell follicle development remodels the conduit system and allows soluble antigen delivery to follicular dendritic cells*. Blood, 2009. **114**(24): p. 4989-4997.
70. Liu, C., et al., *A Balance of Bruton's Tyrosine Kinase and SHIP Activation Regulates B Cell Receptor Cluster Formation by Controlling Actin Remodeling*. The Journal of Immunology, 2011. **187**(1): p. 230-239.
71. Liu, C., et al., *Actin Reorganization Is Required for the Formation of Polarized B Cell Receptor Signalosomes in Response to Both Soluble and Membrane-Associated Antigens*. Journal of Immunology, 2012. **188**(7): p. 3237-3246.
72. Muiznieks, L.D. and F.W. Keeley, *Molecular assembly and mechanical properties of the extracellular matrix: A fibrous protein perspective*. Biochimica et Biophysica Acta (BBA) - Molecular Basis of Disease, 2013. **1832**(7): p. 866-875.
73. Batista, F.D. and N.E. Harwood, *The who, how and where of antigen presentation to B cells*. Nat Rev Immunol, 2009. **9**(1): p. 15-27.
74. Batista, F.D., D. Iber, and M.S. Neuberger, *B cells acquire antigen from target cells after synapse formation*. Nature, 2001. **411**(6836): p. 489-494.

75. Endlich, N., et al., *Movement of stress fibers away from focal adhesions identifies focal adhesions as sites of stress fiber assembly in stationary cells*. Cell motility and the cytoskeleton, 2007. **64**(12): p. 966-76.
76. Kim, D.-H., et al., *Matrix nanotopography as a regulator of cell function*. The Journal of Cell Biology, 2012. **197**(3): p. 351-360.
77. Bettinger, C.J., R. Langer, and J.T. Borenstein, "*Engineering Substrate Micro- and Nanotopography to Control Cell Function*". Angewandte Chemie (International ed. in English), 2009. **48**(30): p. 5406-5415.
78. Driscoll, M.K., et al., *Cellular Contact Guidance through Dynamic Sensing of Nanotopography*. ACS Nano, 2014. **8**(4): p. 3546-3555.
79. le Digabel, J., et al., *Microfabricated substrates as a tool to study cell mechanotransduction*. Medical & Biological Engineering & Computing, 2010. **48**(10): p. 965-976.
80. Berry, C.C., et al., *The influence of microscale topography on fibroblast attachment and motility*. Biomaterials, 2004. **25**(26): p. 5781-5788.
81. Biela, S.A., et al., *Different sensitivity of human endothelial cells, smooth muscle cells and fibroblasts to topography in the nano–micro range*. Acta Biomaterialia, 2009. **5**(7): p. 2460-2466.
82. Kim, D.-H., et al., *Mechanosensitivity of fibroblast cell shape and movement to anisotropic substratum topography gradients*. Biomaterials, 2009. **30**(29): p. 5433-5444.
83. Lamers, E., et al., *The influence of nanoscale topographical cues on initial osteoblast morphology and migration*. European Cells and Materials, 2010. **20**: p. 329-343.
84. Lamers, E., et al., *The influence of nanoscale grooved substrates on osteoblast behavior and extracellular matrix deposition*. Biomaterials, 2010. **31**(12): p. 3307-3316.
85. Ottani, V., M. Raspanti, and A. Ruggeri, *Collagen structure and functional implications*. Micron, 2001. **32**(3): p. 251-260.

86. Xie, J., et al., *Neurite Outgrowth on Electrospun Nanofibers with Uniaxial Alignment: The Effects of Fiber Density, Surface Coating, and Supporting Substrate*. ACS Nano, 2014. **8**(2): p. 1878-1885.
87. Nagata, I., A. Kawana, and N. Nakatsuji, *Perpendicular contact guidance of CNS neuroblasts on artificial microstructures*. Development, 1993. **117**(1): p. 401-408.
88. Nagata, I. and N. Nakatsuji, *Rodent CNS neuroblasts exhibit both perpendicular and parallel contact guidance on the aligned parallel neurite bundle*. Development, 1991. **112**(2): p. 581-590.
89. Teixeira, A.I., et al., *Epithelial contact guidance on well-defined micro- and nanostructured substrates*. Journal of Cell Science, 2003. **116**(10): p. 1881-1892.
90. Teixeira, A.I., et al., *The effect of environmental factors on the response of human corneal epithelial cells to nanoscale substrate topography*. Biomaterials, 2006. **27**(21): p. 3945-3954.
91. Dalby, M.J., et al., *The control of human mesenchymal cell differentiation using nanoscale symmetry and disorder*. Nat Mater, 2007. **6**(12): p. 997-1003.
92. Oh, S., et al., *Stem cell fate dictated solely by altered nanotube dimension*. Proceedings of the National Academy of Sciences, 2009. **106**(7): p. 2130-2135.
93. Sun, X., et al., *Asymmetric nanotopography biases cytoskeletal dynamics and promotes unidirectional cell guidance*. Proceedings of the National Academy of Sciences of the United States of America, 2015. **112**(41): p. 12557-12562.
94. Kwon, K.W., et al., *Nanotopography-Guided Migration of T Cells*. The Journal of Immunology, 2012. **189**(5): p. 2266-2273.
95. Saino, E., et al., *Effect of Electrospun Fiber Diameter and Alignment on Macrophage Activation and Secretion of Proinflammatory Cytokines and Chemokines*. Biomacromolecules, 2011. **12**(5): p. 1900-1911.
96. Ketchum, C., et al., *Ligand Mobility Regulates B Cell Receptor Clustering and Signaling Activation*. Biophysical Journal, 2014. **106**(1): p. 26-36.

97. Manz, B.N. and J.T. Groves, *Spatial organization and signal transduction at intercellular junctions*. Nature Reviews Molecular Cell Biology, 2010. **11**(5): p. 342-352.
98. Lohmüller, T., Q. Xu, and J.T. Groves, *Nanoscale Obstacle Arrays Frustrate Transport of EphA2 – Ephrin-A1 Clusters in Cancer Cell Lines*. Nano letters, 2013. **13**(7): p. 3059-3064.
99. Salaita, K., et al., *Restriction of Receptor Movement Alters Cellular Response: Physical Force Sensing by EphA2*. Science, 2010. **327**(5971): p. 1380-1385.
100. Selhuber-Unkel, C., et al., *Cell Adhesion Strength Is Controlled by Intermolecular Spacing of Adhesion Receptors*. Biophysical Journal, 2010. **98**(4): p. 543-551.
101. Cavalcanti-Adam, E.A., et al., *Cell Spreading and Focal Adhesion Dynamics Are Regulated by Spacing of Integrin Ligands*. Biophysical Journal, 2007. **92**(8): p. 2964-2974.
102. Batista, F.D. and M.L. Dustin, *Cell:cell interactions in the immune system*. Immunological Reviews, 2013. **251**(1): p. 7-12.
103. Junt, T., et al., *Subcapsular sinus macrophages in lymph nodes clear lymph-borne viruses and present them to antiviral B cells*. Nature, 2007. **450**(7166): p. 110-114.
104. Pape, K.A., et al., *The Humoral Immune Response Is Initiated in Lymph Nodes by B Cells that Acquire Soluble Antigen Directly in the Follicles*. Immunity, 2007. **26**(4): p. 491-502.
105. Phan, T.G., E.E. Gray, and J.G. Cyster, *The microanatomy of B cell activation*. Current opinion in immunology, 2009. **21**(3): p. 258-265.
106. Suzuki, K., et al., *Visualizing B cell capture of cognate antigen from follicular dendritic cells*. The Journal of Experimental Medicine, 2009. **206**(7): p. 1485-1493.
107. Unanue, E.R. and M.J. Karnovsky, *LIGAND-INDUCED MOVEMENT OF LYMPHOCYTE MEMBRANE MACROMOLECULES : V. Capping, Cell Movement*,

*and Microtubular Function in Normal and Lectin-Treated Lymphocytes*. The Journal of Experimental Medicine, 1974. **140**(5): p. 1207-1220.

108. Harwood, N. and F. Batista, *Visualizing the Molecular and Cellular Events Underlying the Initiation of B-Cell Activation*, in *Visualizing Immunity*, M. Dustin and D. McGavern, Editors. 2009, Springer Berlin Heidelberg. p. 153-177.

109. Szakal, A.K., M.H. Kosco, and J.G. Tew, *A novel in vivo follicular dendritic cell-dependent iccosome-mediated mechanism for delivery of antigen to antigen-processing cells*. The Journal of Immunology, 1988. **140**(2): p. 341-353.

110. Liu, W., et al., *Antigen-Induced Oligomerization of the B Cell Receptor Is an Early Target of FcγRIIB Inhibition*. Journal of Immunology, 2010. **184**(4): p. 1977-1989.

111. Treanor, B. and F.D. Batista, *Organisation and dynamics of antigen receptors: implications for lymphocyte signalling*. Current Opinion in Immunology, 2010. **22**(3): p. 299-307.

112. Harwood, N.E. and F.D. Batista, *The Cytoskeleton Coordinates the Early Events of B-cell Activation*. Cold Spring Harbor Perspectives in Biology, 2011. **3**(2): p. a002360.

113. Depoil, D., et al., *CD19 is essential for B cell activation by promoting B cell receptor-antigen microcluster formation in response to membrane-bound ligand*. Nat Immunol, 2008. **9**(1): p. 63-72.

114. Weber, M., et al., *Phospholipase C-γ2 and Vav cooperate within signaling microclusters to propagate B cell spreading in response to membrane-bound antigen*. The Journal of Experimental Medicine, 2008. **205**(4): p. 853-868.

115. Unanue, E.R., W.D. Perkins, and M.J. Karnovsky, *Ligand-induced Movement of Lymphocyte Membrane Macromolecules: I. Analysis by Immunofluorescence and Ultrastructural Radioautography*. The Journal of Experimental Medicine, 1972. **136**(4): p. 885-906.

116. Fu, X., et al., *Regulation of migratory activity of human keratinocytes by topography of multiscale collagen-containing nanofibrous matrices*. Biomaterials, 2014. **35**(5): p. 1496-1506.

117. Pot, S.A., et al., *Nanoscale Topography–Induced Modulation of Fundamental Cell Behaviors of Rabbit Corneal Keratocytes, Fibroblasts, and Myofibroblasts*. Investigative Ophthalmology & Visual Science, 2010. **51**(3): p. 1373-1381.
118. Felts, R.L., et al., *3D visualization of HIV transfer at the virological synapse between dendritic cells and T cells*. Proceedings of the National Academy of Sciences of the United States of America, 2010. **107**(30): p. 13336-13341.
119. Szakal, A.K., et al., *Isolated follicular dendritic cells: cytochemical antigen localization, Nomarski, SEM, and TEM morphology*. The Journal of Immunology, 1985. **134**(3): p. 1349-1359.
120. Adutler-Lieber, S., et al., *Engineering of synthetic cellular microenvironments: Implications for immunity*. Journal of Autoimmunity, 2014. **54**: p. 100-111.
121. El Shikh, M., et al., *Follicular dendritic cells stimulated by collagen type I develop dendrites and networks in vitro*. Cell Tissue Res., 2007. **329**(1): p. 81-89.
122. Vogel, V. and M. Sheetz, *Local force and geometry sensing regulate cell functions*. Nat Rev Mol Cell Biol, 2006. **7**(4): p. 265-275.
123. Liu, C., et al., *Analyzing actin dynamics during the activation of the B cell receptor in live B cells*. Biochemical and Biophysical Research Communications, 2012. **427**(1): p. 202-206.
124. Geahlen, R.L. and J.L. McLaughlin, *Piceatannol (3,4,3',5'-tetrahydroxy-trans-stilbene) is a naturally occurring protein-tyrosine kinase inhibitor*. Biochemical and Biophysical Research Communications, 1989. **165**(1): p. 241-245.
125. Oliver, J.M., et al., *Inhibition of mast cell Fc epsilon R1-mediated signaling and effector function by the Syk-selective inhibitor, piceatannol*. Journal of Biological Chemistry, 1994. **269**(47): p. 29697-29703.
126. Ko, Y.-J., et al., *Piceatannol inhibits mast cell-mediated allergic inflammation*. International Journal of Molecular Medicine, 2013. **31**(4): p. 951-958.

127. Kasza, K.E. and J.A. Zallen, *Dynamics and regulation of contractile actin-myosin networks in morphogenesis*. Current Opinion in Cell Biology, 2011. **23**(1): p. 30-38.
128. Martin, A.C., M. Kaschube, and E.F. Wieschaus, *Pulsed actin-myosin network contractions drive apical constriction*. Nature, 2009. **457**(7228): p. 495.
129. Gorfinkiel, N., *Mechano-Chemical Coupling Drives Cell Area Oscillations during Morphogenesis*. Biophysical Journal, 2013. **104**(1): p. 1-3.
130. van den Dries, K., et al., *Interplay between myosin IIA-mediated contractility and actin network integrity orchestrates podosome composition and oscillations*. Nature Communications, 2013. **4**: p. 1412.
131. Ishizaki, T., et al., *Pharmacological Properties of Y-27632, a Specific Inhibitor of Rho-Associated Kinases*. Molecular Pharmacology, 2000. **57**(5): p. 976-983.
132. Smedler, E. and P. Uhlén, *Frequency decoding of calcium oscillations*. Biochimica et Biophysica Acta (BBA) - General Subjects, 2014. **1840**(3): p. 964-969.
133. Wollman, R. and T. Meyer, *Coordinated oscillations in cortical actin and Ca<sup>2+</sup> correlate with cycles of vesicle secretion*. Nature cell biology, 2012. **14**(12): p. 1261-1269.
134. Oka, T., et al., *FcεRI cross-linking-induced actin assembly mediates calcium signalling in RBL-2H3 mast cells*. British Journal of Pharmacology, 2002. **136**(6): p. 837-846.
135. Paredes, R.M., et al., *Chemical Calcium Indicators*. Methods (San Diego, Calif.), 2008. **46**(3): p. 143-151.
136. Jaumouillé, V., et al., *Actin cytoskeleton reorganization by the tyrosine kinase Syk regulates Fcγ receptor responsiveness by increasing its lateral mobility and clustering*. Developmental cell, 2014. **29**(5): p. 534-546.
137. Pearce, G., T. Audzevich, and R. Jessberger, *SYK regulates B-cell migration by phosphorylation of the F-actin interacting protein SWAP-70*. Blood, 2010. **117**(5): p. 1574-1584.

138. Rolli, V., et al., *Amplification of B Cell Antigen Receptor Signaling by a Syk/ITAM Positive Feedback Loop*. *Molecular Cell*. **10**(5): p. 1057-1069.
139. Breuls, R.G.M., T.U. Jiya, and T.H. Smit, *Scaffold Stiffness Influences Cell Behavior: Opportunities for Skeletal Tissue Engineering*. *The Open Orthopaedics Journal*, 2008. **2**: p. 103-109.
140. Hui, K.L., et al., *Cytoskeletal forces during signaling activation in Jurkat T-cells*. *Molecular Biology of the Cell*, 2015. **26**(4): p. 685-695.
141. Wan, Z., et al., *B Cell Activation Is Regulated by the Stiffness Properties of the Substrate Presenting the Antigens*. *The Journal of Immunology*, 2013. **190**(9): p. 4661-4675.
142. LaFratta, C.N., et al., *Multiphoton Fabrication*. *Angewandte Chemie International Edition*, 2007. **46**(33): p. 6238-6258.
143. Stocker, M.P., et al., *Multiphoton photoresists giving nanoscale resolution that is inversely dependent on exposure time*. *Nat Chem*, 2011. **3**(3): p. 223-227.
144. Miura, K.e.a., *ImageJ Plugin CorrectBleach*. 2014, Zenodo. 10.5281/zenodo.30769.